

©2014

Mahta Samizadeh

ALL RIGHTS RESERVED

ANTI-HIV DRUG CONJUGATES FOR ENHANCED MUCOSAL PRE-EXPOSURE

PROPHYLAXIS

By

MAHTA SAMIZADEH

A dissertation submitted to the

Graduate School-New Brunswick

Rutgers, The State University of New Jersey

In partial fulfillment of the requirements

For the degree of

Doctor of Philosophy

Graduate Program in Pharmaceutical Science

Written under the direction of

Professor Patrick J. Sinko

And approved by

New Brunswick, New Jersey

May, 2014

ABSTRACT OF THE DISSERTATION

ANTI-HIV DRUG CONJUGATES FOR ENHANCED MUCOSAL PRE-EXPOSURE PROPHYLAXIS

By Mahta Samizadeh

Dissertation Director:

Professor Patrick J. Sinko

To combat HIV pandemic, targeting HIV mucosal transmission appears to be more effective than targeting later stages of the infection owing to the viral vulnerability and higher efficacy of antiretrovirals at this very early stage of HIV infection. The objective of the current project is to investigate the complementary benefits of combining an anti-HIV drug (amprenavir, APV), a cell-penetrating peptide (bactenecin 7, Bac7 CPP) and poly (ethylene glycol) (PEG) together as a nanocarrier conjugate for fast and efficient cytosolic delivery of the drug. The nanocarrier is to be incorporated into an alcohol-free thermosensitive foam for colonic/rectal delivery.

In the initial studies, APV-PEG conjugates were prepared using 2 to 30 kDa PEGs and protease inhibition properties were assessed in buffer using FRET-based protease inhibition assay. The results suggested that PEG size between 2 and 5 kDa is the optimum range for maintaining the protease inhibition activity. For further studies, APV-PEG_{3,4}-FITC (APF) and a PEGylated APV conjugated with Bac7 CPP (APV-PEG_{3,4}-Bac7 CPP; APB) were prepared. The anti-HIV-1 activities were assessed based on the

potency of the conjugates to inhibit the viral replication in HIV-1 infected CD4⁺ MT-2 T-cells. Compare with free APV (IC₅₀ = 50.29 nM), 160-fold reduction in potency was observed in APF activity (IC₅₀ = 8.064 μM) whereas APB conjugate exhibited anti-viral activity close to APV (IC₅₀ = 78.29 nM), suggesting the poor cell penetration of APV-PEG was remedied by conjugating Bac7 CPP.

Aerosol foams have some distinct advantages for rectal and vaginal drug delivery over conventional dosage forms including greater degree of spread, ease of application and enhanced drug delivery efficiency. Alcohol-free thermosensitive aerosol foams were prepared containing 0.5% to 2.0% of xanthan gum (XG). The foam with 1.5% XG showed the best performance among all the formulations; it was stable at room temperature for over 2 h while *in vivo* MRI of the foam in mice showed excellent colonic/rectal coverage with little discharge compare with saline enema or a conventional gel formulation. Histology of the colorectal tissue following daily application of the foam for 5 consecutive days showed no significant inflammation in the applied area.

DEDICATION

To my parents, Parvin and Cyrus,
and
my husband, Khosro,
for their endless support and unconditional love

AKNOWELEDGMENTS

I would like to thank my dissertation advisor, Professor Patrick Sinko, for giving me the opportunity to be part of his productive lab. Following his guidance and suggestions during my graduate study, I learned how to think independently. I would like to thank my committee members; Professors Bozena Michniak, Paul Thomas and Lauren Aleksunes for their time and supports.

Many thanks to the Sinko Research Group past and present for their help and support. Special thanks to Dr. Xiaoping Zhang, Dr. Shahriar Pooyan, Dr. Simi Gunaseelan, Dr. Yashveer Singh, Dr. Manjeet Deshmukh, Dr. Dayuan Gao, Dr. Zoltan Szekely, Derek Adler and Steven Johnson for sharing their experience in the areas of chemistry and biology. Christal Louison, Amy Grabowsky, Hui Pung, Marianne Shen and Sharana Taylor are recognized for their assistance.

Spray Products Corp., Gerstung Aerosol Inc., Dr. Charles Rohn (Malvern Instruments) and Theresa Choi (CORE Facility, Rutgers) are acknowledged for their helps with some important studies and technical problem solving. NIH MERIT AI51214, NIH HIT-IT (R01AI084137-03) and the Parke-Davis Endowed Chair in Pharmaceutics and Drug Delivery are also acknowledged.

I would like to thank Professor Gary Merrill and all other instructors who taught me not only about science, but about how to be a better human being.

Finally, I am grateful to my family and friends, for bright words on dim days.

Table of Contents

ABSTRACT OF THE DISSERTATION	ii
DEDICATION	iv
AKNOWELEDGMENTS	v
1. INTRODUCTION	1
2. BACKGROUND AND SIGNIFICANCE	4
2.1 Human Immunodeficiency Virus	4
2.1.1 HIV Mucosal Invasion and its Contribution to Global Infections	5
2.1.2 Gut Mucosal Immune Function and HIV Infection	6
2.1.3 Female Genital Tract and HIV Infection	7
2.1.4 Antiretroviral Therapy and HIV Treatment	8
2.1.5 Protease Inhibitors	9
2.1.6 Amprenavir and Foasamprenavir	10
2.1.7 HIV Vaccine Development	11
2.1.8 Preventing Mucosal HIV Transmission with Topical Microbicides	11
2.2 Poly(ethylene glycol) and PEGylation	13
2.2.1 PEGylation of Proteins and Polypeptides	14
2.2.2 PEGylation of Small Molecular agents	15
2.2.3 Different Configurations of PEGylation of Small Molecule Drugs	16
2.2.4 Targeted Delivery of PEGylated Small Molecule Drugs	18
2.2.5 PEGylated Anti-Viral Drugs	18
2.3 Peptides with Cell-Penetrating Properties	20
2.3.1 Cell-Penetrating Peptides	21
2.3.2 Antimicrobial Peptides with Cell-Penetrating Characteristics	22
2.3.3 Bactenicin 7 as a Potent and Effective Cell-Penetrating Peptide	24
2.4 Mucosal Drug Delivery	24
2.4.1 Advantages of Mucosal Drug Delivery	25
2.4.2 Drug Delivery in the Lower Gastrointestinal Tract	25
2.4.3 Vaginal Drug Delivery	26
2.4.4 Foams for Pharmaceutical Applications	26
2.4.5 Foam Quality and Breakability	27

2.4.6 Application of Foams for Rectal and Vaginal Drug Delivery	28
2.4.7 Pharmaceutical Foams for Nanoparticles Delivery to Mucosal Membranes.....	29
3. SPECIFIC AIMS	30
4. DESIGN, SYNTHESIS AND HIV-1 PROTEASE INHIBITION OF DIFFERENTLY SIZED, NON-RELEASABLE AMPRENAVIR-POLYETHYLENE GLYCOL CONJUGATES.....	32
4.1 Introduction.....	32
4.2 Materials and Methods.....	34
4.2.1 Materials	34
4.2.2 Extraction of APV from Agenerase [®] capsules	35
4.2.3 Preparation of APV-O-acetyl.....	36
4.2.4 Preparation of PEG _x -APV-O-acetyl and PEG _x -APV-OH	36
4.2.5 Stability of Amide Bonds in PBS	37
4.2.6 Protease Inhibition Activity of PEG _x -APV-OH (x = 2, 5, 10, and 30 Da) in Buffer	38
4.2.7 Statistical Analysis.....	38
4.3 Results.....	39
4.3.1 Synthesis and Characterization Studies	39
4.3.2 Stability of Amide bonds	40
4.3.3 Evaluation of HIV-1 Protease inhibition in Buffer: PEG Influences the HIV-1 Protease Inhibition in a Size-Dependent Manner	40
4.4 Discussion.....	43
5. DESIGN, SYNTHESIS AND CHARACTERIZATION OF A PEGYLATED.....	46
AMPRENAVIR NANOCARRIER CONJUGATED TO Bac7 CELL-PENETRATING PEPTIDED AND EVALUATION OF ANTI-HIV-1 REPLICATION INHIBITION IN T- CELLS.....	46
5.1 Introduction.....	46
5.2 Materials and Methods.....	47
5.2.1 Materials	47
5.2.2 Synthesis of FITC Labeled Amprenavir-PEG Conjugate (APF).....	49
5.2.3 APF Concentration Determination Using a Standard Curve Generated with FITC- PEG	49
5.2.4 Synthesis of Bac7 CPP.....	50
5.2.6 Cysteine Standard Curve (Ellman's Assay).....	51
5.2.7 Synthesis of FITC Labeled Bac7 CPP-PEG _{3,4} Conjugate (BPF).....	51

5.2.8 Stability of Amide Bonds in Cell Culture Medium Containing 10% Fetal Bovine Serum (FBS)	51
5.2.9 Cytotoxicity of Conjugates	52
5.2.11 Flow Cytometry	53
5.2.12 Confocal Microscopy	54
5.3 Results	55
5.3.1 Synthesis and Characterization Studies	55
5.3.2 Amide bond Stability Studies	56
5.3.3 Cytotoxicity Studies	57
5.3.4 HIV-1 Replication Inhibition Studies	57
5.3.5 Flow Cytometry and Confocal Microscopy	59
5.4 DISCUSSION	61
6. FORMULATION, CHARACTERIZATION AND EVALUATION OF ALCOHOL-FREE COLORECAL FOAM-BASED MICROBICIDE DELIVERY VEHICLES AND INVESTIGATE THEIR PEFORMANCE IN MICE USING IMAGING TECHNIQUES	64
6.1 Introduction	64
6.2.1 Materials and Equipments	65
6.2.2 Preparation of Foam Concentrates	66
6.2.3 Preparation of FITC-PEG Loaded Foam Concentrate	66
6.2.4 Crimping / Gassing Process	67
6.2.5 Foam Appearance and Microscopic Analysis	67
6.2.6 Thermosensitivity Studies	67
6.2.7 Evaluation of Rheological Properties; Experimental Set-up	68
6.2.7.1 Amplitude and Frequency Sweep Tests	68
6.2.7.2 Yield Stress Studies	69
6.2.8 Loss on Drying	69
6.2.9 In vitro Release Studies	69
6.2.10 <i>In Vivo</i> Characterization of Foams using MRI	70
6.2.11 Fluorescence Imaging	70
6.2.12 Preliminary Toxicology Assessment	71
6.3 Results	72
6.3.1 Preparation of Xanthan Gum Foams	72
6.3.2 Foam Appearance	72
6.3.3 Foam Light Microscopy Analysis	73

6.3.4 Thermosensitivity Studies.....	73
6.3.5 Foam Rheology and Dynamic Measurements	73
6.3.6 Loss on Drying.....	74
6.3.7 <i>In vitro</i> Conjugate Release Study	75
6.3.8 <i>In Vivo</i> Characterization of Formulations using MRI.....	76
6.3.9 Colonic/Rectal Distribution of FITC-PEG _{3,4} -COOH-Loaded Foam Using a MS FX PRO System	77
6.3.10 Mouse Colorectal Irritation test	77
6.4 Discussion.....	78
7. SUMMARY AND CONCLUSION	83
LIST OF TABLES	
Table 1. Contribution of different HIV transmission routes to global HIV infections.....	86
Table 2. HIV protease inhibitors approved for clinical use	87
Table 3. FDA-approved PEGylated drugs	88
Table 4. PEGylated small molecular drugs conjugates in clinical trials.....	89
Table 5. Examples of commonly used CPPs and AMPs and their proposed mechanisms.....	90
Table 6. Anti-HIV-1 activity of APV-PEG conjugates in buffer using FRET assay	91
Table 7. Foam Concentrates with Different Xanthan Gum Concentrations	92
Table 8. Residue Levels for Different Formulations	93
LIST OF SCHEMES	
Scheme 1. Synthesis of PEG _x -APV-O-acetyl and PEG _x -APV-OH conjugates.....	94
Scheme 2. FRET-based protease activity inhibition assay in buffer	95
Scheme 3. Synthesis of Fluorescein-Labeled Amprenavir-PEG Conjugate (APF).....	96
Scheme 4. Structure of modified Bac7 CPP	97
Scheme 5. Synthesis of APV-PEG-Bac7 CPP (APB)	98
Scheme 6. Synthesis of fluorescein-labeled PEG-Bac7 CPP (BPF).....	99
LIST OF FIGURES	
Figure 1. HIV Infection and Gut Mucosal Immune Function	100
Figure 2. HIV Transmission Through Vaginal Mucosa	101
Figure 3. Pathways of HIV-1 passage between dendritic cells (DCs) and T cells	102
Figure 4. Molecular modeling of amprenavir interactions with HIV-1 protease	103
Figure 5. proposed mechanisms to explain cellular uptake of cell-penetrating peptides	104
Figure 6. Types of Aerosol Foams.....	105
Figure 7. MALDI-TOF-MS (<i>m/z</i>) profiles of purified PEG-APV conjugates.....	106
Figure 8. HPLC of PEG-APV conjugates.....	107

Figure 9. Cleavage kinetics of HIV-1 protease peptide substrate.....	108
Figure 10. Determination of anti-HIV-1 activity of APV (0 – 5 μ M).....	109
Figure 11. Plots of $\ln(F_{\infty} - F_t)$ vs. time for PEG-APV conjugates.....	110
Figure 12. Effect of PEG size on the HIV-1 protease inhibition potency of APV-PEG conjugates	111
Figure 13. FITC-PEG Standard Curve.....	112
Figure 14. MALDI-TOF-MS of FITC-Labeled PEG-APV	113
Figure 15. HPLC of Bac7 CPP	114
Figure 16. MALDI-TOF-MS of Bac7 CPP	115
Figure 17. MALDI-TOF-MS of APV-PEG-Bac7 CPP	116
Figure 18. MALDI-TOF-MS of FITC-Labeled PEG-Bac7 CPP.....	117
Figure 19. MTT Cytotoxicity Assay.....	118
Figure 20. Syncytia Formation in MT-2 T-Cells.....	119
Figure 21. Anti-HIV-1 Activity of APV and APV-PEG Conjugates.....	120
Figure 22. Quantitative Fluorescence-Activated Cell Sorting (FACTS) Assay.....	121
Figure 23. Confocal Microscopy	122
Figure 24. Macroscopic Foam Quality and stability at room temperature	123
Figure 25. Foam Light Microscopy Analysis	124
Figure 26. Foam Volume Stability (FVS) at Body Temperature.....	125
Figure 27. Foam Volume Stability (FVS) at Body Temperature (2).....	126
Figure 28. Determination of Linear Viscoelastic Region	127
Figure 29. Evaluation of the Elastic Modulus, G' , for the Formulations at 38 $^{\circ}$ C.....	128
Figure 30. Changes in Instantaneous Viscosity, η , with Increase in Shear Stress.....	129
Figure 31. Determination of Yield Stress Values	130
Figure 32. Loss on Drying	131
Figure 33. Kinetics of % Cumulative Release and the Release Rate of FITC-Labeled PEG	132
Figure 35. <i>In Vivo</i> Characterization of XG (1.5%) Foam in the Mice Rectum	134
Figure 36. <i>In Vivo</i> Characterization of Foam in the Mice Colon.....	135
Figure 37. Colorectal Distribution of FITC-PEG _{3.4kDa} -COOH Loaded XG Foam.....	136
Figure 38. Mice Colorectal Irritation Test at Day 1 Post Dose	137
Figure 39. Mice Colorectal Irritation Test after 5 Consecutive Days of Dose Application	138
Figure 40. Mucosal Pre-Exposure Prophylaxis (PrEP) Concept	139
APPENDIX.....	140

8. Formulation of Pharmaceutical Foams	140
9. Caco-2 Cell Culture for Prediction of Intestinal Absorption of Nanoparticles	151
REFERENCES	155

1. INTRODUCTION

According to UNAIDS report (2012) “an estimated 35.3 million people are globally living with HIV, 2.3 million people became newly infected with HIV, and 1.6 million people died from AIDS related illnesses.” Highly active antiretroviral therapy (HAART) is effective at suppressing HIV replication and restoring CD4⁺ T cell numbers in peripheral blood and has contributed to a significant decrease in morbidity and mortality of HIV-infected patients^{1, 2}. However, complete elimination of HIV from the body is almost impossible. Even when antiretroviral therapy (ART) limits HIV to undetectable levels in blood, the virus remains active in tissues³. Recent studies show that in patients with undetectable levels of HIV in the blood after a few months of ART, abundant amount of the virus was found in lymphatic cells³. One hypothesis is that fully suppressive concentrations of the antiretroviral drugs may not be uniformly achieved in the infected cells and the lymph nodes^{3, 4}

For almost thirty years, attempts have been made on producing a safe and effective preventative HIV vaccine⁵. Meantime, there is a growing interest in alternative HIV preventative strategies. Clinical trial data suggest that topical application of HIV drugs through the vaginal and rectal routes are superior over oral route in preventing sexual transmission of HIV-1 because much higher drug concentrations in vaginal and rectal tissues will be achieved with topical application⁶. Intestinal and genital tract transmission contributes the most to HIV cases worldwide (Table 1)^{7, 8}. In addition, host mucosa biology indicates that targeting HIV mucosal transmission is likely to be more

effective than targeting later stages of infection in suppressing the viral replication and preventing the viral spread within an infected individual ⁶. This is due to viral vulnerability and high efficacy of antiretrovirals at this earliest stage of HIV infection ⁶. Once locally expanded HIV spreads to draining lymph nodes to start systemic infection, complete viral inactivation and annihilation of infected cells (especially latently infected cells) is almost impossible. The gut associated lymphoid tissue (GALT) houses most of the body's lymphocytes, including activated memory CD4⁺ T cells that are preferential targets for HIV ⁹. HIV-1 commonly targets the lower gastrointestinal tract as an initial infection site following receptive anal intercourse, and as a secondary infection site following rapid dissemination from mucosal foci or acute systemic infection ¹⁰. Previous reports of the analysis of viral quasispecies during primary acute HIV infection revealed a homogeneous population of early founder viruses, with the majority of infections being initiated by a few transmitted viral variants ¹¹. HIV may cross the epithelium and initiate infection by transcytosis across intact epithelial cells or M cells, adhering to mucosal dendritic cells or direct passage through epithelial breaches thus, rapidly infect and deplete intestinal CD4⁺ T cells (Figure 1) ⁹. Thus, initiation of anti-HIV therapy at the mucosal site as pre-exposure prophylaxis (PrEP) has the potential to prevent or reduce HIV transmission.

In a large South African study reported in July 2010, the efficacy of tenofovir vaginal gel in preventing HIV transmission was investigated ¹². In that trial, known as CAPRISA 004, women were instructed to use the tenofovir gel before and after sex rather than every day. CAPRISA 004 found that the product reduced the risk of infection by 39%. In the high adherers, who reported using the gel more than 80% of the time that

they had sex, the efficacy went up to 54%. In another study, the acceptability of 1% tenofovir microbicide gel was investigated¹³. The participants liked features such as easy use of the gel and its protective effect against HIV. However, acceptability was significantly lower in those participants who reported 'messiness' as the most disliked feature.

In the pharmacy, foams represent new vehicles for drug delivery. Foams feature some application advantages compared to the standard vehicles such as suppositories, creams, gels and ointments. Foams are thermodynamically and mechanically unstable systems that offer both convenient application and one-step administration within one product¹⁴. Little leak of the vehicle takes place during application and it does not leave large amount of residues. Moreover, the residence time of the active pharmaceutical ingredients can be controlled through the use of bio-adhesive polymers. Therefore, foams may be preferable dosage forms for mucosal anti-HIV drug delivery.

For an effective HIV transmission inhibition, it is essential to maintain enough antiretroviral concentration in the area where the virus starts invasion. Current microbicides are small molecule drugs, capable of diffusing through mucosal epithelium to enter the cells of submucosa but easily and quickly being removed by blood circulation^{15, 16}. The proposed thesis herein focuses on investigating the feasibility of developing a non-releasable amprenavir-polyethylene glycol (APV-PEG) conjugated to a cell-penetrating peptide (Bac7 CPP). For colonic/rectal delivery of the anti-HIV-1 nanocarrier, alcohol-free thermosensitive foams are formulated which expand and produces full coverage inside the rectum and the descending colon cavity (Figure 40).

2. BACKGROUND AND SIGNIFICANCE

2.1 Human Immunodeficiency Virus

Human immunodeficiency virus (HIV) is a member of the genus Lentivirus, a member of the family of Retroviridae. Lentiviruses are transmitted as single-stranded, positive-sense, enveloped RNA viruses. HIV is a zoonosis in which efficient human-to-human spread takes over from zoonotic infections¹⁷. HIV attacks the immune system and leaves the body vulnerable to a variety of life-threatening infections and cancers. According to US Global Health Policy Fact Sheet (2012) there are approximately 34 million people globally living with HIV¹⁸ and nearly 30 million people have died of HIV related cause since the beginning of the epidemic. Therefore, HIV is one of the most studied viruses. AIDS (acquired immune deficiency syndrome) is the final stage of HIV disease, which causes severe damage to the immune system. AIDS is the sixth leading cause of death (in 2012) among people ages 25-44 in the United States, down from number one in 1995.

Other than attacking the immune system directly, HIV has the ability to integrate into the host genome and thus to maintain itself within the host cell while presenting no target for immune response¹⁷. Furthermore, HIV is a rapidly evolving virus. Based on homologies among genomic sequences of HIV viruses, it is possible to distinguish two HIV types: HIV-1 and HIV-2¹⁹. Both types are transmitted by sexual contact, through blood, and from mother to child. Worldwide, the predominant virus is HIV-1, and

generally when it is referred to HIV without specifying the type of virus it means HIV-1. There are three major groups of HIV-1: M (Major), O (Outlier) and N (non-M/non-O). Also, viruses within the same HIV-1 subtype may differ by up to 20%, and in places such as Africa, where there are multiple subtypes, the sequences of highly variable envelope proteins can differ up to 38%. HIV-2 is endemic in West Africa, but has spread to Europe (especially Portugal) and to India. Like HIV-1, HIV-2 can be subdivided into a number of major groups, which appear to represent separate zoonoses from a primate host.

2.1.1 HIV Mucosal Invasion and its Contribution to Global Infections

The fastest growing phase of HIV-1 pandemic is sexual transmission (UNAIDS 2009) and the vast majority of new HIV infections are acquired via the lower genital and rectal mucosa²⁰. Although advances in antiretroviral therapies and access to treatment has made HIV from a lethal to a chronic disease, prevention of sexual mucosal transmission, the principal route of acquisition, is clearly needed to contain the continuing growth of the pandemic and ultimately eradicate AIDS⁶. Contribution of mucosal HIV invasion sites to global HIV infections is summarized in Table 1. Targeting HIV mucosal transmission is likely to be more effective than targeting later stages of infection. This is due to viral vulnerability and high efficacy of antiretrovirals at this earliest stage of HIV infection⁶. The target CD4⁺ T-cells are scattered in the vaginal and GI submucosa and the innate immunity suppresses initial infection, resulting in a small founder population of infected cells. If the basic reproductive rate (R_0) of the founder cells drops below 1, the founder population of the infected cells shrinks, resulting in aborted infection. In addition, local expansion must produce critical mass of virus for dissemination to systemic secondary lymphatic tissues and systemic infection to occur.

These two viral vulnerabilities create two prevention opportunities. That is, early intervention can succeed by reducing R_0 to less than 1 and limiting the expansion level so the number of virus falls short of a critical threshold for systemic dissemination, not necessarily by completely inactivating virus and killing all infected cells. This window of opportunity lasts about a week from the time of sexual exposure to HIV ⁶. Once locally expanded HIV spreads to draining lymph nodes to start systemic infection, complete viral inactivation and annihilation of infected cells (especially latently infected cells) are required to eradicate infection, which is impossible at present. The concept of early prevention has been supported by studies in non-human primate models ^{21, 22, 23}. Microbicides that block binding and co-receptor-mediated entry and reverse transcription have been shown to protect against SHIV and SIV vaginal and rectal challenges in the rhesus macaque model ^{6, 22}. Inhibition of recruiting target cells necessary for local expansion using glycerol monolaurate prevented mucosal SIV transmission ²⁴, suggesting that limiting local expansion to below a critical threshold level alone can be effective in prevention.

2.1.2 Gut Mucosal Immune Function and HIV Infection

HIV-1 commonly targets the lower gastrointestinal tract as an initial infection site following receptive anal intercourse, and as a secondary infection site following rapid dissemination from mucosal foci or acute systemic infection ¹⁰. Gastrointestinal (GI) tract houses most of the body's lymphocytes, including activated memory CD4⁺ T cells that are preferential targets for HIV ⁹. HIV infected individuals have histological abnormalities of the GI mucosa, malabsorption, and lymphocyte depletion, generally known as "HIV enteropathy" ²⁵. The presence of physiologic baseline inflammation with

immune cell activation, and increased co-receptor expression on intestinal T cells and macrophages²⁶ make the GI tract a prime target for HIV infection. HIV may cross the epithelium and initiate infection by transcytosis across intact epithelial cells or M cells, adhering to mucosal dendritic cells or direct passage through epithelial breaches thus, rapidly infect and deplete intestinal CD4⁺ T cells (Figure 1). Also, in HIV infected patients tight junctions in the intestinal epithelium are compromised and the lamina propria gathers an influx of CD8⁺ T cells. Therefore, initiation of anti-HIV therapy during early HIV infection has the potential to revert or limit mucosal pathogenesis to some extent while preserving HIV-specific CD8⁺ T cell functions^{27,28}.

2.1.3 Female Genital Tract and HIV Infection

Women appear to be at higher risk for HIV infection than men, with an estimated 30% to 40% of annual worldwide infections occurring through HIV invasion of the female genital tract via exposure to virus-containing semen⁷. Intact multilayered squamous epithelium of the vaginal mucosa and ectocervix offers better mechanical protection against pathogen invasion than the single-layer columnar epithelium of the endocervix. Therefore, most genital HIV transmission in women likely happens through the endocervix. However, the surface area of the vaginal mucosa and ectocervix is approximately 15 times larger than that of the endocervix, providing more opportunities for HIV to encounter breaches in the epithelium through which it more easily penetrates the mucosa⁸. Cell-free and cell-associated HIV-1 penetrates the cervicovaginal epithelium through microabrasions and/or intact tissue (Figure 2). Within a few hours, the virus reaches Langerhans cells (LC) and intraepithelial CD4⁺ T lymphocytes within the epithelium or dendritic cells (DC) and resting CD4⁺ T cells in the lamina propria. CD4⁺ T

cells are activated by direct contact with antigen-presenting (AP) LC or DC, or indirectly through cytokine secretion by epithelial and other immune cells (Figure 3). This happens focally at the ports of entry. Pre-existing inflammation and chemokine-mediated recruitment of new cells expand the number of activated CD4⁺ T cells, which fuel the initial infection by a small number of founder viruses. Dissemination of infected T cells, DC, LC and AP cell complexes from the initial cervicovaginal infection foci to the draining lymph nodes or directly into systemic circulation leads to an established infection^{6, 29}. Therefore, microbicide formulations must deliver their active ingredient(s) to all these cells and places if they want to prevent the irrevocable step of systemic dissemination.

2.1.4 Antiretroviral Therapy and HIV Treatment

Combination antiretroviral therapy (cART) decreases the replication of HIV-1 and improves the survival of infected persons. In a collaboration of 12 prospective cohort studies from Europe and the United States (the HIV-CAUSAL Collaboration) that included 62760 HIV-infected patients, effect of cART was followed for an average of 3.3 years³⁰. According to the results of that study, it was estimated that initiation of cART reduced the overall incidence of mortality of HIV-infected individuals by 50%. The use of combination therapy against HIV eventually gave rise to highly active anti-retroviral therapy (HAART) which potentially controls HIV infection and prevents progression to AIDS¹. With this treatment, three or more drugs from at least two drug classes are used often in lower doses compare with monotherapy. HAART could involve more than 20 pills everyday at precise times however it is still the main approach to control of infection

in HIV-positive patients. Combination therapy is further simplified since some anti-HIV drugs are now available in combined forms.

2.1.5 Protease Inhibitors

Protease inhibitors (PIs) have been designed to bind the viral protease with high affinity but tend to occupy more space than the natural substrates. Thus, they are competitive inhibitors of HIV protease (PR). Currently, there are nine PIs approved for clinical use: saquinavir, ritonavir, indinavir, nelfinavir, fosamprenavir (a prodrug of amprenavir), lopinavir, atazanavir, tipranavir and darunavir (Table 2)^{31,32}. Most of them are prescribed with a concomitant low dose of ritonavir as boosting agent. All of them, with the exception of tipranavir, possess peptidomimetic structure containing a hydroxyethylene core, which prohibits cleavage of the protease inhibitor from the HIV-1 PR^{32, 33, 34, 35, 36, 37, 38, 39, 40}. Instead of a peptidomimetic hydroxyethylene core, tipranavir contains a dihydropyrone ring as a central scaffold. There are side effects related to current HIV PIs. It has been demonstrated *in vitro* that several PIs show decreased insulin-mediated glucose disposal through an acute blockade of glucose transporter-4 (GLUT4)^{41, 32}. In addition, new onset diabetes mellitus, exacerbation of pre-existing diabetes mellitus and increased risk for cardiovascular events has been reported in many HIV-infected patients receiving systemic protease inhibitor therapy. Other adverse events, such as increased nephrotoxicity, hyperbilirubinemia and elevation of liver enzymes may depend more on the enhanced bioavailability of specific boosted PIs^{42, 43, 44}. Ritonavir has been strongly associated with lipid abnormalities and gastrointestinal side effects⁴⁵.

2.1.6 Amprenavir and Fosamprenavir

Amprenavir (APV) is an HIV-1 protease inhibitor designed to be used in HIV-1 treatment regimen. APV is a small molecule drug (MW, 505.6) and passive diffusion is the mechanism of its absorption. APV has very low water solubility (< 5 mg/L, $\log P > 2$). It is also a substrate of P-glycoprotein (P-gp) and this transporter may play a role in APV absorption^{46, 47}. In caco-2 cell model, the ratio (B \rightarrow A / A \rightarrow B) for APV was 2.8 in the absence of a potent P-gp inhibitor (elacridar) and 1.0 in its presence; (B \rightarrow A) is the apparent permeability from the basolateral to the apical side of the cell membrane and (A \rightarrow B) is the apparent permeability from the apical to the basolateral side of the cell membrane. Also, administration of ¹⁴C-amprenavir to multidrug resistance (MDR) *1a/1b* genetic double knockout mice showed higher concentration of radioactivity in blood (1.3 to 2.0 fold) and tissues including brain (13.2 to 27 fold), muscle (1.5 to 2.1 fold) and CSF (3.3 fold) compared with control mice⁴⁶⁻⁴⁷. APV has also demonstrated induction of P-gp in a human intestinal cell line⁴⁸. The principal route of APV elimination is hepatic metabolism by cytochrome P450 (CYP) 3A4⁴⁹. There are two major metabolites for APV. The predominant APV metabolite, GW549445X (42% of administered dose), results from the di-oxidation of the tetrahydrofuran portion of the molecule. The next most prevalent metabolite, GW549444X (22% of administered dose), results from the di-oxidation of the tetrahydrofuran portion of the molecule with additional oxidation of the aniline portion of the molecule. Glucuronides of the oxidative metabolites have also been identified.

Fosamprenavir, the phosphate ester prodrug of amprenavir, was designed to replace the large pill burden and undesirable excipients of the amprenavir soft gelatin

capsule formulation (Agenerase[®])^{42, 47}. Approximately 10-fold increased aqueous solubility was observed with fosamprenavir compare with amprenavir. Fosamprenavir is converted almost entirely (99%) to amprenavir by alkaline phosphatase at or near the intestinal epithelium^{50, 51} reaching all the disadvantages related to APV.

2.1.7 HIV Vaccine Development

In order for a vaccine to be active, the immune response that it stimulates must provide protection against infection. The HIV Vaccine Trials Network (HVTN) records 13 completed and 15 current trials¹⁷. Unfortunately, the number of experimental HIV vaccines that have failed to deliver protective immunity continues to rise. After so many disappointments, a vaccine appeared still to be a long way off. In September 2009, the RV144 trial of two anti-HIV vaccine candidates that had not produced a protective response individually showed promise with a combined approach. The trial was sponsored by the US and Thai governments and involved over 16000 individuals^{17, 52}. Vaccine recipients were treated with an ALVAC live recombinant virus expressing 3 HIV proteins followed by a multivalent formulation containing the subtype B and E of the viral gp120 glycoprotein with an aluminum adjuvant. The combined treatment was intended to include both cell-mediated and serological immunity⁵³. The result represented a 31.2% decrease in infections, the first time a candidate HIV vaccine has produced a significant benefit⁵². Nevertheless, a treatment that leaves the recipients with the two-thirds of the usual chance of becoming infected is still far from ideal.

2.1.8 Preventing Mucosal HIV Transmission with Topical Microbicides

In spite of considerable advances in prevention and treatment of HIV infection in the United States, the rate of new infections has remained stable⁵⁴. Only five of 37

randomized controlled trials, which tested 39 HIV prevention strategies, have demonstrated protection against sexual transmission of HIV infection ⁵⁵. Hence, HIV prevention technologies that can be used conveniently remain a pressing priority. Although earlier prevention interventions mainly were behavioral, recent data demonstrate the strong impact of antiretroviral therapy (ART) on sexual HIV transmission. The most effective strategy to prevent the spread of HIV will probably be a combination of behavioral, biological and pharmacological interventions ⁵⁶. In a study involving 1763 serodiscordant couples (when one partner is HIV positive and the other is HIV negative) in which HIV-1 infected participants had a CD4 count of 350 to 550 cells per cubic millimeter, there was a relative reduction of 89% in the total number of HIV-1 transmissions resulting from the early initiation of antiretroviral therapy, regardless of viral linkage with the infected partner ⁵⁶. The sustained suppression of HIV-1 in genital secretions resulting from antiretroviral therapy was the most likely mechanism for the prevention of HIV-1 transmission ^{56, 57, 58}.

Microbicides are products that can be applied to the vagina or rectum to reduce the acquisition of sexually transmitted infections (STIs) including HIV. An effective microbicide has the potential to alter the progression of the global HIV pandemic ^{12, 59}. In the CAPRISA 004 trial, effectiveness and safety of a 1% vaginal gel formulation of tenofovir, a nucleoside reverse transcriptase (NRT) inhibitor, was assessed for prevention of HIV acquisition in women ¹². In a double-blind, randomized controlled trial tenofovir gel (n=445) was compared with placebo gel (n=444) in sexually active, HIV-uninfected 18-40 year-old women in South Africa for 30 months. In high adherers (gel adherence >80%), HIV incidence was 54% lower (p=0.025) in the tenofovir gel group. In

intermediate adherers (gel adherence 50-80%) and low adherers (gel adherence < 50%) the HIV incidence reduction was 38% and 28% respectively. These results suggest that antiretroviral microbicides could potentially fill an important HIV prevention gap, especially for women unable to successfully negotiate mutual monogamy or condom use.

2.2 Poly(ethylene glycol) and PEGylation

Poly(ethylene glycol), PEG, is a synthetic polymer comprised of repeating ethylene oxide subunits (MW, 44). Being nontoxic, non-immunogenic, non-antigenic and amphiphilic, PEG has been approved by FDA for human oral, intravenous, and topical applications^{60, 61}. Because of these favorable properties, PEG as modifying polymer now plays an important role in drug delivery, a strategy termed “PEGylation”. PEGylation is generally described as the modification of proteins, peptides or small organic molecules by covalent binding with one or more PEG chains with different molecular weights. It has been over thirty years since Davis and Abuchowsky first reported PEG coupling to bovine serum albumin^{62, 63} and thereafter, PEGylation has become a well-established technology in the field of biopharmaceutical formulation and it is used to ameliorate the stability, solubility, bioavailability, and immunological properties of bioactive compounds. PEGylation of liposome surface was able to dramatically improve stability and circulation time of liposomes after intravenous administration. This kind of liposome was then named “Stealth” because of its ability to evade interception by the immune system and reticuloendothelial system (RES), likewise the stealth bomber is able to evade radar^{64, 65}.

In vivo, PEG chains shorter than 400 Da are transformed to toxic metabolites by alcohol dehydrogenase, whereas longer PEG chains (> 1000 Da) are not subjected to

enzymatic degradation, but are eliminated through a mechanism which is dependent to its molecular mass ⁶⁶. Antibodies to PEG have been generated only when the PEG is attached to a highly immunogenic molecule under an immunization protocol with Freund's adjuvant ^{67, 68, 69}.

2.2.1 PEGylation of Proteins and Polypeptides

So far, the most successful approach to solve the intrinsic shortcomings of several proteins and polypeptides (i.e., immunogenicity, short half life, enzymatic degradation) has been the PEGylation ^{70, 71}. PEGylation can shield antigenic epitopes of the polypeptide, thus reducing RES clearance and recognition by the immune system. PEGylation also reduces degradation by proteolytic enzymes and increases the apparent size of the polypeptide, thus reducing renal filtration and altering biodistribution. Contributing factors that affect the abovementioned properties are: (1) the number of PEG chains attached to the polypeptide, (2) the molecular weight and structure of PEG chains attached to the polypeptide, (3) the location of the PEG sites on the polypeptide and (4) the chemistry used to attach the PEG to the polypeptide ⁷². At present, most of the PEGylated proteins commercially available have been produced by random PEGylation although the reproducibility of the reaction needs to be FDA proved for these mixtures (Table 2) ^{72,73}. Recently, new strategies have been developed to avoid the formation of heterogeneous mixture of PEG isomers by shifting from random to site-specific PEGylation reactions which may lead to a better preservation of the native protein activity in the conjugate.

Some researchers proposed degradable linkages in the attempt to maintain minimal loss of activity ^{74, 75, 76}. Degradable linkages are designed to break and release

the active native conjugated drug or protein from the conjugate through enzymatic degradation, hydrolytic cleavage or reduction. The degradable linkage could be ester bonds in which the releasing rate can be tuned by changing the neighboring chemical groups. Compounds PEGylated with degradable linkages generally show higher *in vitro* biological activity, but shorter circulation half-life compared to stable PEG-protein conjugates. Two examples of releasable and non-releasable PEGylated drugs are PegIntron[®] which releases the native protein from the releasable urethane bond, and Pegasys[®] which is a stable PEG-IFN derivative and has been synthesized via a stable amide bond. Although PegIntron owns a better specific activity than Pegasys (28% vs. 7%, respectively), its half-life is 50% shorter compare to Pegasys⁷⁷.

2.2.2 PEGylation of Small Molecular agents

Small molecular drugs, especially the antitumor agents, often suffer some problems such as low solubility, high toxicity, rapid excretion or untargeted biodistribution^{78, 79}. One promising approach to overcome these obstacles is to use PEGylation strategy. Although no approved product has yet reached the market, four PEGylated small organic drugs are currently undergoing clinical trials (Table 3)⁶⁰. NKTR-118 (PEG-naloxol), an orally administered PEGylated naloxol (an opioid antagonist), is the only small molecule drug PEGylated with a small linear PEG now under phase III clinical trials for the treatment of debilitating conditions such as opioid-induced bowel dysfunction (OBD) and opioid-induced constipation (OIC), both of which can occur during opioid pain management⁷⁸⁻⁷⁹. NKTR-102 (PEG-irinotecan), a PEGylated form of the topoisomerase I inhibitor irinotecan, is now under phase III/II clinical trials for the treatment of solid tumors⁷⁹⁻⁸⁰. EZN-2208 (PEG-SN38) is being

developed by Enzon Pharmaceuticals under phase II for the treatment of advanced colorectal cancer. Its prodrug, pegamotecan (PEG-camptothecin), was dropped by Enzon during phase II b trials in 2005 due to a lack of efficacy⁷⁹. NKTR-105 (PEG-docetaxel) is a conjugate of PEGylated docetaxel that is now under phase I clinical trials for the treatment of solid tumors⁸¹.

Compared to biological macromolecules, small organic molecules present fewer problems in the chemistry of PEGylation since they have fewer functional groups, lower conformational constraints, and easier purification and characterization steps^{79, 82}. PEG can be linked to small active agents via releasable or permanent bonds. Permanent PEG links create novel compounds for increasing oral bioavailability and decreasing penetration of specific barriers, such as NKTR-118 (permanent PEGylation of naloxol). In case of permanent PEGylation, PEGs may block activity of small active agents at the target cells via steric hindrance. Therefore the size of PEG to be chosen is important. For releasable PEG attachments, which result in forming prodrugs, the conjugate must be chemically or enzymatically transformed into their active form after administration. In this type of PEGylation, large molecular weight PEGs can be used to increase the circulating half-life, modify biodistribution and enhance water solubility. With releasable PEG systems, too rapid breakdown of the conjugate can lead to spiking of the parent drug and possible toxicity, while too slow a release rate will attenuate the drug efficacy.

2.2.3 Different Configurations of PEGylation of Small Molecule Drugs

In PEGylation, linear PEGs are the simplest and most often used conjugate agents. Active small molecules are conjugated to the distal ends of a PEG carrier and the simple PEG carrier could substantially enhance the properties of the drugs^{62, 75}. The most

obvious effect of PEGylation in this system is to increase solubility or sustained release of parent drug, which in turn increases cellular drug availability, decreases toxicity and enhances specific activity^{79, 83}. Since linear PEG has only two sites available for the conjugation, only one or two drug molecules may be conjugated, which limits the loading capacity. In addition, the comparatively large molecular weight PEG conjugation may impede the release of the small molecular weight drugs, so that they do not reach therapeutic concentrations at the target sites.

Branched PEG (PEG2) has an umbrella like structure, linking two linear mPEGs to active groups of amino acids (e.g. glutamate, lysine). These structures give better protection than linear PEG toward approaching proteolytic enzymes, antibodies, etc. However, this technology is preferred in protein PEGylation, but is not applied as frequently with small molecules^{70, 84}.

Forked PEG provides multi-proximal reactive groups at the end of one or both ends of a linear PEG chain. This structure effectively increases the drug load of the PEG by increasing active sites, but some investigators point out that the maximum number of active ingredients that can be conjugated to the dendritic termini is limited mainly by the solubility of components⁸⁵.

A multi-armed PEG is a star-like structure carrying same functional groups. This structure can be used in conjugation of small molecules. NKTR-102 (PEG-irinotecan), EZN-2208 (PEG-SN38), and NKTR-105 (PEG-docetaxel) are examples of this type of PEGylation (Table 4)⁶⁰.

2.2.4 Targeted Delivery of PEGylated Small Molecule Drugs

Conjugating large size PEGs to small molecule drugs via releasable bonds can significantly prolong the circulation time of low molecular weight therapeutic agents because the macromolecules barely permeate the endothelium of normal blood vessels. Thus, macromolecular prodrugs are more likely to be retained in tumors or other pathological tissues with disorganized vasculature⁸⁶, exhibiting enhanced permeability and retention (EPR). This is an example of passive targeting of PEGylated small drugs. In a few studies, biodistribution of a series of PEGylated doxorubicin (PEG-Dox) was evaluated in mice, with results showing that PEG-Dox conjugates had higher doxorubicin concentrations than free doxorubicin in tumor tissues. Also, doxorubicin had low concentrations in other organs such as heart tissues^{86, 87, 88}. Heart toxicity is one of the severe therapeutic limitations of free doxorubicin.

This form of passive targeting still suffers several limitations, including variable vascular hyperpermeability for different tumor tissues and low cellular uptake for macromolecular prodrugs^{60, 89}. To overcome the drawbacks and enhance the therapeutic index, one proposed model consists of a water-soluble PEG, a drug that is conjugated to the PEG backbone via a biodegradable or a stable bond and an active targeting moiety. Because pathogenic cells tend to over-express specific antigens, receptors, or transporters, various targeting moieties can be used in this model such as antibodies, antibody fragments, peptides, aptamers, and small molecule ligands^{86, 88-89}.

2.2.5 PEGylated Anti-Viral Drugs

Saquinavir (SQV), the first HIV-1 protease inhibitor approved by FDA, suffers from several problems such as low oral bioavailability in clinical formulations, cellular

uptake and retention, metabolism, stability, and poor solubility. Gunaseelan et al.⁹⁰ prepared various PEG-based prodrug conjugates of the SQV that were all inactive *in vitro* until the ester bond was cleaved and active SQV was released. They evaluated anti-HIV-1 activity of the conjugates in MT-2 cells infected with HIV-1 strain LAV/LAI (MOI of 0.01) and monitored the release of active drug from the conjugates. The activity of SQV-PEG₃₄₀₀ was reduced after PEGylation (EC_{50} , 900 nM vs. 15 nM for the free drug), but restored when the PEGylated SQV was conjugated to biotin (EC_{50} , 125 nM), or retro-inverso Tat cell penetrating peptide (EC_{50} , 15 nM). The cytotoxicity (LD_{50}) of all prodrugs was in the micromolar range⁹⁰ which suggested a favorable therapeutic index.

Zidovudine (AZT), the first anti-HIV reverse transcriptase inhibitor, is an important component in HAART. However, the effectiveness of its therapy suffers from several clinical limitations, especially its short terminal half-life (1.2 h) and significant dose-related toxicity. Li et al.^{91, 92} designed and synthesized a mPEG₂₀₀₀-AZT prodrug conjugate and they evaluated the pharmacokinetic properties by oral administration of the conjugate in mice. Compared to free AZT, the absorption half-life ($t_{1/2ka}$) and elimination half life ($t_{1/2kb}$) of AZT released from the conjugate were increased to 0.51 ± 0.03 h and 2.94 ± 0.24 h, respectively. The *in vitro* anti-HIV activity assay showed that the conjugate exhibited good inhibition of HIV-1, with an EC_{50} value of $0.0634 \mu\text{M}$, but lower than that of free AZT.

Acyclovir, a synthetic purine nucleoside analog derived from guanine, is mainly used for the treatment of herpes zoster virus infections. To avoid its poor solubility in water and increased chemical stability, Zacchigna et al. prepared two acyclovir prodrugs⁹³. They coupled activated PEG with either acyclovir or valacyclovir (esterified prodrug

of acyclovir). *In vitro* drug release studies demonstrated that the conjugates were both stable in buffer solutions at pH 7.4 and 5.5. However, only PEG-valacyclovir₂ was stable at pH 1.2.

2.3 Peptides with Cell-Penetrating Properties

The recent discoveries of new potent therapeutic molecules which do not reach the clinic due to poor delivery and low bioavailability have made scientists look for new effective ways of drug delivery in therapeutic development. One of the technologies to improve plasma membrane restrictions is to design peptide-based transport systems⁹⁴. In this context, cell-penetrating peptides (CPPs) have come into focus and their efficiency has been demonstrated in many different applications. More recently, also some antimicrobial peptides (AMPs) with cell-penetrating properties have been used as efficient vectors for intracellular translocation of various active molecules. These peptides represent a new and innovative concept to bypass the problem of bioavailability of drugs and were first discovered based on the potency of several proteins to enter cells. Two CPP strategies have been described to date⁹⁵; the first one requires chemical linkage between the drug and the carrier for cellular drug internalization, and the second is based on the formation of stable complexes with drugs, depending on their chemical nature. Nowadays, peptides with cell-penetrating properties constitute very promising tools for non-invasive cellular delivery of cargo and have been successfully applied for *in vitro* and *in vivo* cellular import of therapeutic molecules such as small chemical molecules, nucleic acids, proteins, peptides and liposomes. The ability of CPPs to enhance the absorption of drugs through intestinal epithelium has also been studied for a few number of drugs which their oral delivery is a major barrier⁹⁶.

2.3.1 Cell-Penetrating Peptides

Cell-penetrating peptides (CPPs) have been successfully used since their discovery 20 years ago. CPPs are a family of peptides that are structurally diverse but share the ability to translocate a wide range of different bioactive molecules into living cells⁹⁷. Tat and penetretin (pAntp) were the first intracellular proteins discovered with the ability to pass the cell membrane. Since then, many other proteins that contain peptide domains responsible for membrane-translocating properties have been identified (Table 5)⁹⁴. Their amino acid compositions confer various structural properties, including amphipathicity, cationic charge, shape and size, interaction with the microbial surface, insertion into the lipid bilayer and induction of membrane lesions. The number of CPPs developed so far is growing, all of them being derived from different sources that can be divided into natural, synthetic or chimeric. The mechanism of cellular uptake of CPPs is still not completely understood and is controversially discussed. Several different models have been proposed to depict the consequences of this mode-of-action, including the ‘barrel-stave’ and ‘toroidal-pore’ mechanisms, the formation of ‘aggregate channels’ and the detergent-like ‘carpet’ effect^{98,99} (Figure 5).

Furthermore, CPPs are mostly low in toxicity. A wide range of different applications for translocation of macromolecules by CPPs into living cells has been described including transport of proteins, oligonucleotides, quantum dots, polysaccharides, nanoparticles, chemotherapeutics, polymers, and liposomes. Raagel et al.¹⁰⁰ studied recycling pathway in trafficking of 3 different CPPs (transportan, oligoarginine and Tat) complexed to avidin-TexasRed in Cos-7 cells in relation to trans-Golgi network and they reported the marginal role of Golgi network for CPP intracellular

trafficking. Dubikovskaya et al.¹⁰¹ showed that conjugation of an octaarginine peptide transporter through a releasable linker to a model small-molecule chemotherapeutic agent (Taxol) could produce conjugates with significantly improved activity against malignant cells that were resistant to the therapeutic agent alone. They further show that this approach was effective in animal models of ovarian cancer.

In another study, when methotrexate (MTX) was conjugated to CPPs, YTA2 and YTA4, the peptide–MTX conjugates were shown to overcome MTX resistance and kill the cells more efficiently than MTX alone¹⁰².

2.3.2 Antimicrobial Peptides with Cell-Penetrating Characteristics

Antimicrobial peptides (AMPs) are a diverse group of innate immune effector molecules utilized by multicellular organisms to prevent or combat microbial infections. Several categories of AMPs have been described based on common structural features or conserved sequence motifs¹⁰³. AMPs typically interact directly with and rapidly permeabilize microbial membranes and, in fact, they act via lytic mechanisms (Table 5). ‘Lytic’ AMPs generally have broad spectrum activity covering both Gram-positive and Gram-negative bacteria as well as fungi, while their selectivity for microbial with respect to host cells is proposed to derive from distinctive features of microbial membranes¹⁰⁴. Some AMP classes, particularly the proline-rich antimicrobial peptides do not conform to this predominant lytic mode of action. Proline-rich AMPs are a group of peptides of widespread natural origin, whose quite diverse sequences show some common characteristics: (1) the unusually high content of proline residues, (2) a net cationic charge mainly due to the presence of arginine residues, and (3) they act without extensive membrane damage, mostly targeting Gram-negative bacteria^{104, 105, 106}. Differences in

structure and primary sequence of proline-rich AMPs¹⁰³ suggest that the different families are the product of convergent evolution, although they are all characterized by a high content of proline (typically from 25 to 50%), as well as of arginine, often arranged in short recurrent motifs. In most cases, proline-rich peptides display low cytotoxicity and a cell-penetrating efficiency similar to that of TAT-derived peptides, although they are less hydrophilic¹⁰⁷.

Most of what is known about the mechanism of action of proline-rich AMPs comes from studies on the insect peptides pyrrhocoricin, apidaecin and drososcin, and from the mammalian cathelicidins Bac7, Bac5 and PR-39. From these studies it is evident that the antimicrobially active domains generally correspond with specific segments of the peptides. The three cathelicidin-derived peptides Bac5, Bac7 and PR-39 can be shortened from the C-terminus until a length of 15–16 residues or less, while maintaining a substantial antimicrobial activity^{108, 109, 110}. Shortening from the N-terminus, the most cationic region in all three peptides, will damage activity, and fragments comprising the central or C-terminal regions such as Bac7(29-56), Bac5(19-43) and PR-39(11-26) are poorly active or inactive as a matter of antimicrobial effects, despite having a considerable transmembrane activity. Therefore, one of the potential applications of proline-rich AMPs is their use as cell-penetrating peptides (CPPs) for the intracellular delivery of impermeant drugs into both bacteria and eukaryotic cells. In one study, fluorescently labeled Bac7 (fragment 1-35) was rapidly detected in the cytoplasm of exposed Gram-negative bacteria using flow cytometry or confocal microscopy¹¹¹, indicating that it can efficiently internalize small molecules such as the fluorophores BODIPY or fluorescein. More recently, a functionalized derivative of Pt(II)

coproporphyrin I (PEPP0) was conjugated to the 15–24 fragment of Bac7 to make an oxygen-sensitive phosphorescent probe for intracellular use¹⁰⁷.

2.3.3 Bactenecin 7 as a Potent and Effective Cell-Penetrating Peptide

The antimicrobial peptide bactenecin 7 (Bac7) is produced by ribosomes in granulocytes and is active against Gram-negative bacteria. This polypeptide is 59 amino acids in length and possesses repeated sequences which form regions with both antimicrobial and cell-penetrating properties¹¹². Sadler et al. showed that similar to Tat (fragment 49-57), bactenecin 7 (fragment 1-24) enters the RAW 264.7 murine monocytes however unlike Tat, it dispersed throughout intracellular space and not to the nucleus and endosomes¹¹³. They also showed that in the sequence, a short 10 amino acid residue fragment (15–24) harbors a cell-penetrating ability in the absence of antimicrobial ability, and does not influence the function of mammalian cells (e.g. DNA synthesis), which was observed for the (1–35) fragment¹¹³⁻¹¹⁴. The short (15–24) fragment (hitherto Bac7 CPP) contains five prolines (50% of the 10 residues) and, when carrying a small cargo (e.g. FITC) or even a large cargo (60-kDa NeutrAvidin), is able to penetrate mammalian cells.

2.4 Mucosal Drug Delivery

Mucosal delivery can be defined as the application of a drug containing formulation to the mucus membrane to directly treat mucosal disorders (e.g. vaginal infections) or the mucosal manifestations of a general disease (e.g. ulcerative colitis). Mucosal drug delivery also contains the pharmacological or other effect of the drug to the surface of or within the mucus¹¹⁵. Mucosal drug delivery is a multistep process which comprises (a) targeting of the delivery system at a specific region or cell type in a mucosa, (b) retention of that delivery system where it is anchored, (c) drug release from

the delivery system, and (*d*) access of the drug to the epithelial cells ¹¹⁵. Examples of commonly used vehicles for mucosal drug delivery are: lotions, gels, ointments, suppositories, enemas, vaginal tablets, aerosols and foams.

2.4.1 Advantages of Mucosal Drug Delivery

Some advantages of drug delivery directly to mucosal membranes are: avoiding first pass metabolism, avoiding the risks and inconveniences of intravenous therapy and of the variable conditions of absorption (pH changes, presence of enzymes, gastric emptying time etc.), achieving efficacy with lower total daily dosage of drug by continuous drug input, avoiding fluctuation in drug levels inter- and intra-patients, possibility to easily terminate the medications when needed, ability to deliver drug more selectively to a specific site, avoiding GI incompatibility, providing safer way of utilization of drugs with short biological half-life and narrow therapeutic window, and finally, suitability for self-medication ^{116, 117, 118}.

2.4.2 Drug Delivery in the Lower Gastrointestinal Tract

The colon is part of the gastrointestinal (GI) tract and may be affected by specific diseases. Treatment of such diseases preferably involves the local administration of drugs to the colon. The type of delivery system for administration of drugs to the colon is thus important for the treatment of colonic disease, whether for local treatment alone, or for a combination of local and systemic treatment ¹¹⁹. Rectal delivery vehicles offer the advantage of delivering high local concentrations of active medication to the site with minimum systemic side effects. Examples of methods of rectal administration are suppositories, liquid enemas and foams.

Rectal drug administration can be directed to both local and systemic drug delivery. Peptides and proteins are large molecules, which usually poorly absorbed in the upper GI tract. These molecules are degraded by luminal and brush border peptidases in the upper GI tract and generally have very short half-lives with low and variable bioavailability. Woodley *et al.* have shown that there is much lower peptidase activity in the colon relative to the upper intestinal tract ¹²⁰. Moore and Yoshikawa studied the absorption of series of peptide and proteins and they have concluded that these molecules may be regionally absorbed in the colon ¹²¹.

2.4.3 Vaginal Drug Delivery

Vaginal drug delivery systems (VDDS) are comfortable and convenient to administer for local targeted treatment of female genital diseases ¹²². VDDS could preferentially deliver high levels of medication directly to the uterine circulation (first uterine-pass effect), thereby providing high levels of drug to the endometrial tissue ^{123, 124} and causing much greater regional effects ¹²⁵.

2.4.4 Foams for Pharmaceutical Applications

According to European Pharmacopoeia, foams are formulations consisting of a large amount of gas dispersed in a liquid phase. The US Pharmacopoeia lists “foam aerosols” as a sub-part of the aerosol section. Many therapeutically active ingredients have been administered to the body by aerosol dosage forms. Commonly, foam is defined as a dispersion of gas in a liquid or a solid, where the volume fraction of gas is usually between 0.5 and 0.9. The bubble size in foams is mostly between 0.1 and 3 mm ¹⁴.

Foams are colloids composed of two or three distinct phases: a hydrophilic liquid continuous phase with a foaming agent, throughout which a gaseous dispersion phase

(which is called propellant) is distributed. There may be a third hydrophobic dispersed phase (Figure 6). Pure liquids will not foam, therefore foaming and bodying agents are used to generate and stabilize foams^{14, 126}. A propellant is defined as an essentially non-toxic material capable of producing pressure in a sealed container at ambient temperatures. When the nozzle of the spray head is opened so that there is a connection with the external air; the fluid phase will be pressed out of the aerosol canister. At atmospheric pressure the dissolved propellant immediately evaporates, generating the foam. The two basic classes of aerosol propellant include the compressed gas propellants (carbon dioxide, nitrous oxide, and nitrogen) and the liquefied gas propellants (hydrocarbons, fluorocarbons, and ethers)¹⁴. The concentration of propellant in the aerosol canister is usually between 3% and 12% w/w¹²⁷.

2.4.5 Foam Quality and Breakability

One way to study foam stability is to measure the initial foam volume and compare it with the subsequent volumes measured as the foam ages. A cylinder method can be used as an easy method for routine evaluations^{14, 128, 129}. Another important foam quality, which has a high significance, is the foam breakability. According to this property, foams can be classified into several categories:

- 'Quick breaking' foams are thermally unstable and collapse upon exposure to body temperature. Hydro-ethanolic foams are typically thermally unstable but their application to mucus membranes as well as large areas is not recommended.
- 'Lathers' are soapy foams that remain stable as they are formed or increase in volume when rubbed (like shaving foam).

- 'Breakable' foams are stable at body temperature, but collapse and spread easily upon application of mild shear forces. The thermal stability of the 'breakable' foams together with their fast collapse and high spreading properties make them ideal for use in dermatological and mucosal tissue application.

2.4.6 Application of Foams for Rectal and Vaginal Drug Delivery

Rectal drug delivery has been effectively used to treat anorectal diseases as well as an alternative for oral administration. Current formulations for rectal administration (suppositories, creams, ointments, liquid enemas) still have significant disadvantages¹³⁰. They are difficult to insert through anorectal orifice, they are difficult to spread through the cavity and if spreadable, they tend to leak, causing a lot of discomfort to the patients. Conventional dosage forms for vaginal drug delivery include lotion, gels, suppository, tablets, pessaries and creams. The efficacy of all of these dosage forms is greatly decreased by the fact that the drug cannot fully spread in rectum or vagina and contact the disease sites, which located in rectal or vaginal mucous membrane folds tightly. Induction of irritation by higher local drug concentration or by insoluble ingredients is another deficiency. In addition, these conventional dosage forms are susceptible to be removed by the self-cleansing action of the vaginal tract^{131, 132}. It is reported that patients are generally tolerate gels better than other dosage forms¹³³; however, an obvious shortcoming with classic gels is that they are very difficult to spread uniformly in vaginal and rectal canal because of their higher viscoelasticity¹³⁴.

Aerosol foams have some distinct advantages for colorectal and vaginal drug delivery including greater degree of spread, ease of application, enhanced topical drug delivery efficiency and comfortable feeling^{14, 122}. In addition, the potential of

contaminating the unused portion of the medication is minimized as the foam is often administered from a sealed airtight container. As a result of their benefits, patient compliance is greatly improved with foams¹⁴.

2.4.7 Pharmaceutical Foams for Nanoparticles Delivery to Mucosal Membranes

Nanoparticles have already been confirmed to be appropriate as carriers for mucosal delivery. Zhou and Neutra tried ferritine antigen by rectal route and concluded that rectal administration effectively induced mucosal immunity¹³⁵. Another study by Watarai carried out using gangliosides GMI encapsulated liposomal vaccine in mice, reported higher IgA antibody titer¹³⁶. Despite the proposed benefits of topical nanoparticles, very few therapeutic agents are presented in this form in commercial products. The reason behind it is that therapeutic agents that have sufficient affinity to the carrier to allow efficient loading and safe storage do not have a high tendency to be released at the biological membrane¹³⁷.

Recent studies suggest that dynamic foams have the potential to break down the nanoparticles loaded within them, improve drug release from nanoparticles, and enhance topical efficacy^{138, 139}. Upon valve actuation, the propellant evaporates rapidly, leaving nonvolatile excipients in the foam residue. Through the manipulation of the excipients, drug release from nanoparticles can be improved and the drug thermodynamic activity in the residual foam vehicle can be enhanced. Because of the dynamic nature of foams, the use of these topical vehicles may be a promising approach to enhance drug release from nanoparticles and thus solve the dilemma of the topical nanoparticle delivery.

3. SPECIFIC AIMS

Intestinal and genital tract transmission contributes the most to HIV cases worldwide. Therefore, early prevention of viral dissemination by local anti-HIV administration may be beneficial in inhibition of viral establishment. The objective of the proposed research is to develop nanocarrier (NC)-based mucosal pre-exposure prophylaxis (PrEP) therapy that blocks in a sustained manner the transmission of HIV in the distal colon and rectum. The developed NCs are prepared with noncleavable bonds and the drug activity will maintain while still connected to the NC. Breakable pharmaceutical foams providing superior colorectal mucosal surface coverage with minimum anal leakage are developed. Once the foam containing anti-retroviral NCs breaks and concentrates on the colorectal mucosa, the NCs displaying cell-penetrating peptides (CPPs) will be taken up into the mucosa. The proposed approach could potentially minimize administration frequency and systemic exposure.

As an anti-HIV-1 model, amprenavir (APV) was used. The small drug molecule contains two reactive sites for chemical modifications; a hydroxyl group which is in the pharmacophore and is necessary for APV protease inhibition and, an amino group which is away from the pharmacophore and can be reacted with a linear PEG chain.

Accordingly, the specific aims of this dissertation are:

1. To design, synthesize and characterize differently sized, non-releasable amprenavir-polyethylene glycol (APV-PEG) conjugates and evaluate their potency in HIV-1 protease inhibition.

Hypothesis: The NCs maintain drug activity while APV still connected to the PEG. This would allow using the NCs' favorable biopharmaceutical properties to avoid cellular efflux or metabolism of the drug thus prolonging its cellular persistence.

2. To design, synthesize and characterize a PEGylated APV that is further conjugated to Bac7 CPP and evaluate the activity of the conjugate in HIV-1 replication inhibition.

Hypothesis: PEGylation of APV will limit the plasma membrane permeability of the conjugate therefore; *in vitro* activity in the presence of T-cells will be lost. Further conjugation of Bac7 CPP will restore the drug's anti-HIV-1 activity.

3. To formulate, characterize and evaluate alcohol-free colonic/rectal vehicles and investigate their performance in mice using imaging techniques.

Hypothesis: The temperature sensitive colonic/rectal foam will be condensed at, and thoroughly cover, the inner wall of the rectum and the descending colon with no significant leakage and irritability. The foam then breaks into a thin gel layer on the mucosal surface depositing the nanoparticles in a sustained manner.

4. DESIGN, SYNTHESIS AND HIV-1 PROTEASE INHIBITION OF DIFFERENTLY SIZED, NON-RELEASABLE AMPRENAVIR- POLYETHYLENE GLYCOL CONJUGATES

4.1 Introduction

Human immunodeficiency virus (HIV) attacks the immune system and leaves the body vulnerable to a variety of life-threatening infections and cancers. Combination antiretroviral therapy (cART) decreases the replication of HIV-1 and improves the survival of infected persons. Although cART reduced the overall incidence of mortality of HIV-infected individuals by 50%³⁰, HIV replication continues because of inadequate patient's adherence to therapy, drug-drug interactions and, resistance issues. Therefore, it is essential to (i) achieve sufficient anti-retroviral drug levels at HIV sanctuaries¹⁴⁰, (ii) avoid their inactivation resulting from *in vivo* binding to plasma glycoproteins¹⁴¹ and, (iii) limit their rapid metabolism, inactivation (e.g., by the liver CYP3A4)^{142, 143} and efflux out of the cells by efflux transporters, especially P-glycoprotein (P-gp).

Protease inhibitors (PIs) are competitive inhibitors of HIV protease which are widely used in cART³². Amprenavir (APV) is an HIV-1 PI which interrupts HIV maturation by preventing HIV protease from binding with its normal substrates¹⁴⁴.

Disadvantages related to APV physicochemical and pharmacological properties are low water solubility, variable oral bioavailability and poor penetration into the HIV sanctuaries^{145, 146}. Clinically approved prodrug of APV, fosamprenavir, has been developed to improve patient's compliance by reducing pill size/burden and eliminating food and water restrictions⁴⁷. However, the prodrug is rapidly converted back to the parent drug *in vivo* at or inside the intestinal epithelial cells regaining all the disadvantages.

PEGylation is one of the most successful approaches to solve the intrinsic shortcomings of biomolecules. Similarly, PEGylation has been applied to small molecule drugs constituting the prodrug approach¹⁴⁷. When PEG polymers are attached to drugs through releasable bonds (to produce prodrugs) the loss of drug potency is not a concern. Some examples are camptothecin¹⁴⁸, SN38¹⁴⁹, paclitaxel^{150,151} and irinotecan¹⁵². However, fluctuation in rate of drug release from the prodrug is a drawback. Too rapid release may cause toxicity and/or accelerated drug clearance whereas too slow release may attenuate drug efficacy. PEGylation of therapeutics through non-releasable bonds (affording novel components) has been extensively used for proteins but not very commonly used for small molecule drugs. Only a few PEGylated small molecule drugs have been used directly as therapeutics (Table 4). One example is PEG-naloxol (NKTR-118), presently in phase 3 clinical trials, prepared by covalently reacting a 550 Da PEG to naloxol (MW, 329.4) via a non-releaseable bond¹⁵³. Naloxol is a reductive metabolite of naloxone and both are effective opioid antagonists. The PEGylated conjugate is produced to eliminate the undesired entry of the drug into the brain while retaining its desired opioid antagonist characteristics in the intestine⁷⁸. Another example is PEGylated

camptothecin, carrying folate as targeting moiety, developed by our group¹⁵⁴. The nanoparticle was prepared by covalently reacting PEG to camptothecin, a chemotherapy agent, via an ester bond and then conjugating the PEGylated camptothecin to folate via a stable amide bond. However, in the later study, the intracellular delivery of PEGylated conjugate was not investigated.

In this chapter, the feasibility of developing non-releasable APV-PEG conjugates with high anti-HIV-1 activity has been investigated. PEG_x-APV-OH ($x = 2, 5, 10,$ and 30 kDa) conjugates were prepared by coupling PEG to amino group present on the aniline moiety of APV, without perturbing the -OH pharmacophore of the drug. The results showed that APV can tolerate PEGylation with PEGs 2 to 5 kDa in size, retaining more than 50% of the activity of free APV in cell-free HIV-1 protease inhibition assay.

4.2 Materials and Methods

4.2.1 Materials

APV as Agenerase[®] capsules was obtained from GlaxoSmithKline (Research Triangle Park, NC). The mPEG_x-NHS ($x = 2, 5, 10,$ and 30 kDa) were purchased from NOF America (White Plains, NY). All other chemicals were purchased from Sigma-Aldrich (St. Louis, MO). The recombinant HIV-1 PR and a SensoLyte[®] 490 HIV-1 Protease Assay Kit (containing the quenched fluorogenic HIV-1 protease substrate along with EDANS fluorescence reference standard and assay buffer) were obtained from AnaSpec Inc (San Jose, CA). Sephadex beads (LH-20 and LH-60) were obtained from Amersham Biosciences (Uppsala, Sweden). Microcon centrifugal filter (MWCO, 1000)

was purchased from Amicon (Beverly, MA). Electro-spray ionization mass spectrometry (ESI-MS) was performed on a Finnigan MAT TSQ 7000 equipped with an atmospheric pressure ionization source. Mass spectrometry using matrix-assisted-laser-desorption-ionization time-of-flight (MALDI-TOF-MS) was performed on ABI-MDS SCIEX 4800. UV and fluorescence were measured using a Tecan GENios multifunction microplate reader (MTX Lab Systems, Vienna, VA). HPLC analysis was carried on a Waters system equipped with UV and fluorescence detectors using a reverse-phase (RP) C₁₈ column (Waters symmetry, 5 μ m, 4.6 x 150 mm, Milford, MA). Ultrahydrogel 250 (7.8 x 300 mm, 6 mm) was used for size exclusion chromatography (Waters Corp., Milford, MA). Deionized water used in the reactions was from a MilliQ system (EMD Millipore, Billerica, MA).

4.2.2 Extraction of APV from Agenerase[®] capsules

APV was extracted from Agenerase capsules since the production of unformulated drug was discontinued from GlaxoSmithKline. The capsule shells were cut open with a sharp blade and contents (white to cream-colored viscous liquid), containing APV and excipients, were mixed with distilled water in a round bottom flask. The drug, which has low aqueous solubility, was precipitated in water. After 5 days, the precipitate was filtered and dried. The crude APV was purified on a silica column (70 - 230 mesh) using an ethyl acetate/methanol gradient. The extracted APV was characterized using RP-HPLC and ESI-MS. HPLC (C-18 column): 0.1% TFA (v/v) in HPLC grade water (mobile phase A) and 100% ACN (mobile phase B), linear gradient (t = 0 min, 100% A, 0% B; t = 5 min, 90% A, 10% B; t = 15 min, 50% A, 50% B; t = 25 min, 10% A, 90% B; t = 35 min, 100% A; 0% B; t = 36 min, 100% A; 0% B, t = 38 min stop), flow rate = 1

ml/min, detection = 265 nm (UV), Rt (retention time) = 18 min; (m/z): calculated, 505.6 Da; observed, 506.74 Da (MW+H)⁺.

4.2.3 Preparation of APV-O-acetyl

APV (0.17 g, 0.34 mmol) was dissolved in N, N-dimethyl formamide (DMF, 3 mL) containing N, N-diisopropyl ethylamine (DIPEA, 2%). Acetic anhydride (0.125 mL, 1.32 mmol) was added drop wise into the solution. The reaction mixture was stirred at room temperature for 12 h. The crude product was purified on a silica column (70 -230 mesh) using a gradient of ethyl acetate/methanol. The pure product was obtained as off-white solid after evaporation on a Rotavap. The product was characterized using RP-HPLC and ESI-MS. HPLC (C-18 column): 0.1% TFA (v/v) in HPLC grade water (mobile phase A) and 100% ACN (mobile phase B), linear gradient (t = 0 min, 100% A, 0% B; t = 5 min, 90% A, 10% B; t = 15 min, 50% A, 50% B; t = 25 min, 10% A, 90 % B; t = 35 min, 100% A; 0% B; t = 36 min, 100% A; 0% B, t = 38 min stop), flow rate = 1 ml/min, detection = 265 nm (UV), Rt = 15 min; (m/z): calculated, 547.7 Da; observed, 570.5 Da (MW+Na)⁺ and 1117.4 Da (2M+Na)⁺.

4.2.4 Preparation of PEG_x-APV-O-acetyl and PEG_x-APV-OH

The mPEG_x-NHS (x = 2, 5, 10 or 30 kDa) polymer (0.01mmol) was reacted with APV-O-acetyl (0.03 mmol, 3 equiv) in DMF (4 mL) containing DIPEA (2%). The reaction mixture was stirred at room temperature for 24 h. The product was purified on Sephadex LH-20 (2 and 5 kDa conjugates) or Sephadex LH-60 column (10 and 30 kDa conjugates) using DMF as eluent. The UV readings of each fraction were monitored at 265 nm (absorption maximum of APV) using a microplate reader. Two separate peaks were obtained from each of the chromatographic runs. The high molecular weight

fractions corresponding to the purified PEG_x-APV-O-acetyl eluted first followed by low molecular weight APV-O-acetyl (unreacted). The eluted high molecular weight fractions were pooled together and re-crystallized from ice-cold anhydrous diethylether. 1,4-dioxane was added drop-wise to enhance the precipitation. The precipitate was collected by centrifugation and the product was washed three times with the ice-cold diethylether. The purified product precipitate was dried using argon, affording PEG_x-APV-O-acetyl as a white powder. The -acetyl group was removed by treating with HCl (0.1 N) at room temperature for 6 h. The HCl was then neutralized with sodium bicarbonate and the solution was lyophilized to obtain crude conjugates as white flakes. The conjugates were purified by size exclusion chromatography (SEC) on Waters Ultrahydrogel 250 column using water as mobile phase (flow rate: 0.8 ml/min, detection at 265 nM) and characterized using MALDI-TOF-MS. Yield: ~50% for all PEGylated conjugates. **2 kDa**: Rt = 24 min; (*m/z*): calculated, 2505.6 Da; observed, 2505.6 Da; **5 kDa**: Rt = 23 min; (*m/z*): calculated, 5505.6 Da; observed, 5625.6 Da; **10 kDa**: Rt = 20 min; (*m/z*): calculated, 10505.6 Da; observed, 10700.1 Da; **30 kDa**: Rt = 17 min; (*m/z*): calculated, 30505.6 Da; observed, 31098.7 Da.

4.2.5 Stability of Amide Bonds in PBS

The stability of PEG-APV conjugates was tested in 100 mM phosphate buffered saline (PBS) for 24 h (pH 7.4). The conjugates were incubated separately at 37 °C. Aliquots were withdrawn at different time points and subjected to ultra-filtration by centrifugation at 14,000g for 90 min with a Microcon filter (MWCO, 1000 Da). The filtrates were subjected to RP-HPLC to quantify the free APV. Each measurement was done in triplicate.

4.2.6 Protease Inhibition Activity of PEG_x-APV-OH (x = 2, 5, 10, and 30 Da) in Buffer

The protease inhibition in the presence of APV conjugates was measured using fluorescence resonance energy transfer (FRET) assay¹⁵⁵, which uses a recombinant HIV-1 protease (PR) and a quenched fluorogenic HIV-1 PR substrate. The substrate corresponds to the naturally occurring HIV gag precursor, synthesized by viral mRNA, with a p17/p24 cleavage site for HIV-1 PR, which cleaves at the Tyr-Pro peptide bond. In a 96-well microplate, HIV-1 protease FRET substrate (50 μ L of 10 μ M) was pre-incubated with different concentrations of unmodified APV (10 μ L) at 37°C for 10 min, following the protocol¹⁵⁵. HIV-1 PR solution (40 μ L of 88 μ M) was then added to the wells (final volume 100 μ L/well, 0.5-5 μ M APV). Fluorescence intensity measurements were immediately started on a Tecan fluorescence microplate reader (Ex/Em: 360 nm/465 nm) at an interval of 2 min until the reaction proceeded to virtual completion (40 min). Similar experimental set-ups were used for PEG_x-APV-OH conjugates (at APV-equivalent concentration of 3.5 μ M). APV-O-acetyl and PEG_{10kDa}-APV-O-acetyl were used as negative controls. The mathematical treatment of the experimental data has been explained in details in the Results section.

4.2.7 Statistical Analysis

GraphPad Prism version 4.0.1 (GraphPad Software, San Diego, CA) was used for analyzing and processing the protease assay data and results are presented as mean \pm SD (n = 3). ANOVA and Tukey's posthoc test were used for statistical analysis of the results and statistical significance was determined by a value of p<0.05. Waters Empower™2

Software (Waters Corporation, Milford, MA) was used for data processing generated from both RP-HPLC and SEC-HPLC runs.

4.3 Results

4.3.1 Synthesis and Characterization Studies

The APV (Ageneras) capsules were obtained from a commercial source and the active ingredient was isolated by precipitation in water and purified on a silica gel column. The purity of the extracted APV was determined by ESI-MS and RP-HPLC and was found to be about 99%. The free aliphatic hydroxyl moiety of APV was acetylated in a basic environment (DMF containing DIPEA) using acetic anhydride to obtain APV-O-acetyl, which was then purified on a silica gel 60 column. The APV-O-acetyl was then PEGylated using mPEGx-NHS polymers ($x = 2, 5, 10, 30$ kDa) of different molecular weights (Scheme 1). The coupling reactions were carried out at room temperature in DMF containing 2% DIPEA. The PEG-O-acetyl conjugates were purified on a sephadex LH-20 or LH-60 columns. The APV-PEG conjugates were obtained by removing the O-acetyl group with 0.1 N HCl at room temperature for 6 h and subsequent purification. Thus, PEGs were covalently attached via a stable amide bond to the amine group present on APV. The conjugate yields were in the range of 50-55%. The yields were slightly lower because PEGylation was performed on relatively less reactive aromatic amine group. These conjugates were characterized using MALDI-TOF mass spectrometry, and observed molecular weights were found in agreement with calculated values (Figure 7, 8).

4.3.2 Stability of Amide bonds

The objective of this study was to assess the feasibility of designing non-releasable PEG-APV conjugates with high anti-HIV-1 activity. Therefore, the stability of the amide bond linking APV to PEG was assessed by incubating APV-PEG_x-OH ($x = 2, 5, 10, \text{ and } 30$ kDa) conjugates ($1 \mu\text{M}$) at 37°C in PBS (pH 7.4) for 24 h and the released drug was monitored using RP-HPLC. All APV-PEG conjugates were found to be stable with less than 2% degradation in PBS over the time course of the study.

4.3.3 Evaluation of HIV-1 Protease inhibition in Buffer: PEG Influences the HIV-1 Protease Inhibition in a Size-Dependent Manner

The PEG polymers attached to drug have been known to shield it in a size-dependent manner. This shielding effect exhibited by PEGs may influence the APV activity against HIV-1 protease. Therefore, the anti-HIV-1 activities of APV-PEG_x-OH conjugates ($x = 2, 5, 10, \text{ and } 30$ kDa) were measured in buffer using FRET-based HIV-1 protease inhibition assay¹⁵⁵. The method utilizes a quenched fluorogenic substrate and a HIV protease FRET peptide with the sequence: DABCYL-GABA-Ser-Gln-Asn-Tyr-Pro-Ile-Val-Gln-EDANS, where EDANS is the fluorophore and DABCYL is the quencher. In the absence of HIV-1 protease, the fluorescence of EDANS in the FRET peptide remains quenched, but when incubated with the recombinant HIV-1 protease at 37°C , the peptide is cleaved leading to the recovery of fluorescence (Ex/Em = 340nm/490 nm) (Scheme 2). However, in the presence of a protease inhibitor, like APV, the cleavage of the fluorogenic HIV-1 peptide substrate by HIV-1 PR is inhibited, leading to a decrease in fluorescence signal in a concentration-dependent manner.

Fig. 9 and Fig. 10 are presented to illustrate how the potencies of APV at different concentrations (0 – 5 μM) in inhibiting the recombinant HIV-1 protease activity were derived from measured fluorescence (F) in buffer. Fig. 9 shows the F kinetics of the FRET enzymatic reactions at different APV concentrations. Fig. 10 (top) shows plots of $\ln (F_{\infty} - F_t)$ against time, where F_{∞} is the maximum fluorescence intensity (0 μM of APV), F_t is fluorescence intensity at time t (min) and $\ln (F_{\infty} - F_t)$ is the natural logarithm of F reduction at a given APV concentration and t. The plots of $\ln (F_{\infty} - F_t)$ values against time yielded straight lines (linear regression $R^2 \geq 0.9711$ for all concentrations), indicating that the assay was accurate. The slope of each line represents the rate of F decline (i.e., the observed rate constant, k_{obs} , in min^{-1}) of a FRET substrate cleavage reaction. The linear regression yielded k_{obs} values (mean \pm s.d.) for 0 – 5 μM concentrations of APV are as follows: -0.3027 (\pm 0.0234) for 0 μM , -0.2239 (\pm 0.0146) for 0.5 μM , -0.1638 (\pm 0.0080) for 1.0 μM , -0.0890 (\pm 0.0049) for 2.0 μM , -0.05704 (\pm 0.0014) for 3.5 μM and -0.03766 (\pm 0.0019) for 5.0 μM .

Since APV loses some potency after PEGylation, the preliminary experiments were carried out to find a concentration that was optimal for comparing potency of APV with that of PEG_x-APV-OH conjugates (x = 2, 5, 10, and 30 kDa) and their two negative controls (APV-O-acetyl and PEG_{10kDa}-APV-O-acetyl). In the two negative controls, the free -OH group on APV necessary for drug activity had been acetylated. It was found that 3.5 to 5.0 μM APV was optimal for suppressing the recombinant HIV-1 PR (with similar potency, $p > 0.05$). Therefore 3.5 μM APV was selected to compare k_{obs} values (Table 6). Anti-HIV-1 protease potency is defined as $[-(1/k_{\text{obs}})]$. Fig. 10 (bottom), plots of $[-(1/k_{\text{obs}})]$ derived from Fig. 10 (top) against APV concentration, shows that APV potency

increases linearly with its concentration increase. Linear regression of the data resulted in a straight line ($R^2 = 0.9858$) that relates the potency (a value of $-1/k_{\text{obs}}$) to APV's concentration. Therefore, Fig. 10 (bottom) was used as a standard curve to fit a $-1/k_{\text{obs}}$ value of an APV-PEG conjugate at $3.5 \mu\text{M}$ to find the corresponding APV concentration that is called the apparent APV concentration (APV_{app}).

Fig. 11 shows the plots of $\ln(F_{\infty} - F_t)$ values against time (R^2 values ≥ 0.9773) for $3.5 \mu\text{M}$ APV and $3.5 \mu\text{M}$ -equivalent concentrations of various PEGylated conjugates, applying the same mathematical procedure to the experimental data as explained above. The obtained k_{obs} values were then converted to $[-(1/k_{\text{obs}})]$ and the latter values were converted to their APV_{app} values using Fig. 10. (Table 6). Fig. 12 shows the compounds' relative potencies in HIV-1 protease inhibition represented by the APV_{app} values relative to the potency of APV (the APV reference being 100% potent). The figure shows that the PEG_x-APV-OH conjugates prepared using 2 and 5 kDa PEGs exhibited 53% and 51% of APV potency, whereas conjugates prepared using 10 and 30 kDa PEGs exhibited 34 and 24% of APV potency. No significance difference was found between the potency of PEG_{2kDa}-APV-OH and PEG_{5kDa}-APV-OH ($p > 0.05$). The two negative controls, with -OH group acetylated, were nearly inactive (9% and 8% of APV potency). Thus, conjugates prepared using smaller-sized PEGs retained half of the drug activity, whereas the ones prepared using larger-sized PEGs suffered significant loss of activity. Among the conjugates prepared, the optimum PEG size for PEG_x-APV-OH is within the range of 2 - 5 kDa.

4.4 Discussion

One promising approach to overcome the obstacles related to small molecule drugs is to use PEGylation strategy. Compare to biological macromolecules, small organic molecules present fewer problems in the chemistry of PEGylation since they have fewer functional groups, lower conformational constraints, and easier purification and characterization steps^{79, 82}.

In this chapter, the feasibility of using non-releasable APV-PEG conjugates with high anti-HIV-1 activity has been investigated. The PEG moiety can impart greater solubility to the poorly soluble APV^{78, 79}. PEG may also serve as a tether to hold a functional molecule, such as a targeting moiety or a cell penetrating peptide (CPP). Moreover, PEG can increase the intracellular persistence of APV by preventing metabolism since PEG is conjugated to APV at the amine group of aniline moiety, where oxidation occurs during metabolism by cytochrome P450 3A4⁴⁹. To investigate the influence of PEG size on the anti-HIV-1 activity of APV, PEG_x-APV-OH conjugates were prepared using 2, 5, 10 and 30 kDa PEGs. The PEG chains were specifically reacted to the amino group rather than to the hydroxyl group, which is essential for protease inhibition (Scheme 1). Anti-HIV-1 activity was measured in buffer using FRET-based protease inhibition assay. The assay uses the quenched fluorogenic substrate consist of an octapeptide with a fluorescent donor, 5-[(2-aminoethyl)amino]naphthalene-1-sulfonic acid (EDANS) attached at the COOH- termini, and a quenching acceptor, 4-(4-dimethylaminophenylazo)benzoic acid (DABCYL) attached at NH₂- termini (Scheme 2). The octapeptide sequence of substrate, SQNYPIVQ, corresponds to the naturally

occurring p17/p24 cleavage site for HIV-1 protease, which cleaves at the Tyr-Pro peptide bond. This sequence has been shown to be a better substrate than synthetic peptides based on other cleavage sites¹⁵⁵. The γ -aminobutyric acid (GABA) spacer inserted between the DABCYL group and the NH₂-terminal Ser in the fluorogenic peptide substrate is present to avoid potential steric hindrance of substrate binding by the bulky acceptor¹⁵⁵. The intrinsic fluorescence of EDANS is dramatically reduced because of intramolecular resonance energy transfer to the DABCYL group. Since FRET becomes insignificant beyond distances of about 100 Å, the full fluorescence quantum yield of EDANS is restored after cleavage of the peptide substrate with liberation of the DABCYL-linked peptide fragment. Hence, proteolytic activity can be monitored by measuring the increase in fluorescence intensity with time. APV, a potent HIV-1 protease inhibitor, withholds the cleavage of the substrate in a dose dependent manner, which was observed as an inhibition in the fluorescence signal (Scheme 2). When APV was conjugated to differently sized PEGs (2 to 30 kDa) via stable amide bonds and APV-PEG conjugates were subjected to FRET assay, it was observed that conjugates with up to 5 kDa PEGs retain half of the drug activity (Figure 12). The observed decrease in protease inhibition with increase in PEG size is not surprising, due to the shielding properties of PEG. Both the acetylated APV (APV-O-acetyl) and PEGylated acetylated APV (PEG_{10kDa}-APV-Oacetyl) showed negligible inhibitory effect. Molecular modeling of amprenavir interactions with HIV-1 protease also confirms these results (Figure 4). Amide bonds stability studies showed that these bonds are very stable, with less than 2% cleaved over 24 h incubation periods.

The target for the APV is HIV-1 protease, located inside the cytosol. Therefore,

effective anti-HIV-1 activity *in vitro* is achieved only when APV-PEG conjugates transport across the plasma membrane. This requirement may be accomplished by appending additional chemical groups to multivalent PEG molecules. Examples include targeting agents, such as the macrophage-specific peptide, N-formyl-Met-Leu-Phe^{156, 157,}¹⁵⁸ and cell-penetrating peptides, such as bactenecin 7¹¹²⁻¹¹⁴ explained with details in next chapter. Thus, by using an already active drug-PEG conjugate, it might be possible to control the pharmacological properties of the drug, without requiring a prodrug cleavage reaction to occur.

5. DESIGN, SYNTHESIS AND CHARACTERIZATION OF A PEGYLATED AMPRENAVIR NANOCARRIER CONJUGATED TO Bac7 CELL- PENETRATING PEPTIDES AND EVALUATION OF ANTI-HIV-1 REPLICATION INHIBITION IN T- CELLS

5.1 Introduction

Topical microbicides in currently available dosage forms operate within a thin margin of safety in HIV prevention; missing one daily dose could subject to failure of protection. Another challenge is microbicide penetration into vaginal and rectal mucosa. Lots of efforts have been made to overcome the epithelial barrier, notably through the use of cell penetrating peptides (CPPs) ¹⁵⁹.

Antimicrobial peptides (AMPs) are a group of peptides that are active against a diverse spectrum of microorganisms. AMPs are strongly membrane-active and some of them are known to be able to translocate into cells without lytic properties or permanent membrane permeabilization ⁹⁴. Some AMPs with cell-penetrating properties have recently been used as efficient vectors for intracellular delivery of various active molecules. Bactenecin 7 is a 59 amino acids AMP and possesses repeating sequences which form regions with both antimicrobial and cell-permeant properties ¹¹². Peptide mapping has narrowed the cell penetration function to a 10 amino acid region (fragment 15–24) that is devoid of the antimicrobial activity ¹¹³⁻¹¹⁴. The short (15–24) fragment,

hitherto as Bac7 CPP, contains five prolines in its sequence and is one of a few most potent CPPs with no cytotoxicity. Bac7 CPP is capable of carrying small (fluorescein isothiocyanate, FITC) or large (60-kDa NeutrAvidin) cargo into mammalian cells with efficiency comparable with that of the TAT peptide, a gold standard for CPPs^{107, 113}.

In the previous chapter, it was shown that the anti-HIV drug APV could tolerate PEGylation with PEGs up to 2 to 5 kDa in size, retaining more than 50% of the free APV HIV-1 protease inhibition when the potency was evaluated in buffer with a SensoLyte[®] 490 HIV-1 Protease Assay Kit. However, PEGylation usually makes small molecule drugs membrane-impermeable. In this chapter, a strategy to enhance the APV-PEG bioavailability is proposed. This strategy also has the incidental benefits of reducing dose frequency and improving patients' adherence. For this purpose, three APV-PEG conjugates, APV-PEG_{3.4kDa}-FITC (APF), APV-PEG_{3.4kDa}-Bac7 CPP (APB) and Bac7 CPP-PEG_{3.4kDa}-FITC (BPF) were synthesized. The potencies of APF and APB in HIV-1 replication inhibition in HIV-1 infected MT-2 T-cells were studied. Although PEGylated APV (APF) lost the anti-HIV-1 potency of free APV, further conjugation to Bac7 CPP essentially restored the drug activity. Confocal microscopy with APF and BPF and anti-HIV-1 activity assays with APF and APB suggest that APB effectively entered the cytoplasm of MT-2 T-cells with little endosomal entrapment.

5.2 Materials and Methods

5.2.1 Materials

APV as Agenarase[®] capsules was obtained from GlaxoSmithKline (Research Triangle Park, NC). FITC-PEG_{3,4}-COOH and maleimide-PEG_{3,4}-COOH were purchased

from NANOCS (Burlington, MA), amino acids from AnaSpec Inc. (Fremont, CA), NovaSyn[®] TG Sieber resin from EMD Millipore (Billerica, MA), O-(7-Azabenzotriazole-1-yl)-N,N,N',N'-tetramethyluronium hexafluorophosphate (HATU) and 1-hydroxy-7-azabenzotriazole (HOAt) from GenScript (Piscataway, NJ). Diisopropylethylamine (DIPEA), N-methylpyrrolidone (NMP), methanol (MeOH), dichloromethane (DCM), piperidine, triisopropylsilane (TIS), trifluoroacetic acid (TFA), ethanedithiol (EDT), acetonitrile (ACN), acetic acid, α -cyanohydroxy-cinnamic acid (CHCA) and all other chemicals were purchased from Sigma-Aldrich (St. Louis, MO). Dialysis membrane (MWCO, 3000) was purchased from Cole-Parmer (Rancho Domingues, CA). The MT-2 cells were obtained from NIH AIDS Research and Reference Reagent Program. Fetal bovine serum (FBS), phenol red-free RPMI Medium, penicillin/streptomycin 100 \times solution, tetramethylrhodamine dextran, diamidino-2-phenylindole dihydrochloride (DAPI) were purchased from Life Technologies Corp (Carlsbad, CA). Chambered coverglasses (Lab-Tek[™] II) were purchased from ThermoScientific (Waltham, MA).

Electro-spray ionization mass spectrometry (ESI-MS) was performed on a Finnigan MAT TSQ 7000 equipped with an atmospheric pressure ionization source. Mass spectrometry using matrix-assisted-laser-desorption-ionization time-of-flight (MALDI-TOF-MS) was performed on ABI-MDS SCIEX 4800. UV and fluorescence were measured using a Tecan GENios multifunction microplate reader (MTX Lab Systems, Vienna, VA). HPLC analysis was carried on a Waters system (Milford, MA) equipped with UV and fluorescence detectors. Agilent Technologies (3.5 mm, 4.6 \times 50 mm, Santa

Clara, CA) C₁₈ column was used for reverse-phase (RP) HPLC. Deionized water used in the reactions was from a MilliQ system (EMD Millipore, Billerica, MA).

5.2.2 Synthesis of FITC Labeled Amprenavir-PEG Conjugate (APF)

Amprenavir (APV) was extracted from Agenerase capsules and the crude APV was purified and characterized as explained in previous chapter (4.2.2). The FITC-PEG_{3.4kDa}-COOH (0.03 mmol) was activated by 1-Ethyl-3-(3'-dimethylamino propyl)carbodiimide (WSC, 4 equiv., 0.12 mmol) and 1-hydroxy-7-azabenzotriazole (HOAt, 3 equiv., 0.09 mmol) in DMF (3 ml) while protected from light. After 2 min, APV (2 equiv., 0.06 mmol) was added to the solution and the reaction mixture was stirred in dark at room temperature for 16 h. The conjugate was purified by dialysis (MWCO, 3000 Da) against water (3 × 2 L for 24 h) and lyophilized to obtain APF as yellow flakes. APF was quantified using a FITC standard curve and characterized by MALDI-TOF-MS (*m/z*): calculated, 4714.72 Da; observed, 4800.9 Da.

5.2.3 APF Concentration Determination Using a Standard Curve Generated with FITC-PEG

The Standard curve was created by dissolving 5 to 150 nM FITC-PEG_{3.4}-COOH in PBS. The fluorescence of each sample was measured using a Tecan GENios microplate reader at Ex/Em of 485 nm/535 nm. Data was obtained in triplicate. Lyophilized APF was dissolved in PBS and, from the standard curve; the concentration of the APF stock solution was determined assuming APF and FITC-PEG have the same fluorescence.

5.2.4 Synthesis of Bac7 CPP

The modified cell-penetrating peptide NH₂-Cys-Gly-Pro-Arg-Pro-Leu-Pro-Phe-Pro-Arg-Pro-Gly-COOH (Bac7 CPP) was synthesized on NovaSyn[®]TG Sieber resin at 0.077 mmole synthesis scale using a Nautilus 2400 automated peptide synthesizer (Argonaut Technologies, Redwood City, CA). The resin was swollen with DCM and washed several times with NMP. The Fmoc approach of solid-phase peptide synthesis (SPPS) was then used to assemble the resin-bound Bac7 CPP. The peptide was cleaved from the resin using TFA, EDT, H₂O, and TIS (94/2.5/2.5/1). The cleaved peptide was precipitated in and washed twice with ice-cold diethyl ether. The product was characterized using RP-HPLC and MALDI-TOF-MS. HPLC (C18 column, Agilent Technologies): 0.05% TFA (v/v) in HPLC grade water (mobile phase A) and 0.05% ACN (v/v) in HPLC grade water (mobile phase B), linear gradient of 95% (A) to 0% (A) in 12 min; (*m/z*): calculated, 1333.71; observed, 1334.6 (M + H)⁺.

5.2.5 Synthesis of APV-PEG_{3,4}-Bac7 CPP Conjugate (APB)

The Bac7 CPP (0.01 mmol) was reacted with maleimide-PEG_{3,4kDa}-COOH (0.01 mmol, 1 equiv.) in DMF (0.5 mL). The reaction was monitored by measuring the reduction in free thiol using Ellman's assay at 0, 0.5, 1.0, 1.5, 2, and 4 h¹⁶⁰ as described in 5.2.6. The reaction was ~85% complete in 4 h. The product was purified by dialysis (MWCO, 3000 Da) against water (3 × 2 L for 24 h). The COOH-PEG_{3,4}-Bac7 CPP was characterized by MALDI-TOF-MS (*m/z*): calculated, 4733.6 Da; observed, 4732.7 Da. In the next step, COOH-PEG_{3,4}-Bac7 CPP (0.02 mmol) was reacted with APV (0.04 mmol, 2 equiv.) by a method similar to one described earlier in 5.2.3. The product was purified by dialysis against water (MWCO, 3000 Da) and then lyophilized to obtain pure APB as

white flakes. The conjugate was characterized by MALDI-TOF-MS (m/z): calculated, 5219.9 Da; observed, 5010.18 Da.

5.2.6 Cysteine Standard Curve (Ellman's Assay)

The reaction between maleimide-PEG_{3,4}-COOH and Bac7 CPP thiol group was followed by Ellman's assay. To create a standard curve, serial dilutions of cysteine were prepared in PBS (ranging zero to 1.5 mM). Ellman's reagent (5,5'-dithio-bis-2-nitrobenzoic acid) in PBS was then added; each sample was vortexed and incubated for 15 min at room temperature. Ellman's reagent reacts with free sulfhydryl groups to form yellow-colored 2-nitro-5-thiobenzoic acid. The absorbance of each sample was measured at 412 nm. The experiment was performed in triplicates. The concentration of unreacted thiol group in modified Bac7 CPP at each time point was determined using the standard curve.

5.2.7 Synthesis of FITC Labeled Bac7 CPP-PEG_{3,4} Conjugate (BPF)

The maleimide-PEG_{3,4}-FITC (0.01 mmol) was reacted with Bac7 CPP (0.03 mmol, 3 equiv.) in dry DMF (0.5 mL). The reaction mixture was stirred in dark at room temperature. The product was purified by dialysis (MWCO, 3000 Da) and then lyophilized to obtain BPF as yellow flakes. The product was characterized by MALDI-TOF-MS (m/z): calculated, 4710.6 Da, observed: 4732.74 Da.

5.2.8 Stability of Amide Bonds in Cell Culture Medium Containing 10% Fetal Bovine Serum (FBS)

The APB and APF conjugates were incubated with RPMI medium containing 10% of FBS and 5×10^4 cells/ml of MT-2 T-cells at 37°C for 5 days. At the end of 5 days culture period, MT-2 cells were removed by centrifugation. Each cell-free supernatant

was centrifuged through a Microcon filter (MWCO, 3000 Da). The filtrate was analyzed using MALDI-TOF-MS and anti-HIV-1 activity assay for any traces of free APV.

5.2.9 Cytotoxicity of Conjugates

Cytotoxicities of the conjugates were determined, based on cell viability, using the colorimetric [4,5-dimethylthiazol-2-yl]-2,5-diphenyltetrazolium bromide (MTT) assay¹⁶¹. The MT-2 T-cells were cultured in phenol red-free RPMI 1640 medium supplemented with FBS (10%), penicillin (100 units/ml) and streptomycin (0.1%). The cells were plated into 96-well plates at 5×10^3 cells/well and 200 μ l/well in triplicate in medium containing APB (0-350 nM), APF (0-11 μ M) or APV (0-280 nM). The plates were incubated at 37°C for 5 days in a CO₂ incubator. Each experiment was repeated at least twice. At the end of 5 days incubation period, 25 μ l of MTT at 5 mg/mL in PBS was added to each well. The plates were incubated at 37 °C in a CO₂ incubator for 3 h to allow for the formation of purple crystals. The plates were spun at 1000 g to settle the cells and the majority of the liquid was removed, followed by the addition of 150 μ l/well isopropanol to dissolve the crystals. The absorbance at 570 nm was measured in a microplate reader. Cell viability is expressed as the percentage ratio of Abs₅₇₀ of cells treated with a compound over that of untreated cells.

5.2.10 Anti-HIV-1 Activity of APB and APF in MT-2 T-cells

The anti-HIV-1 activity was quantitatively determined *in vitro* using the syncytium count assay¹⁶² based on inhibition of HIV-1-induced cell syncytium formation. Serial dilutions of APV, APF and APB in complete RPMI medium (100 μ L/well) were prepared in 96-well tissue culture plates. MT-2 T-cells (5×10^4 cells/well) with or without the X-4 HIV-1 strain III_B (at 0.03 multiplicity of infection; MOI) of a

known tissue culture infection dose (TCID) were also added to wells. Final concentrations were: APV, 0 - 560 nM; APF, 0 - 22 μ M; and APB, 0 - 700 nM. After incubating the plates for 5 days at 37 °C under 5% of CO₂, the virus-induced syncytia in each well were counted under a microscope. The experiment was performed in triplicates to derive mean and standard deviation (SD).

5.2.11 Flow Cytometry

For human colon carcinoma Caco-2 cells (American type culture collection, ATCC), conjugate uptakes was carried out in 6-well tissue culture plates. The cells were cultured in Dulbecco's Modified Eagle Medium (DMEM) containing 10% FBS until reached confluence. The cells were then incubated with DMEM (control), fluorescence-equivalent 10 μ M APF (actual molar concentration = 16 μ M) or BPF (actual molar concentration = 10 μ M) for 2h. The cells were then trypsinized and washed with Hank's Balanced Salt Solution (HBSS) using centrifugation. Similar procedure was used for conjugate uptake into MT-2 T-cells, except for the modification of culturing 5×10^5 cells in 500 μ l of serum-containing RPMI medium in a well of a 24-well plate. A Gallios fluorescent-activated flow cytometer (Beckman Coulter) was used for flow cytometry acquisition. Three gating events were used. The first gating, by forward and side scattering, selected intact cells from cell debris. The second gating, by forward scattering, selected singlet cells from doublet cells that also included cell-associated dead cells and/or cell debris. The third gating was based on FITC fluorescence to select cells with fluorescence above the histogram of unstained cells. FITC intensity of 5000 cell events was recorded for each treatment. At least two independent experiments were performed

for each type of cells. Statistical analysis was carried out using GraphPad Prism version 4.0.1 (GraphPad Software, San Diego, CA).

5.2.12 Confocal Microscopy

MT-2 cells were incubated for 4 h in medium containing fluorescence-equivalent 10 μ M of APF or BPF, the fluid phase endocytosis marker, tetramethyl rhodamine dextran (Rho Dex, 10 kDa, 30 μ g/mL) and the nuclear counterstain diamidino-2-phenylindole (DAPI, 5 μ g/mL). The cells were then washed with PBS by centrifugation and were re-suspended in HBSS. Part of the cells was transferred to a chambered coverglass pre-coated overnight with 50 mg/ml poly-D-lysine hydrobromide and prewashed with PBS so cells were densely packed on the coverglass surface. The cells were let settle down and become adherent to the bottom of the chambered coverglass for 60 min at room temperature. Similar procedure was used for Caco-2 cells, except for that the cells were growing on chambered coverglass until three days past confluence so a monolayer of Caco-2 cells were formed. Confocal imaging of the cells was performed on a Leica TSC SP5 confocal microscope (Leica Microsystems CMS GmbH, Germany). Sequential scanning was employed to minimize color spills from one color channel to another. Z stacks of images of 0.5 microns per section in the XYZ mode were acquired with a 40 \times objective. Z stack upper and lower limits were set so only about middle 50% of total cell height was scanned, which avoided the inclusion of occasional dead cell and/or cell debris at cell surface of some cells that artificially adsorbed fluorescent conjugates. There was no cell surface fluorescence observed on the X-Y plane. Quantification of intracellular fluorescence was carried out using the companion software of the confocal microscope on each un-zoomed Z-stack of densely packed MT-2 cells or

confluent Caco-2 cell monolayer. The Z-stacks of images for quantification were not subject to any image editing and contained over 500 cells to ensure objectivity and statistical power. The results were shown as mean \pm s.d. values of each stack of 13 to 17 sections of entire field. In figure 22, a $2.47\times$ -zoomed, blue/green/red merged image of Caco-2 cells of a middle section of its Z-stack is shown.

5.2.13 Statistical Analysis

Results are represented as the mean \pm standard deviation (SD). Statistical analyses were performed by GraphPad Prism Software, version 4.0.1 (GraphPad Software, Inc., San Diego, CA) by analysis of variance (ANOVA) and Tukey's posthoc test. Statistical significance was determined when $p < 0.05$. Non-linear regression analysis was performed by the same GraphPad Prism Software for statistical analysis between curves and curve parameters.

5.3 Results

5.3.1 Synthesis and Characterization Studies

The fluorescein-labeled APV-PEG conjugate was prepared using a 3.4 kDa PEG (Scheme 3). The FITC-PEG_{3,4}-COOH was activated with WSC, and then coupled to APV. The conjugate was purified by dialysis and quantified using a FITC standard curve (Figure 13). Successful formation and purification of APF was confirmed by MALDI-TOF-MS (Figure 14). The PEG-APV conjugate containing Bac7 CPP was also prepared and characterized. Bac7 CPP was synthesized using Fmoc-based solid-phase peptide synthesis (SPPS) protocols (Scheme 4). An extra cysteine in the sequence of the peptide

was designed for reaction with the PEG. A glycine between cysteine and the CPP sequence served to reduce steric hindrance of the PEG-Bac7 CPP reaction. The product was analyzed using PR-HPLC (C18 column) and characterized by MALDI-TOF-MS (Figures 15, 16). The product was obtained in a high purity (87%). To synthesize APV - PEG_{3,4}-Bac7 CPP (APB) conjugate, the maleimide-PEG_{3,4}-COOH was coupled to the cysteine residue present on Bac7 CPP peptide via a stable thioether linkage. In the next step, Bac7 CPP-PEG_{3,4}-COOH was coupled to APV via an amide bond using a procedure similar to one described above for the synthesis of FITC-PEG_{3,4}-APV (Scheme 5). The conjugates were characterized using MALDI-TOF mass spectrometry, and observed molecular weights were found in agreement with calculated values (Figure 17). Similarly, Bac7 CPP-PEG_{3,4}-FITC (BPF) was obtained by coupling maleimide-PEG-FITC to the cystein residue of Bac7 peptide via a thioether linkage (Scheme 6). Successful synthesis and purification was confirmed using MALDI-TOF-MS (Figure 18). The slight difference between observed and calculated molecular weight of the PEGylated conjugates could be explained by the fact that PEGs are not absolutely monodispersed molecules¹⁶³. All conjugates were obtained in high purity. The conjugates exhibited higher solubility in water than free APV.

5.3.2 Amide bond Stability Studies

The objective of this chapter was to assess the feasibility of designing non-releasable APV-PEG conjugates with high anti-HIV-1 activity. Therefore, the stability of the amide bond linking APV to PEG was studied in MT-2 cell culture medium containing fetal bovine serum. The stability of amide bonds in APF and APB conjugates was assessed at about 12- and 4-fold higher concentrations than their respective IC₅₀ values

(96 μ M and 350 nM). The two conjugates were incubated at 37 °C for 5 days in RPMI medium containing MT-2 cells with 10% FBS, conditions similar to those used for cell-based anti-HIV-1 activity assay (see 5.3.4). After incubation period, the cells were removed by centrifugation and cell-free supernatants were centrifuged through a Microcon filter (MWCO, 3000 Da) to separate the released drug from the conjugate. The filtrates were analyzed in triplicates (n=3) for APV traces using the drug's anti-HIV-1 function in inhibition of syncytium formation of HIV-1 infected MT-2 cells (see 5.3.4). Less than 0.08% free APV was found in the filtrates suggesting that negligible amount of APV was released. Thus, the amide bonds were stable during the period of exposure to MT-2 cells and the medium in this study.

5.3.3 Cytotoxicity Studies

The cytotoxicities of APF and APB conjugates were assessed using the MTT cell viability assay. The MT-2 T-cells were incubated with different concentrations of APF, APB, and APV at 37 °C for 5 days, and the untreated MT-2 T-cells were used as controls. The viabilities in cells treated with APF, APB, and APV exhibited no statistical difference in comparison to untreated cells, at the concentrations tested (Figure 19). No significant cytotoxicity was observed for APB up to 350 nM and for APF up to 11 mM, which are several-fold higher than their respective IC₅₀ values.

5.3.4 HIV-1 Replication Inhibition Studies

After ascertaining the optimum PEG size for PEG_x-APV-OH conjugates (Aim 1, previous chapter), APV-PEG_{3,4}-FITC (APF), was synthesized using a 3.4 kDa PEG to investigate the HIV-1 replication inhibition in HIV-1 infected CD4⁺ MT-2 T-cells. Preliminary results indicated that although PEG_x-APV-OH (x = 2 to 5 kDa) conjugates

retained above half of the drug's HIV-1 protease inhibition (using FRET-based protease inhibition assay); their potency in suppressing HIV-1 replication in MT-2 T-cells was very low, suggesting that APF is unable to enter cells effectively. To overcome low cell penetration, another conjugate, APV-PEG_{3,4}-Bac7 CPP (APB) was synthesized by conjugating PEG_{3,4}-APV to a Bac7 CPP (Scheme 5).

The anti-HIV-1 activities of APF and APB conjugates were investigated in human CD4⁺ MT-2 T-cells infected with an HIV-1 X-4 strain, III_B. Infecting the cells with the enveloped HIV-1 virus led to the formation of syncytia (i.e., cells fusing together to form large multinuclear cells, as shown in Figure 20). Anti-HIV-1 activities were assessed by scoring the reduction in syncytia formation in infected cells in the presence of the conjugates. Other readouts, such as the reduction in viral matrix protein p24 production and cell viability, showed more variability in results (data not shown). Statistical analysis was conducted after normalization of the results of the treatment groups to untreated wells (Figure 21). The APF conjugate exhibited over 160-fold less potency ($IC_{50} = 8064$ nM) compare to APV ($IC_{50} = 50.29$ nM), suggesting the PEGylated conjugate is unable to reach HIV-1 protease located in the cytosol. When FITC was replaced with the modified Bac7 CPP (to synthesize APB), the conjugate exhibited anti-HIV-1 activity ($IC_{50} = 78.29$ nM) close to that of free APV. Incorporation of Bac7 CPP in APV-PEG effectively overcame the cell permeability problem observed with APV-PEG conjugate. Comparing the IC_{50} values of APV and APB, no difference was found statistically between the potency of the conjugates ($p > 0.05$). Since it has already been shown that amide bonds linking APV to PEG are stable under the conditions used in these studies (see 5.3.2), the anti-HIV-1 activity observed was due to intact APB in the medium.

5.3.5 Flow Cytometry and Confocal Microscopy

To study the intracellular fate of APV-PEG conjugates, a fluorescein-labeled analog of APB, FITC-PEG_{3,4}-Bac7 CPP (BPF) was synthesized by replacing APV with a surrogate fluorescent molecule, FITC (Scheme 6). To compare the extent of uptake of APF and BPF into mucosal epithelial cells and target T-cells, flow cytometry and confocal microscopy were performed with respective representative Caco-2 cells and human MT-2 T cells.

In flow cytometry, Caco-2 cells or MT-2 T-cells were incubated with culture medium (blank), FITC-fluorescence-equivalent 10 μ M of APF (molar concentration of 16 μ M) or BPF (molar concentration of 10 μ M). Fluorescence-equivalent concentrations were used because APF is weaker than BPF in fluorescence, likely due to partial intramolecular quench in APF by the APV moiety. Figure 22 Shows that total cell-associated fluorescence level of BPF in Caco-2 cells was 4.1 fold higher than that of APF and 2.0 fold higher in MT-2 cells while the blank was zero. These results are consistent with the superior anti-HIV-1 activity of APB over APF in MT-2 cells presented above (5.3.4).

The intracellular uptake of the APF and APB conjugates was investigated using confocal microscopy (Figure 23). Compare to Caco-2 cells, significantly less intracellular fluorescence was observed in Z-stack of sections of MT-2 cells (data not shown), consistent with above flow cytometry data. No cell surface fluorescence in the sections of XY-plane was observed, indicating that the fluorescence was exclusively intracellular. Quantification of the intracellular fluorescence was performed using the companion software of the confocal microscope over the entire Z-stack of sections for APF or BPF

in either cell types. Figure 23 (lower panel) shows that intracellular fluorescence level of BPF was 3.5 fold higher than APF in Caco-2 cells and 2.0 fold higher in MT-2 cells. The trends were consistent with that obtained by flow cytometry. Also, the absolute total cell-associated fluorescent levels of APF and BPF were 3 and 6 fold higher in Caco-2 cells compare with MT-2 cells, respectively; suggesting Caco-2 cells have higher uptake capacity and/or rate for the conjugates. Therefore, vesicular (punctate) vs. diffused (cytosolic/nuclear) localization of APF and BPF in MT-2 cells was not clear. Figure 23 (top panel) shows the blue, green and red color merged images of APF and BPF in Caco-2 cells, in the 2.47 \times -zoomed magnification. No punctate (vesicular) orange color resulted from colocalization of FITC and Rho-Dex (the fluid endocytosis marker) was observed. The undetectable BPF in intracellular endosomes/lysosomes (no orange color) and detectable BPF as the intracellular green fluorescence are mostly due to the conjugate's cytosolic localization. Control experiments confirmed that cells incubated with free FITC did not show any intracellular fluorescence (data not shown); suggesting that the intracellular green fluorescence of cells incubated with the FITC-labeled conjugates is associated with intact conjugates, and not free FITC. Combined with the anti-HIV-1 activities of APF and APB in MT-2 T-cells, confocal microscopy results suggest that APF did not efficiently enter the cells by endocytosis, while APB entered the cytosol efficiently without being trapped in the endosomes. The results also suggest that the main mechanism responsible for Bac7 CCP-assisted cell entry of the PEG-APV conjugate is either direct translocation across the plasma membrane, or endocytosis followed by very efficient endosomal escape.

5.4 DISCUSSION

According to the study results explained in chapter 4, APV PEGylated with 2 to 5 kDa PEGs retain about half of the drug activity. Following up on these results, the fluorescently labeled APF conjugate was prepared using 3.4 kDa PEG and its anti-HIV-1 activity in human CD4⁺ MT-2 T-cells was investigated. Interestingly, APF exhibited 160-fold decrease in anti-HIV-1 activity ($IC_{50} = 8064$ nM) compare to the free drug ($IC_{50} = 50.29$ nM), suggesting a poor cell penetration by this conjugate. It was therefore decided to use Bac7 CPP to improve the cell penetration of APV-PEG conjugates. Bac7 CPP was attached to PEG_{3.4kDa}-APV conjugate via a relatively stable thioether bond to obtain the APB conjugate, which showed anti-HIV-1 potency in MT-2 T-cells ($IC_{50} = 78.29$ nM) close to the potency of free APV ($IC_{50} = 50.29$ nM). These results suggest very efficient intracellular (cytosolic) entry of APB, providing effective APB molar concentration in cytosol for HIV-1 protease inhibition. Since APB differs from APF mainly in the presence of covalently attached Bac7 CPP, the promising outcomes with this conjugate suggest that the CPP is able to drag PEGylated APV across the cell membrane to the cytoplasm.

Flow cytometry and confocal microscopy were used to investigate the extent of cellular uptake and intracellular fate of APV-PEG conjugates in both Caco-2 cells (a human *in vitro* intestinal mucosal epithelial model) and MT-2 T-cells (a representative of HIV target T cells). APF and BPF (a FITC-labeled structural analog of APB) were used for those studies. Consistent with HIV-1 replication inhibition assay in MT-2 cells, both methods showed that intracellular BPF levels in both cell types were significantly higher than that of APF (Figure 22 and Figure 23). With BPF, very little intracellular punctuate

(vesicular) but significant diffused (cytosolic) fluorescence was observed in Caco-2 cells (Figure 23, top panel). It was concluded that BPF (APB analog) efficiently entered the cytosol, similar to non-PEGylated free APV. This no loss in cytosolic entry of APB is in contrast to PEGylated TAT. It has been reported that after conjugating to a 1.3 kDa linear PEG, the PEG-TAT at 2 μ M entered CHO-K1 cells by endocytosis. The conjugate was entrapped in the endosomes and was unable to reach the cytosol ¹⁶⁴. It is remarkable that the 10 amino acid residue in bactenecin 7 antimicrobial peptide is able to deliver the cargo into the cytosol with almost the same efficiency as a 29-residue chimeric CPP consisting an 11-residue TAT CPP and an 18-residue membrane disrupting peptide ¹⁶⁵.

The Bac7 CPP was used because its cell penetration efficiency rivals that of TAT, which is among the best known CPPs ^{113,166}. However, Bac7 CPP differs from TAT in several ways. Bac7 CPP is highly rich in proline (Pro) ¹¹², whereas TAT is highly rich in arginine (Arg) ¹⁶⁷. Mechanistic studies have shown that the cell entry of Arg-rich CPPs requires binding to negatively charged glycosaminoglycans (GAGs) that are part of cell surface proteoglycans, while Pro-rich Bac7 CPP enters cell in an energy-independent manner and is mainly localized in cytosol and not entrapped in endosomes ¹¹³, suggesting direct plasma membrane crossing unlike Arg-rich CPPs ^{168,169}. Bac7 CPP contains repeating (PX)_n motif that is different from all other known cell-permeant peptides. The (PX)_n motif possesses both hydrophobic character and a distinct secondary structure, both of which may be implicated in the translocation activity. Proline has a moderate hydrophobicity and poly proline peptides have a distinct conformation containing a hybrid of the PPII helix and the α -helix which may be the basis of Bac7 cell penetration properties.

It is known that PEGylation of hydrophobic small molecule drugs makes the PEGylated drug no longer susceptible to cellular efflux by P-gp and other efflux transporters^{170, 171}. It is expected that PEGylated and Bac7 CPP-conjugated APV can overcome the cellular efflux *in vivo*. P-gp efflux is a drawback related to the free APV. Moreover, because a PEGylated conjugate tends to linger inside cells, a CPP-PEG-microbicide conjugate is expected to reside in vaginal or colonic-rectal mucosa for a longer time. Future studies are needed to confirm this expectation, which is critical for the proposed PrEP strategy.

6. FORMULATION, CHARACTERIZATION AND EVALUATION OF ALCOHOL-FREE COLORECTAL FOAM-BASED MICROBICIDE DELIVERY VEHICLES AND INVESTIGATE THEIR PERFORMANCE IN MICE USING IMAGING TECHNIQUES

6.1 Introduction

The efficacy of all of conventional dosage forms for rectal drug delivery (suppository, enema, ointments, foams and gels) and vaginal drug delivery (lotion, gels, suppository, tablets, foam, pessaries and creams) are greatly decreased by the fact that the drug cannot fully spread and contact the disease sites which located in rectal or vaginal mucous membrane folds. The induced irritation by higher local drug concentration or by insoluble ingredients is another documented deficiency^{122, 172}. The patients' comfort while administering these dosage forms is also a critical component. It is reported that patients are generally better tolerant to gels than other topical dosage forms^{173, 174} however, a documented shortcoming with this dosage form is that it is very difficult for classic gels to spread uniformly in rectal and vaginal canal because of their higher viscosity¹³⁴. Other drawbacks are low residence in the area they applied and leakage.

An ideal rectal or vaginal drug delivery system should have (1) a long retention time to maximize drug release, (2) a proper spreading over the epithelium to obtain fast absorption or to maximize the effect in case of local treatment and (3) be easy to administer (allow self-administration) and not cause discomfort to improve patient

compliance. Aerosol foams have some distinct advantages for rectal and vaginal drug delivery including a greater degree of spread, ease of application, enhanced drug delivery efficiency and comfortable feeling^{14, 126, 130}. In addition, the potential of contaminating the unused portion of the medication is minimized as the foam is often administered from a sealed airtight container. As a result of their benefits, patient compliance is greatly improved with foams^{14, 175}.

The purpose of the studies in this chapter was to develop and characterize an alcohol-free foam aerosol for colonic/rectal anti-HIV drug application. Thirteen preliminary formulations were investigated consisting of various combinations of foaming agents, surface-active agents (surfactants), solvents (aqueous and hydrophobic), polymers (natural and synthetic) and propellants. Four basic formulations were developed with different concentrations of xanthan gum (XG, 0.5% to 2.0%). Colonic/rectal distribution of the foams was investigated in mice using an Aspect MRI and a MS FX PRO small animal imaging system and the foams rheology and dynamic measurements were done using a Malvern rheometer. The foam containing 1.5% XG was selected as the most satisfactory. FITC-PEG_{3,4kDa}-COOH as a model of PEGylated small molecule drugs was incorporated into 1.5% XG foam and the release was studied over 72 h. The results of distribution and release studies were compared with that of a conventional gel and saline enema.

6.2 Materials and Methods

6.2.1 Materials and Equipments

Xanthan gum and disodium EDTA were purchased from Sigma-Aldrich (St. Louis, MO). Methyl 4-hydroxybenzoate was obtained from Acros organics (Geel,

Belgium). Brij L23 was purchased from Alfa Aesar (Heysham, LA) and FITC-PEG_{3,4kDa}-COOH was obtained from NANOCS (Burlington, MA). Transwell[®] polycarbonate membrane inserts (0.4 μm pore size) were purchased from Corning Incorporation (Corning, NY).

Deionized water used for formulations was obtained from a MilliQ system (EMD Millipore, Billerica, MA). A Barnant Mixer Head (Barrington, IL) was used to mix the formulations. A Malvern Bohlin Gemini HRnano (Malvern Instrument, Westborough, MA) was used at controlled stress mode for the rheology studies. An Aspect M2 MRI system (Netanya, Israel) operating at field strength of 1.0 T was used for magnetic resonance imaging and an In-Vivo MS FX PRO small animal imaging system (Wood Bridge, CT) was used for fluorescent imaging.

6.2.2 Preparation of Foam Concentrates

In a round bottom glass container, deionized water was warmed up to 55 °C. Disodium EDTA was dissolved in water while stirring. Different quantities of xanthan gum (0.5% to 2.0%, Table 7) were also mixed with the aqueous phase using a Barnant Mixer Head (Barrington, IL). In a separate glass container, Brij L23 was warmed up to 55 °C. Methyl 4-hydroxybenzoate was then dissolved in Brij L23 while stirring. The oil phase was gradually added to the aqueous phase and the mixture was stirred for 20 min more. The foam concentrates were then cooled to room temperature.

6.2.3 Preparation of FITC-PEG Loaded Foam Concentrate

The FITC-PEG_{3,4kDa}-COOH (5 μM) was dissolved in deionized water (300 ml) while protected from light. The mixture was warmed up to 55 °C and the formulation containing 1.5% xanthan gum was prepared as explained in 6.2.2.

6.2.4 Crimping / Gassing Process

The foam concentrates were transferred to tin-plate aerosol canisters (58 × 163 mm, 382 ml) in 150 ml aliquots. A continuous Standard Valve (Precision valve, Rye Brook, NY) was crimped onto the canister and propellant AP-70 was delivered through the valve at 7% (w/w) to achieve an internal pressure of 70 psi. A Juno Spout nozzle (Precision valve, Rye Brook, NY) was fixed on the valve to ease the foam delivery. The aerosol package was shaken well immediately and was kept at a cool place until tested. Crimping and gassing process was done in Spray Products Corporation (Plymouth Meeting, PA).

6.2.5 Foam Appearance and Microscopic Analysis

Foam quality was assessed using an in-house ranking of fine to coarsely porous, as well as viscous or runny. For light microscopy analysis, foam samples were applied from the canister with a continuous valve to a glass slide and then a digital image of the foam appearance was quickly taken using an Olympus TH4-100 light microscope (Tokyo, Japan). Ten robust bubbles of each foam capture were arbitrarily chosen for size quantification. Three independent experiments were conducted to ensure that the observations were reproducible.

6.2.6 Thermosensitivity Studies

Foam was expelled into a graded glass cylinder, which was immediately placed in a 38 °C bath. Initial volume of foam (20 ml) and the subsequent volume of aged foam after 1, 5, 15, 30, 45 and 60 minutes were recorded. Foam volume stability (FVS) was defined as:

$$\text{FVS (\%)} = \frac{V(\text{foam } t)}{V(\text{foam } int)} \times 100$$

With $V(\text{foam}_t)$, volume of foam at time “t”; $V(\text{foam}_{int})$, initial volume of foam. GraphPad Prism version 4.0.1 (GraphPad Software, San Diego, CA) was used for analyzing and processing the FVS data and results were presented as mean \pm SD (n = 3).

6.2.7 Evaluation of Rheological Properties; Experimental Set-up

Viscoelastic properties of the foams were determined through frequency sweeps, which measures the viscoelastic moduli, G' and G'' , and the complex viscosity, η^* . After calibrating the system, the sample was carefully placed at the center of the lower fixture on the rheometer (Malvern Bohlin Gemini HRnano, Westborough, MA). The sample was allowed to rest and physically and thermally stabilize for 2 min before the experiment started. The parallel plate sensor (40 mm in diameter) was lowered slowly into the sample at controlled speed (7.5 mm/min) to produce minimal disruption to the formulation structure during set-up. Temperature was maintained constant at 38 °C during the experiment.

6.2.7.1 Amplitude and Frequency Sweep Tests

The range of amplitude of oscillation for which the structure of the foam sample remains intact was found by gradually increasing the amplitude (0.1 to 1.0 Pa) on the sample at constant angular velocity (ω , 5 rads/s). The response was observed at 38 °C (n = 20) while G' values remained constant. Angular velocity is defined as:

$$\omega = 2\pi F$$

With π , 3.4 and F, frequency.

The frequency sweep test was performed at ω of 0.1 to 100 rads/s (n = 30). The data collected for this experiment included the elastic modulus G' (a measure of

contribution of elastic forces to flow), viscose modulus G'' (a measure of the contribution of viscous force to flow) and the complex viscosity, η^* .

6.2.7.2 Yield Stress Studies

The yield stress was determined by linearly increasing the shear stress from 1.0 to 50 Pa in a sweep time of 60 s and response of the samples was observed ($n = 50$). The location of the change in response from no flow (the structure only stretches) to flow determined the yield point of the formulation.

6.2.8 Loss on Drying

Approximately 3 g to 4 g of foam was expelled into a pre-weighted beaker and the foam quantity was determined. The beaker was placed in a 65 °C oven and weighted at intervals until constant weight achieved, typically after 5 to 7 days.

6.2.9 *In vitro* Release Studies

In vitro release studies were conducted by placing 500 μ l of either the FITC-PEG_{3,4kDa}-COOH loaded foam (1.5% XG) or the FITC-PEG_{3,4kDa}-COOH loaded Gel (containing 1.5% XG foam concentrate with no propellant added) in Transwell[®] polycarbonate membrane inserts (400 nm pore size). The receptor was filled with 1500 μ l preheated release medium (phosphate buffer 10 mM, pH 7.4, 38 °C), followed by figure 8 shaking (Nutator Innovative Medical System, Ivyland, PA) for 72 h in dark at 38 °C. The amount of FITC-PEG_{3,4}-COOH release was detected at each time point by a Tecan GENios multifunction microplate reader (MTX Lab Systems, Vienna, VA) at Ex / Em of 485 nm/ 535 nm. Sink condition was kept throughout the experiment. The study was done in batches of 3 for 3 times.

6.2.10 *In Vivo* Characterization of Foams using MRI

An Aspect M2 MRI system (Netanya, Israel) was used for *in vivo* characterization of the formulations, operating at field strength of 1.0 T. Coronal fast spin-echo (FSE) images were acquired using a 265×250 matrix; slice thickness, 0.8 mm; TR, 3029 ms; TE, 80 ms; and total scan time of 7 min and 58 sec. Axial FSE images were acquired with TR/TE, 6059/80; slice thickness, 0.08 mm; field of view, 64 mm; and number of slices, 32. Groups of three male adult CD1 mice (~ 25 g) were used for *in vivo* imaging studies. Mice were fasted overnight. Before and during imaging, the mice were anesthetized by 1.5% isoflurane in 70% N₂O / 30% O₂. The foams (0.5% to 2.0% XG), gel (1.5% XG) or saline enema (pH 7.4) was then applied intrarectally at 100 μ l and the mice were scanned with the MRI at different time points over 2h. Foams included no contrasting agent. Magnetic resonance imaging data were analyzed using inviCRO's VivoQuant (1.22) software. Mice were observed for signs of swelling or inflammation for 5 days (visual and MRI).

6.2.11 Fluorescence Imaging

Fluorescence imaging was performed using an In-Vivo MS FX PRO small animal imaging system (Wood Bridge, CT). FITC Ex / Em (480 nm / 535 nm) filters were used. Identical illumination settings such as exposure time (60 sec), binning factor (1×1), etc. were used for all image acquisition. Groups of three male CD1 mice (~ 25 g) were used for *ex-vivo* imaging studies. Mice were fasted overnight and were anesthetized by isoflurane. FITC-PEG_{3.4kDa}-COOH loaded foam (1.5% XG) was then applied intrarectally at 100 μ l. Three mice were euthanized by CO₂ asphyxiation at each time point and 7 cm of the lower GI (from anus to descending colon) was removed and imaged. Imaging time

points were: untreated (control), 30 sec, 15 min, 30 min, 1 h, 2 h, 3 h and 4 h after application. Fluorescent and photographic images were acquired and overlaid. Background fluorescence was subtracted prior to analysis. Images were acquired and analyzed using the Carestream molecular imaging software (Carestream Health, Wood Bridge, CT).

6.2.12 Preliminary Toxicology Assessment

The study was conducted in accordance with the requirements of Good Laboratory Practice Standards. Male adult CD1 mice (~ 25 g) were treated intrarectally with either XG foam (1.5%) or saline enema at 100 μ l. For each formulation as well as the control group, three animals were used. Before and after each dosage application, the mice were examined for clinical signs of rectal irritation, discharge or bleeding from the rectum. The mice were dosed once in a day for one day or for 5 consecutive days. At the end of the time points, the mice were euthanized and necropsied. Samples of the colonic/rectal tissues of each animal were dissected out and embedded in paraffin after being rinsed with saline. The tissues were stained with hematoxylin and eosin, and then examined microscopically by a pathologist at HistoMic (Highland Park, NJ) for the severity of ulceration (an area of mucosa where the epithelial lining was missing). The severity of the findings was described by one of the four following grades: normal, mild, moderate or severe.

Statistical Analysis

Results are represented as the mean \pm standard deviation (SD). Statistical analyses were performed by GraphPad Prism Software, version 4.0.1 (GraphPad Software, Inc., San Diego, CA) by analysis of variance (ANOVA) and Tukey's posthoc test. Statistical

significance was determined when $p < 0.05$. Non-linear regression analysis was performed by the same GraphPad Prism Software for statistical analysis between curves and curve parameters.

6.3 Results

6.3.1 Preparation of Xanthan Gum Foams

Xanthan gum (XG) foams were prepared with different concentrations of XG (0.5% to 2.0% w/w). In order to dissolve XG, the aqueous phase containing disodium EDTA (a chelating agent) was warmed up to 55 °C. The oil phase containing a surfactant (Brij L23) and a preservative (methyl 4-hydroxy benzoate) was gradually added to the aqueous phase once warmed up to the same temperature. The resultant mixture is called 'foam concentrate'. In case of FITC-PEG-loaded foams, FITC-PEG_{3.4kDa}-COOH was dissolved in the aqueous phase before adding XG. The foam concentrate containing 0.5% XG appeared to be a clear viscous liquid whereas other foam concentrates with higher concentration of XG formed clear, homogenous gels. After delivering the hydrocarbon propellant AP-70 (containing 31% propane, 23% isobutane, 46% n-butane) at 7% w/w through the valve, the internal pressure of the canisters was measured between 65 to 70 psi.

6.3.2 Foam Appearance

The foams quality was assessed by an in-house ranking method introduced by Abram et al ¹⁷⁶. When expelling the sample from the canister, a white to off-white foam was observed (Figure 24). All foams were characterized as being three-dimensional,

semi-solid creamy structures that did not readily flow away from dispensing area when dispensed. The foams had relatively small bubble size and they exhibit characteristics like whipped cream. The foams containing %1.5 to %2.0 XG could retain over %70 of the original volume at room temperature over a period of 2 h.

6.3.3 Foam Light Microscopy Analysis

The foams were applied from the canisters to glass slides and digital images of the foam appearance were quickly taken with 10× objective. The bubble sizes were quantified, using Olympus TH4-100 Infinity Capture software with an average diameter of 87.82, 110.28, 157.27 and 104.7 μm for the foams containing 0.5%, 1.0%, 1.5% and 2.0% XG respectively (Figure 25). By time-lapsed imaging, the foam's ageing process (gas diffusion across the liquid film, liquid drainage and film rupture) was recorded.

6.3.4 Thermosensitivity Studies

In vitro foam stability is commonly measured by foam volume stability (FVS) that reflects changes in a foam volume as the foam ages. FVS was studied over a period of 1 h. The foams were expelled into graded glass cylinders and the cylinders were immediately placed into a 38 °C water bath. Changes in FVS over time (Figure 26) showed that foam with lower concentration of XG (0.5%) is significantly less stable ($p < 0.05$) compare to the foams with higher concentrations of XG. The highest stability at the end of the study was found with the foam consisting of 1.5% XG (Figure 27).

6.3.5 Foam Rheology and Dynamic Measurements

The linear viscoelastic region, following where the structure of the foams remained intact, was studied to isolate the region of testing for the frequency sweeps (Figure 28). The elastic modulus, G' , describes the amount of energy stored in the

structure of the material during the oscillatory testing, as plotted in Figure 29. G' is a function of ω , the angular velocity. The elastic modulus is used for differentiating the materials since it provides a map of the behavior of the macrostructure of each formulation. The ranking of the observed G' of the formulations was: gel > foam (1.5% XG) > foam (2.0% XG) > foam (1.0% XG) > foam (0.5% XG). The foam with 0.5% XG had the lowest G' , suggesting that the flexibility of the formulation network was the weakest. On the other hand, the foam with 1.5% XG was highly elastic. The instantaneous viscosity (η) however, was reduced for all the formulations with increase in the applied shear stress (Figure 30). This reduction in viscosity with increase in shear stress was significantly more considerable for the gel formulation.

The point at which the flow changes from elastic deformation to plastic deformation is known as the yield stress. The yield stress of the foams was evaluated with the parallel plate sensor in controlled stress (CS) mode by gradually increasing the imposed shear stress and monitoring the deformation of the foams. At low stresses, the foam deformed elastically but did not break. At higher stresses, the yield stress was overcome and the material began to flow; the structure deformed plastically and irreversibly. Plotting the deformation (γ) and the applied stress (σ) showed a linear region for each of these flow systems (Figure 31). The yield stress values calculated by the software were 19.43, for the conventional gel and 25.77, 15.86, 7.33, and 3.43 for the 2.0%, 1.5%, 1.0% and 0.5% XG foams.

6.3.6 Loss on Drying

Loss on Drying represents residue remaining after all volatiles evaporated from the dried down formulation. Samples of the foams were placed in a 65 °C oven and

weighted at intervals. Loss on Drying and percentage residue was evaluated when constant weight was achieved (Table 8). Comparing loss on drying results using one way ANOVA analysis of variance showed no significant difference between the foams residues (Figure 32) suggesting that the same volume of the formulations with different concentrations of XG (0.5% to 2%) will produce the same volume of the foams.

6.3.7 *In vitro* Conjugate Release Study

FITC-PEG_{3.4kDa}-COOH was used as a model conjugate for studying the *in vitro* NC release from the foam and the conventional gel both containing 1.5% XG. In the assay, 500 μ l of the foam or gel was applied to the donor side of Transwell inserts (membrane pore size, 400 nm). At each time point (0.17, 0.5, 1, 2, 4, 6, 8, 24, 48 and 72 h) the amount of NC released to the receptive side of the Transwell (containing 1500 μ l phosphate buffer) was determined using a FITC-PEG standard curve. Plotting the cumulative release of FITC-PEG_{3.4kDa}-COOH over time yielded a release profile that started to plateau after 20 h (Figure 33). The release rate (% / h) was calculated from the initial linear slopes of the graphs (0 to 8 h). Release rate from the foam formulation (1.07% / h) was 4.6 fold faster than that of the gel formulation (0.23% / h). The absolute cumulative release (ng/cm^2) up to 8 h was not significantly different between the two formulations (Figure 34).

Non-specific adsorption of FITC-PEG_{3.4kDa}-COOH to the Transwell[®] polycarbonate membranes was investigated by a control experiment. Individual insert membranes were excised at the end of the release assay, quickly and thoroughly rinsed, cut into small pieces and individual membrane pieces were soaked in phosphate buffer for 24 h in dark while shaking. The amount of released NC was determined as explained

earlier. The amount of recovered NC was at the baseline level of detection (~ 0.05 ng/cm²). The non-specific adsorption of the NC was therefore negligible compare to its cumulative release from each formulation (175.96 ng/cm² for the foam and 496.22 ng/cm² for the gel).

6.3.8 *In Vivo* Characterization of Formulations using MRI

The Institutional Animal Care and Use Committee (IACUC) of Rutgers University approved the protocol of this animal study. Mice were fasted overnight and were anesthetized with isoflurane prior to formulation application and imaging. Before application of the test formulations, individual mice were scanned with MRI (control images). Then, about 100 μ l of the foams (0.5% to 2.0% XG), gel (1.5% XG) or saline enema was intrarectally applied and MRI scans were repeated every 10 min up to 1 h. Among all the formulations, the foam containing 1.5% XG showed the best coverage and intensity (an indication of foam breaking and concentrating on the mucosal membrane surface) in the rectum and the descending colon. The conventional gel only covered the rectal cavity with little expansion to the descending colon (data not shown). The saline enema expelled out of the rectum immediately after application and showed the weakest intensity in MRI scans (data not shown). The experiment was repeated with 1.5% XG foam for 2h (Figure 35 and 36). The foam was visible within 10 min but the intensity of the newly formed foam was low. The intensity of the foam images increased over time, producing a complete coverage inside the rectum and the descending colon (approximately 3.5 cm in height). All the imaging studies were repeated for at least 3 mice.

6.3.9 Colonic/Rectal Distribution of FITC-PEG_{3,4}-COOH-Loaded Foam Using a MS FX PRO System

Colonic/rectal distribution of the foam (1.5% XG) containing 5 μ M FITC-PEG_{3,4kDa}-COOH, as a model NC for small molecule drug-PEG conjugates, was investigated using an In Vivo MS FX PRO small animal imaging system that detects fluorescence signals. Mice were euthanized immediately after dose, 15, 30, 60, 120, 180 or 240 min post-dose and 7 cm of the lower intestine was removed and imaged. The conjugate immediately covered the rectum and the descending colon in a fairly uniform manner (Figure 37). Although the MS FX PRO system successfully demonstrated *ex vivo* colonic/rectal distribution of the NC-loaded foam, it was not able to detect the fluorescent signal *in vivo* in the whole body animals.

6.3.10 Mouse Colorectal Irritation test

There were no mortalities in any of the groups during the 1 day or the 5 days of once in a day application period. Clinical examination of the mice prior to each administration revealed no signs of anal or rectal irritation, discharge or bleeding for all the untreated control, foam or saline enema groups. Histological examination performed after one day of formulation application (Figure 38) showed that the epithelium of all the three groups was normal with crypts and goblet cells arranged in series. The histological examination of the group of 5 days of daily application showed the same normal results for the control and the saline enema group. For the XG (1.5%) foam group, occasional missing of crypts was observed in the histology samples (Figure 39). A small ulceration in one of the three mice was produced during dose application and it was not related to

the foam formulation. The severity of inflammation was graded normal to mild. Overall, the foam appeared safe but more studies are needed to confirm the safety.

6.4 Discussion

Hydrogel foams were successfully prepared using different concentrations of XG (0.5% to 2.0%). XG is a natural high molecular weight polysaccharide produced by fermentation of sugars^{177, 178}. Due to its exceptional rheological properties it is a very effective stabilizer for water-based systems¹⁷⁹. The formulations prepared for this study do not contain aliphatic alcohols, making them non-irritating and non-drying. Brij L23 was used as a non-ionic naturally derived surfactant with high foamability properties. Surfactant rearrangement has a major role in foam production¹³⁷. Once the foam expelled outside the canister, the surfactant must quickly rearrange to reduce the surface tension and stabilize the bubbles^{180, 181}. Surfactants with higher hydrophilic-lipophilic balance (HLB > 10) produce oil in water (o/w) systems and once ejected from the canister, their adsorption to air/water interface leads to the production of stable foam. In contrast, surfactants with lower HLB (< 10) produce a w/o system with a delay in surfactant partitioning into the aqueous phase before adsorption, therefore generating a quick-breaking foam. Having a high hydrophilic-lipophilic balance (HLB 16), Brij L23 produces stable foams.

The propellant generally is regarded as the “heart” of the aerosol package¹²⁷. The propellant not only supplies the necessary force to expel the product but it must also act as a solvent and diluent. For our purpose, propellant AP-70 consisting of propane (31%),

isobutene (23%) and n-butane (46%) was used to produce an aerosol internal pressure of 70 psi. Hydrocarbon propellants (eg. AP-70) have a greater range of solubility and a lower cost compare with HFC propellants, that are extremely poor solvents and will not dissolve a sufficient amount of surfactants ¹²⁷. Although the low toxicity of hydrocarbon propellants makes them biologically safe, their flammability used to limit their use. However with the development of newer types of dispensing valves, the flammability drawback has been reduced considerably. Hydrocarbons' extreme chemical stability makes them very resistant to hydrolysis thus useful with water-based aerosols.

All the produced foams after expelling from canisters were characterized as being three-dimensional, semi-solid creamy structures that did not readily flow away from dispensing area (Figure 24). The foams were quantified by light microscopy and the bubble sizes were within the normal range, which is 100 μm to 3 mm ¹⁴.

The foams stability and aging process were studied *in vitro* at 38 °C, which is close to the anorectal temperature ¹⁸². The most common way of determining foam stability is by measuring the changes of the foam column height in a graded glass cylinder as a function of time ^{183, 184, 185}. Percentage foam volume stability (FVS %) was studied over time. Arzhavitina et al. has defined the higher FVS values as a mark of higher foam stability ¹⁴. The foam containing 1.5% XG had the highest stability over the period of the study (Figure 27), suggesting the optimum concentration of XG to maintain the desired stability as the other components remained consistent in quantities for all the foams formulations.

Rheological properties of foams, such as elasticity, plasticity and viscosity, play major roles in foam production and applications ^{186, 187, 188}. Various experimental

techniques are used for characterization and analysis of foams deformation and flow. The macroscopic response to applied shear stress can be measured by rotational rheometers. Parallel plates with smooth surfaces has successfully been used for shear geometries¹⁸⁹. According to the rheological measurements, the XG foams displayed a shear-thinning behavior but this behavior was significantly more obvious in the gel formulation (Figure 30). This result may be a reason why intrarectal gel application *in vivo* was with significantly more discharge and leakage compare with when the foams were applied.

When subjected to a small shear strain, a foam behaves like an elastic material and the shear stress (σ) varies linearly with the strain (γ)^{126, 189}. In this linear regime, the foam bubbles are deformed but the applied stress is not strong enough to modify the topology of the bubbles packing. At higher stresses however, the yield stress is overcome and the foam material begins to flow. The strain at yield is an indication of the elasticity of the structure; more elastic structures will deform more before yielding. In our study, the foams exhibited a variety of strains for the yield point. However in general, foams with higher concentration of XG (1.5% to 2.0%) showed more flexibility with higher yields (Figure 31).

Magnetic resonance imaging (MRI) was selected as the method of choice for visualizing the *in vivo* dynamic process occurring after application of the formulations. MRI scans of the formulations were recorded with T2 mapping. Among all the formulations, the best colonic/rectal coverage and intensity was observed with the foam containing 1.5% XG. At the early MRI (dose to 10 min), when the foam still contained a high amount of propellant, the intensity of the foam image was low. At later time points when the propellant was released and the foam broke and condensed on the lower GI

tract inner wall, an increase in the intensity of the foam images was observed. Little discharge was observed over the time of the study whereas application of the gel (1.5% XG) or the saline enema resulted in significant or immediate discharge. The colonic/rectal distribution of the foam was confirmed when the 1.5% XG foam containing 5 μM FITC-PEG_{3.4kDa}-COOH was investigated with a MS FX PRO small animal imaging system. Both MRI and FX PRO images showed that the foam covers the entire rectum through the descending colon (a total 3.5 cm in length). Fluorescein isothiocyanate (FITC), is a well-known pH indicator and its fluorescence is significantly reduced below pH 7.0^{190, 191, 192}. Since the pH of the descending colon is mildly acidic, a lower fluorescence intensity of the foam images is expected where the foam is in contact with the GI wall secretions (Figure 37). Therefore, the images might have slightly underestimated homogenous distribution of the model NC inside the foam.

The colorectal irritation tests were carried out in mice both by macroscopic and microscopic examination of the exposed tissues at one day and five day time points after daily administration of the XG (1.5%) foam or saline enema. It was concluded that the single dose administration of the foam does not cause colorectal irritation and it is as safe as applying saline enema. Mild inflammation was observed in two mice after 5 days of application of the foam (once in a day). Overall, the foam was classified as non-irritating over the time of the study.

Release of the model PEGylated small molecule conjugate, FITC-PEG_{3.4kDa}-COOH, from the foam (1.5% XG) was compared with that of a conventional gel (1.5% XG). The intestinal mucus layer is a diffusional barrier as well as a physical barrier to the absorption of particles¹⁹³. It has been shown in our lab that a size restriction exists for the

transport of nanoparticles through intestinal mucin and microspheres larger than 500 nm in diameter could not diffuse through the mucin layer¹⁹⁴. Therefore, Transwell[®] polycarbonate membranes (400 nm pore size, 1.12 cm² membrane areas) were used to simulate the intestinal mucin mesh. This specific pore size was assumed to allow free flux of the model NC through the pores, but to exclude XG large molecules, which will be retained in the donor compartment. The average hydrodynamic radius of a 4 kDa PEG molecule has been measured as around 2.0 nm^{195, 196}. The release study was done at pH 7.4 since the pH of the rectal mucus layer is close to normal pH¹¹⁶. Percentage cumulative release relative to the initial amount was about 4.6 fold higher for the foam compared with that for the gel. The rate of release might have been underestimated with *in vitro* studies. Fourier transform infrared (FTIR) spectroscopy can be done in future studies to evaluate possible interactions between the nanoparticles and the excipients used in the formulation. The overall results suggest that the XG (1.5%) foam could be used as a thermosensitive drug delivery system for safe and fast colonic/rectal anti-HIV drug distribution (Figure 40).

7. SUMMARY AND CONCLUSION

Highly active antiretroviral therapy (HAART) is effective in suppressing HIV replication and restoring CD4⁺ T cell numbers in peripheral blood and has contributed to a significant decrease in morbidity and mortality of HIV-infected patients. However, HAART has failed to eradicate viral reservoirs that have been established early in infection, leading to viral persistence and incomplete immune restoration. There is a growing interest in alternative HIV preventative strategies. Clinical trial data suggest that topical application of HIV drugs through the vaginal and rectal tracts are superior over oral PrEP in preventing sexual transmission. The gut-associated lymphoid tissue (GALT) harbors the majority of the body's lymphoid tissue and is an important site for host-pathogen interactions. Moreover, the greatest number of isolated lymphoid follicles, which contain abundant number of antigen presenting cells and activated T cells, are found in rectum. This condition creates the perfect environment for HIV-1 infection. Currently, there is no ideal drug delivery system to eradicate the early viral founder population in the mucosa. An ideal delivery system must fulfill the following criteria: ease of use, homogenous spread over the intended mucosal area and sustained release of anti-HIV drug(s) in the mucosa. Preferably, the anti-HIV drug should also result in the delivery to the mucosal draining lymph nodes that are considered one of the important HIV sanctuaries and possess the capability of enhanced retention of drugs in target cells.

Non-releasable APV-PEG conjugates were prepared with different sizes of PEGs and protease inhibition properties were assessed in buffer using a FRET-based protease inhibition assay. The results suggested that PEG sizes within 2 to 5 kDa (average 3.5 kDa) is the optimum range for maintaining anti-viral activity. For further *in vitro* studies, an APV-PEG conjugate was prepared using a 3.4 kDa PEG and the anti-HIV-1 activities were assessed based on the potency of the conjugates to inhibit syncytium formation in HIV-1 infected CD4⁺ MT-2 T-cells. Compare with free APV ($IC_{50} = 50.29$ nM), 160-fold drop was observed in APF activity ($IC_{50} = 8064$ nM) suggesting poor cell-penetration.

When the PEGylated APV was conjugated with a 10 amino acid residue batenecin 7 cell-penetrating peptide (Bac7 CPP), the resultant conjugate exhibited an anti-viral potency in T cells ($IC_{50} = 78.29$ nM) close to APV potency ($IC_{50} = 50.29$ nM). Therefore, the loss of cell penetration of the PEGylated conjugate was remedied by conjugating the Bac7 CPP.

For colonic/rectal anti-HIV drug delivery, alcohol-free thermosensitive aerosol foams containing 0.5% to 2.0% of xanthan gum (XG) were prepared. The foam with 1.5% XG showed the best performance among all the formulations. It contained small bubble size, good network flexibility and high elasticity. The foam was stable at room temperature over 2 h and percentage residual volume after all volatiles was evaporated was less than 10%. *In vivo* MRI of mice lower GI showed very good colonic/rectal distribution of the foam with little discharge compare to when saline enema or a conventional XG gel was applied. Histology of the colorectal tissue following daily application of the 1.5% XG foam for 5 consecutive days showed no significant inflammation in the intended mucosa. In summary, alcohol-free thermosensitive foam

drug delivery systems were developed for colonic rectal delivery of anti-HIV drugs and nonparticles.

Suggested directions for future studies are:

1. To increase the load of anti-retroviral (ARV) drugs by using branched PEGs or other nanoparticle (NP) platforms. By using hydrolysable linkages, sustained release of the ARVs could be achieved.
2. To covalently cover ARV-loaded NPs with short PEG chains with terminal cell-penetrating peptides or targeting moieties.
3. To incorporate magnetic contrast agents and fluorescent tags into the NPs developed at step two as imaging labels and load the NPs into foam concentrates.
4. To study the NP performance as well as lymphatic distribution using confocal and/or fluorescence detection, MRI and histochemistry after vaginal or rectal administration of the foam.
5. To evaluate the efficacy of the NP-loaded foams in HIV prevention first in ex-vivo rectosigmoidal HIV tissue models and then in humanized HIV transmission animal models.

Table 1. Contribution of different HIV transmission routes to global HIV infections

HIV Invasion Site	Anatomical sub-location	Type of epithelium	Transmission medium	Transmission probability per exposure event	Estimated contribution to HIV cases worldwide
Female genital tract	Vagina	Squamous, non-keratinized	Semen	1 in 200 – 1 in 2000	12.6 million
	Ectocervix	Squamous, non-keratinized			
	Endocervix	Columnar, single layer			
	Other	Various epithelia			
Male genital tract	Inner foreskin	Squamous, poorly keratinized	Cervicovaginal and rectal secretions and desquamations	1 In 700 – 1 in 3000	10.2 million
	Penile urethra	Columnar, stratified			
	Other	Various epithelia			
Intestinal tract	Rectum	Columnar, single layer	Semen	1 in 20 – 1 in 300	3.9 million
	Upper GI tract	Various epithelia		1 in 2500	1.5 million
Placenta	Chronic villi	Two layer epithelium	Maternal blood	1 in 10 – 1 in 20	480000
Blood stream			Blood products, Sharps	95 in 100 – 1 in 150	2.6 million

Table modified from references 7 and 8.

Table 3. FDA-approved PEGylated drugs

Commercial name	Drug name	Company	PEG size (Da)	Indication	Year of approval
Adagen [®]	Pegadamasase	Enzon	Multiple linear 5000	SCID	1990
Oncaspar [®]	Pegaspargase	Enzon	Multiple linear 5000	Leukemia (ALL, CML)	1994
PEG-INTRON [®]	Peginterferon- α 2b	Schering-Plough	Linear 12,000	Hepatitis C	2000
PEGASYS [®]	Peginterferon- α 2a	Hoffman-La Roche	Branched 40,000	Hepatitis C	2001
Neulasta [®]	Pegfilgrastim	Amgen	Linear 20,000	Neutropenia	2002
Somavert [®]	Pegvisomant	Pharmacia & Upjohn	4–6 linear 5000	Acromegaly	2003
Macugen [®]	Pegaptanib	Pfizer	Branched 40,000	Age-related macular degeneration	2004
Mircera [®]	mPEG-epoetin- β	Hoffman-La Roche	Linear 30,000	Anemia associated with chronic renal failure	2007
Cimzia [®]	Certolizumab pegol	UCB	Branched 40,000	Reducing signs and symptoms of Crohn's disease	2008
Puricase1 [®] /Krystexxa [®]	PEG-uricase	Savient	10,000	Gout	2010

Table modified from Alconcel, S.N.S. (2011)³¹ and Li, W. (2012)⁶⁰.

SCID: severe combined immunodeficiency disease; ALL: acute lymphoblastic leukemia; CML: chronic myeloid leukemia; GH: growth hormone

Table 4. PEGylated small molecular drugs conjugates in clinical trials

PEG conjugates	Trade name	Company	PEG size (kDa)	Indication	Stage of development
PEG-naloxol	NKTR-118	Nektar	Linear PEG	Opioid-induced constipation	Phase III
PEG-irinotecan	NKTR-102	Nektar	4-Arm PEG	Solid tumor	Phase III/II
PEG-SN38	EZN-2208	Enzon	4-Arm PEG	Solid tumor	Phase II
PEG-docetaxel	NKTR-105	Nektar	4-Arm PEG	Solid tumor	Phase I

Table redrawn from Li, W. (2012)⁶⁰.

Table 5. Examples of commonly used CPPs and AMPs and their proposed mechanisms

Name	Sequence	Structure	Proposed mechanisms
<i>AMPs</i>			
Pyrrhocoricin	VDKGSYLPRPTPPRPIYNRN ^b	Random coil/reverse turns at the termini	Receptor-mediated
Lactoferricin (hLF peptide)	VSQPEAT KCFQWQRNMRKVRGPPVSCIKR DSPIQI ^b GRRRRSVQWCA	β -Turn/loop	Direct penetration/pore formation
Bac7 (Bac7 1–24)	RRIRPRPRLPRPRPLPFPRPGPRPIRPLPF PRPGPRPIRPLPFPRPGPRPIRP	Hybrid of PPII helix and α -helix	Receptor-mediated/pore formation
PG-1 (SynB1)	RGGRLCYCRRRFCVVCVGR (RGGRLSYSRRRFSTSTGR)	Cationic, amphipathic antiparallel β -sheet	Endocytosis/pore formation
LL-37	LLGDFFRKSKEKIGKEFKRIVQRIKDFLRNLP RTES ^b	α -Helical	Pore formation
Buforin II (BF2d)	TRSSRAGLQFPVGRVIIRLLRK TRSSRAGLQWPVGRVIIRLLRKGGC	Extended amphipathic, α -helical*	Direct penetration
<i>CPPs</i>			
sC18	GLRKRLRKFRNKIKEK	Amphipathic, α -helical	Endocytosis
Tat (48–60)	GRKKRRQRRRPPQ	Random coil/PPII helix*	Direct penetration/ pore formation
Penetratin	RQIKIWFQNRRMKWKK	Amphipathic, α -helical*/ β -sheet (higher conc.)	Direct penetration/ endocytosis
pVEC	LLILRRRIRKQAHASK	Amphipathic, β -sheet*	Direct penetration/ transporter-mediated
Pep-1	KETWWETWTEWSQPKKRKY	Amphipathic, α -helical*	Direct penetration/ pore formation
Transportan (TP10)	GWTLNSAGYLLGKINKALAALAKKIL	Amphipathic, α -helical	Endocytosis/ direct penetration
MAP	KLALKLALKALKAAKLA	Amphipathic, helical	Multiple mechanisms

Table modified from Splith, K. ⁹⁴ (AMPs: antimicrobial peptides, CPPs: cell-penetrating peptides)

* Present at high lipid-to-peptide ratio conditions

When bolded, the listed sequence also includes neighboring dispensable sequence

Table 6. Anti-HIV-1 activity of APV-PEG conjugates in buffer using FRET assay

APV Compound^a	Mean Rate Constant* (k_{obs}, min^{-1})	[APV]_{app} (μM)	HIV-1 Protease Inhibition (%)
Free APV (positive control)	-0.057	3.30	100
PEG _{2kDa} -APV-OH	-0.097	1.73	52
PEG _{5kDa} -APV-OH	-0.101	1.68	49
PEG _{10kDa} -APV-OH	-0.136	1.12	30
PEG _{30kDa} -APV-OH	-0.170	0.80	21
APV-Oacetyl (negative control)	-0.289	0.28	6
PEG _{10kDa} -APV-Oacetyl (negative control)	-0.301	0.25	3

^a All APV compounds tested in the protease inhibition assay contained 3.5 μM APV equivalents

*The k_{obs} in absence of an inhibitor was -0.303 min^{-1}

Table 7. Foam Concentrates with Different Xanthan Gum Concentrations

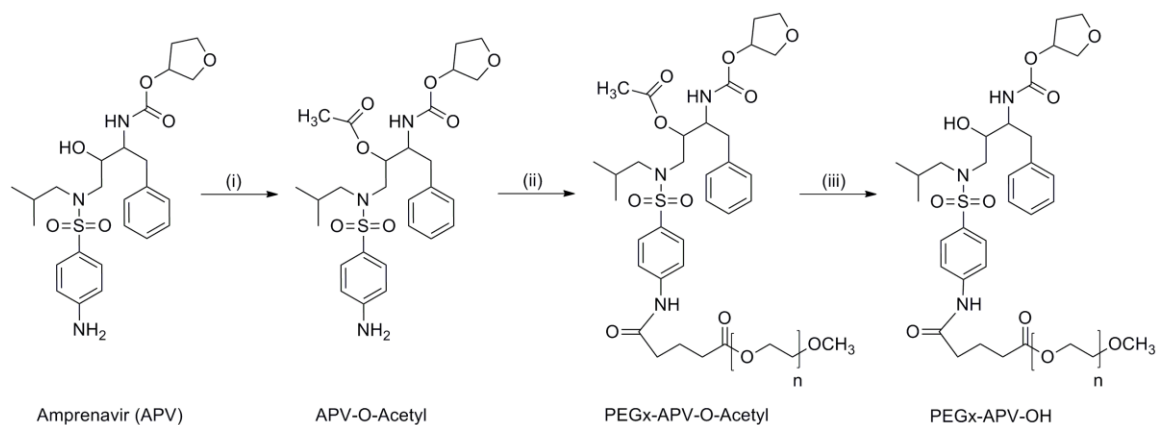
Ingredient	Function	% w/w			
Purified Water	Solvent for aqueous phase	94.38	93.88	93.38	92.88
di-sodium EDTA	Chelating agent	0.55	0.55	0.55	0.55
Xanthan gum	Foam stabilizer, natural Polymer	0.5	1.0	1.5	2.0
Brij L23	Surface active agent	4.35	4.35	4.35	4.35
Methyl-hydroxybenzoate	Antioxidant, preservative	0.22	0.22	0.22	0.22
Aerosol Base ^a		100	100	100	100

a. AP-70 (hydrocarbon propellant) was added later at 7% (w/w)

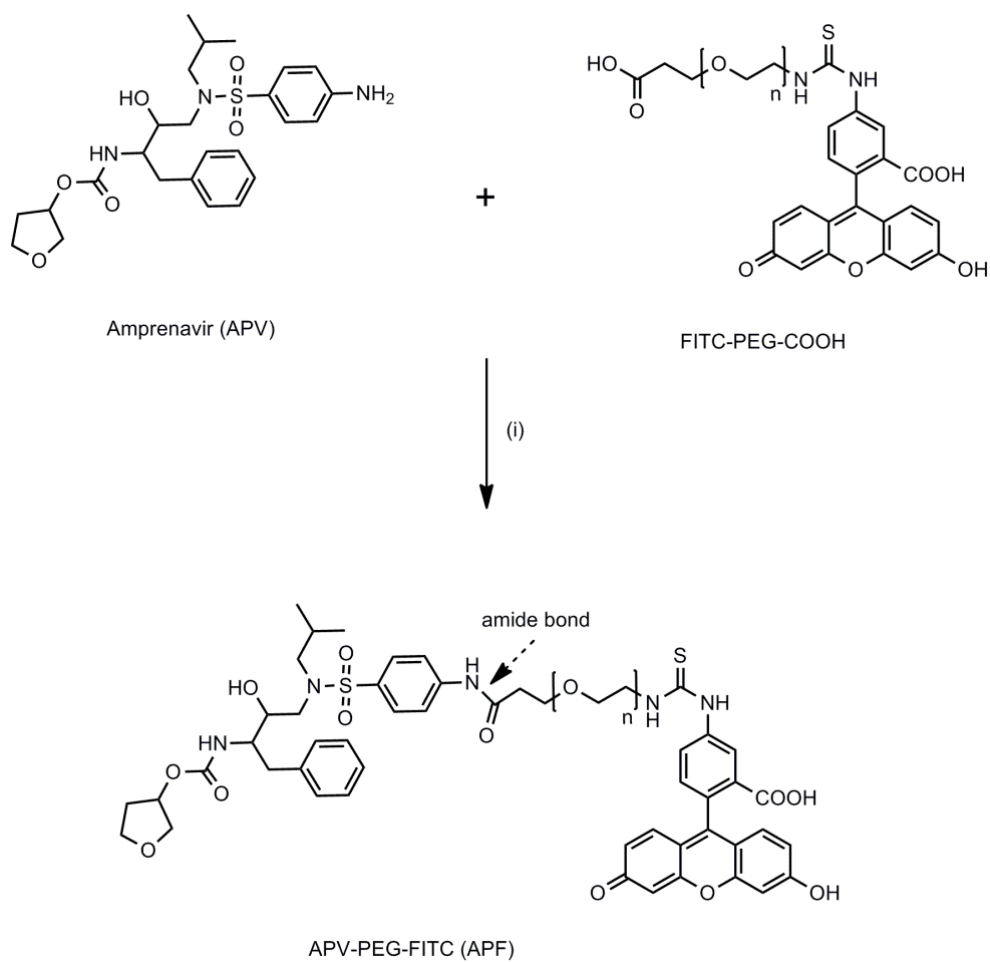
Table 8. Residue Levels for Different Formulations

Formulation #	Xanthan Gum (%)	Loss on Drying (%)	Residue (%)
1	0.5	94.58	5.42
2	1.0	94.56	5.44
3	1.5	93.36	6.64
4	2.0	93.07	6.93

Loss on drying and percentage residue was measured after all volatiles evaporated from the dried down foams.

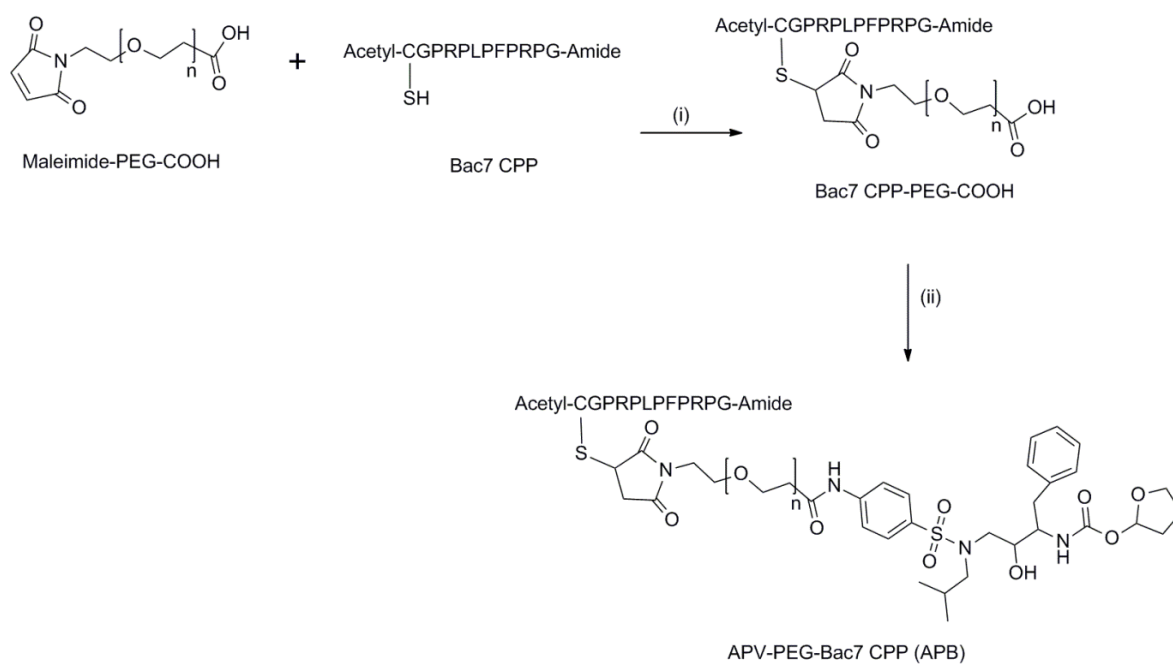
**Scheme 1. Synthesis of PEG_x-APV-O-acetyl and PEG_x-APV-OH conjugates**

Reagents and conditions: (i) DMF, DIPEA, acetic anhydride, room temperature, 12 h; (ii) DMF, DIPEA, mPEG_x-NHS ($x = 2, 5, 10, 30$ kDa), room temperature, 24 h; and (iii) 0.1 N HCl, neutralized with NaHCO₃.



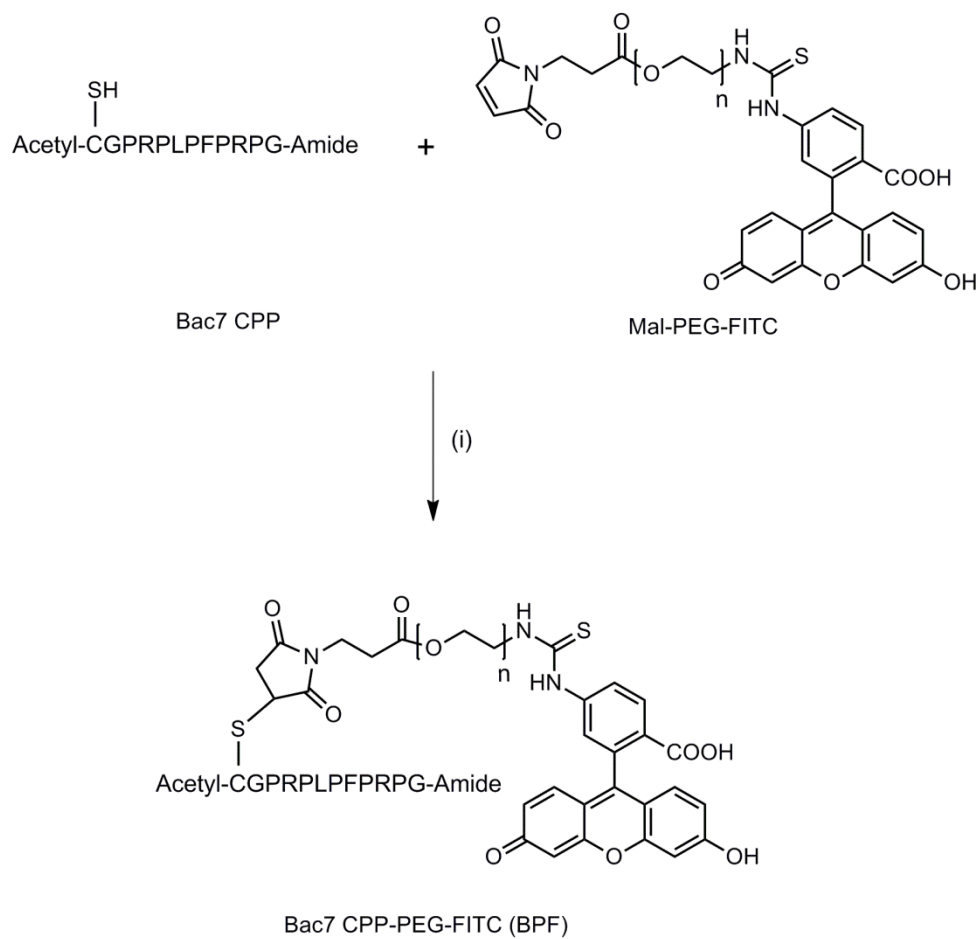
Scheme 3. Synthesis of Fluorescein-Labeled Amprenavir-PEG Conjugate (APF)

The amino moiety on the aniline group of APV was reacted with a FITC labeled PEG_{3.4kDa} via a stable amide bond. (a): DMF containing WSC and HOAt, room temperature, 16 h.



Scheme 5. Synthesis of APV-PEG-Bac7 CPP (APB)

The cell penetrating peptide, Bac7 CPP, was linked to maleimide-PEG_{3,4}-COOH via a thioether bond. APV was linked to Bac7 CPP-PEG_{3,4}-COOH via an amide bond. Reagents and conditions: (i) DMF, room temperature, 4 h. (ii) DMF containing WSC and HOAt, room temperature, 16 h.



Scheme 6. Synthesis of fluorescein-labeled PEG-Bac7 CPP (BPF)

The FITC labeled PEG_{3,4kDa} was reacted to Bac7 CPP via a stable thioether bond. (i) DMF, room temperature, 4 h.

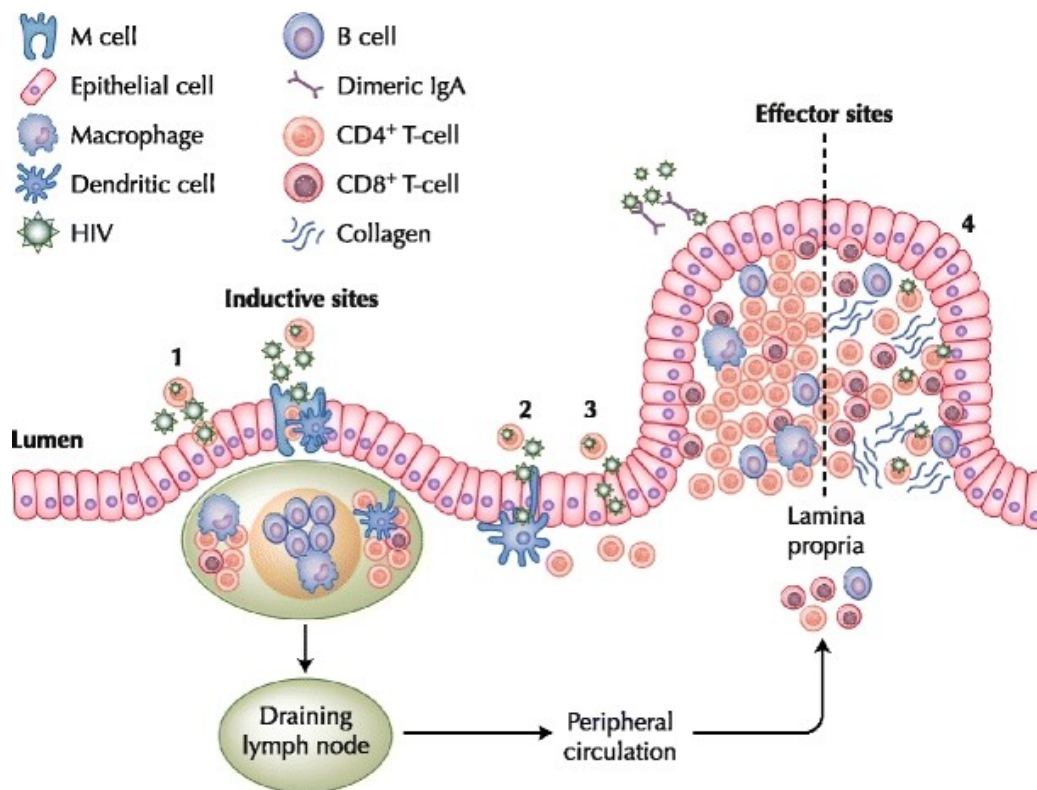


Figure 1. HIV Infection and Gut Mucosal Immune Function

HIV may cross the epithelium and initiate infection (1) by transcytosis across intact epithelial cells or M cells; (2) by adhering to dendrites of mucosal dendritic cells; or (3) by direct passage through epithelial breaches. Intestinal CD4⁺ T cells (in both inductive and effector sites) are rapidly infected and depleted during acute HIV infection. The figure also illustrates some consequences of HIV infection on mucosal integrity (4)⁹. Tight junctions in the intestinal epithelium are compromised. The lamina propria loses most of its CD4⁺ T cells but gathers an influx of CD8⁺ T cells. Collagen deposition occurs and may hinder reconstitution of CD4⁺ T cells.

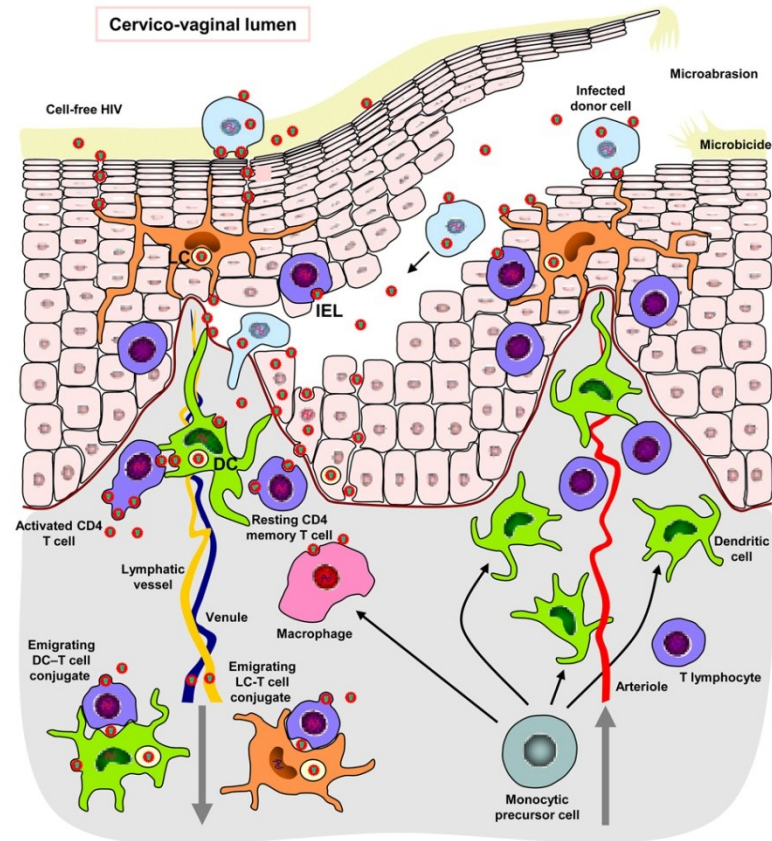


Figure 2. HIV Transmission Through Vaginal Mucosa

Cell-free and cell-associated HIV-1 penetrates the cervicovaginal epithelium through microabrasions and/or intact tissue. LC: Langerhans cells, IEL: intraepithelial CD4⁺ T lymphocytes, DC: dendritic cells²⁹.

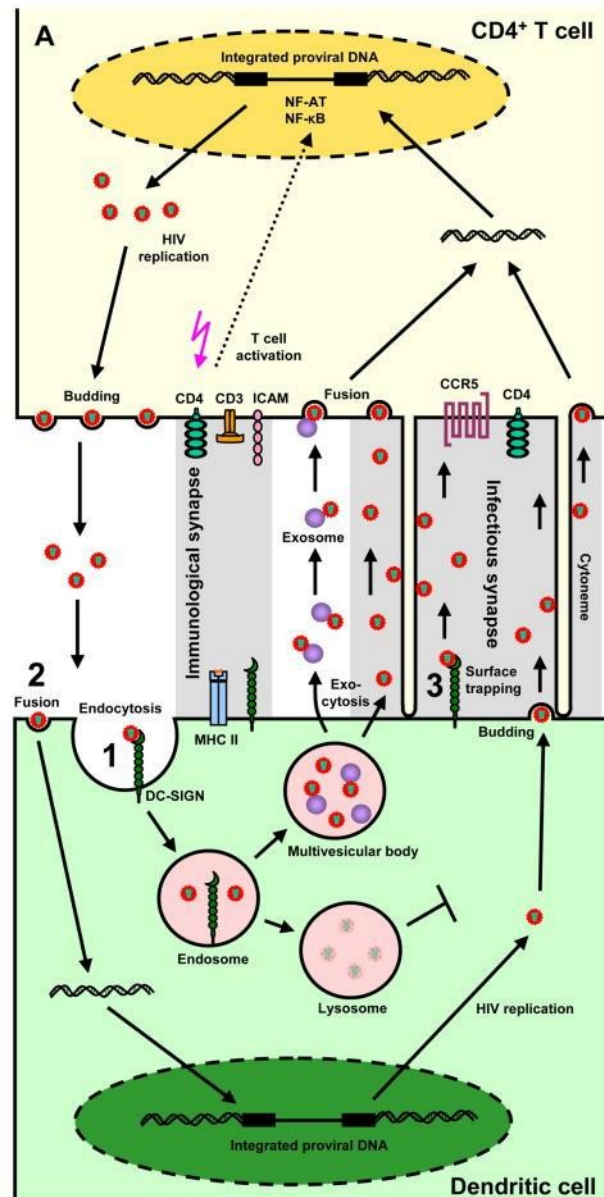


Figure 3. Pathways of HIV-1 passage between dendritic cells (DCs) and T cells

DCs can store HIV-1 in three forms for eventual infection of CD4⁺ T cells: (1) endocytosed intact virions, (2) integrated provirus and, (3) surface-bound intact virions. Passage of HIV-1 from DCs to CD4⁺ T cell occurs most effectively across an infectious synapse, formed by concentration of HIV-1 on the DC side and of HIV receptors such as CD4 and CC-chemokine receptor 5 (CCR5) on the T cell side. The DC also presents antigenic peptides through MHC class II molecules to the T-cell receptor CD3. Signals delivered through the immunological synapse lead to T-cell activation, which ultimately causes transcription factors such as nuclear factor- κ B (NF- κ B) and nuclear factor of activated T cells (NFAT) to translocate into the nucleus of the T cell. There, they bind to the enhancer region of the viral long terminal repeat (LTR) and activate viral gene transcription, driving HIV-1 replication⁷.

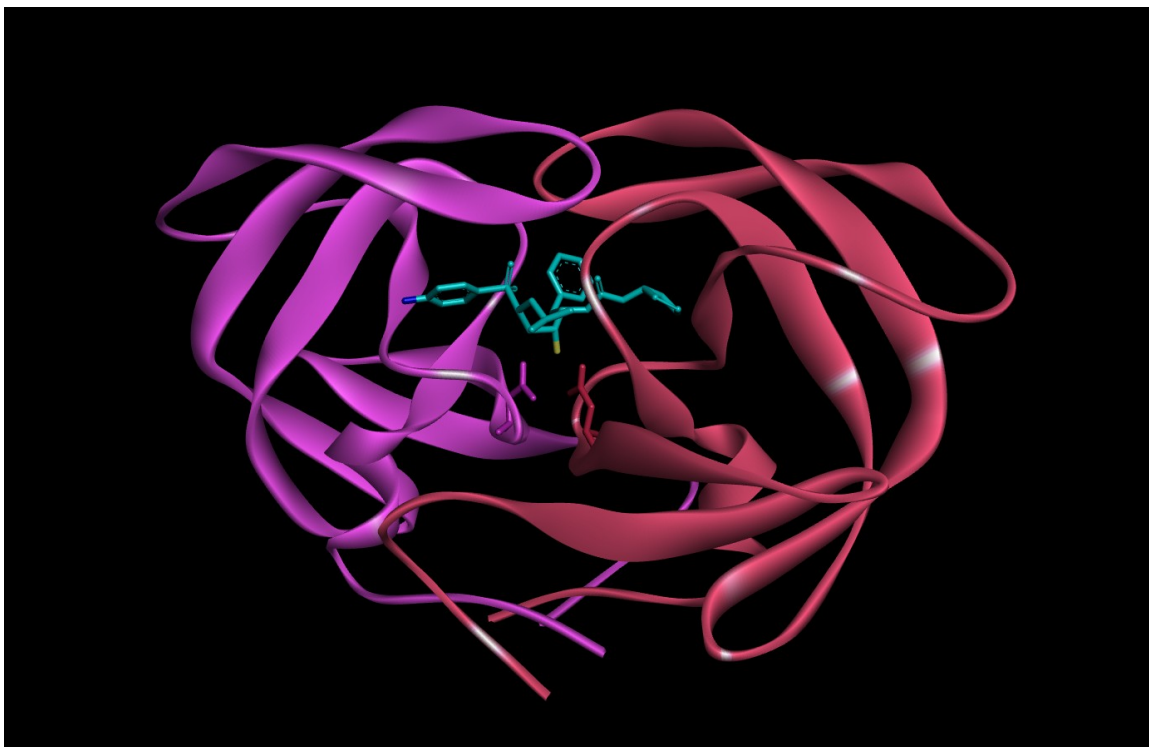


Figure 4. Molecular modeling of amprenavir interactions with HIV-1 protease

Amprenavir is bound in the active site of the HIV protease dimer. Monomers are colored magenta and red. Amprenavir is colored blue. Free hydroxyl group in amprenavir (yellow) is required to interact with the active site of the enzyme while amino group (dark blue) in the aniline moiety stands out.

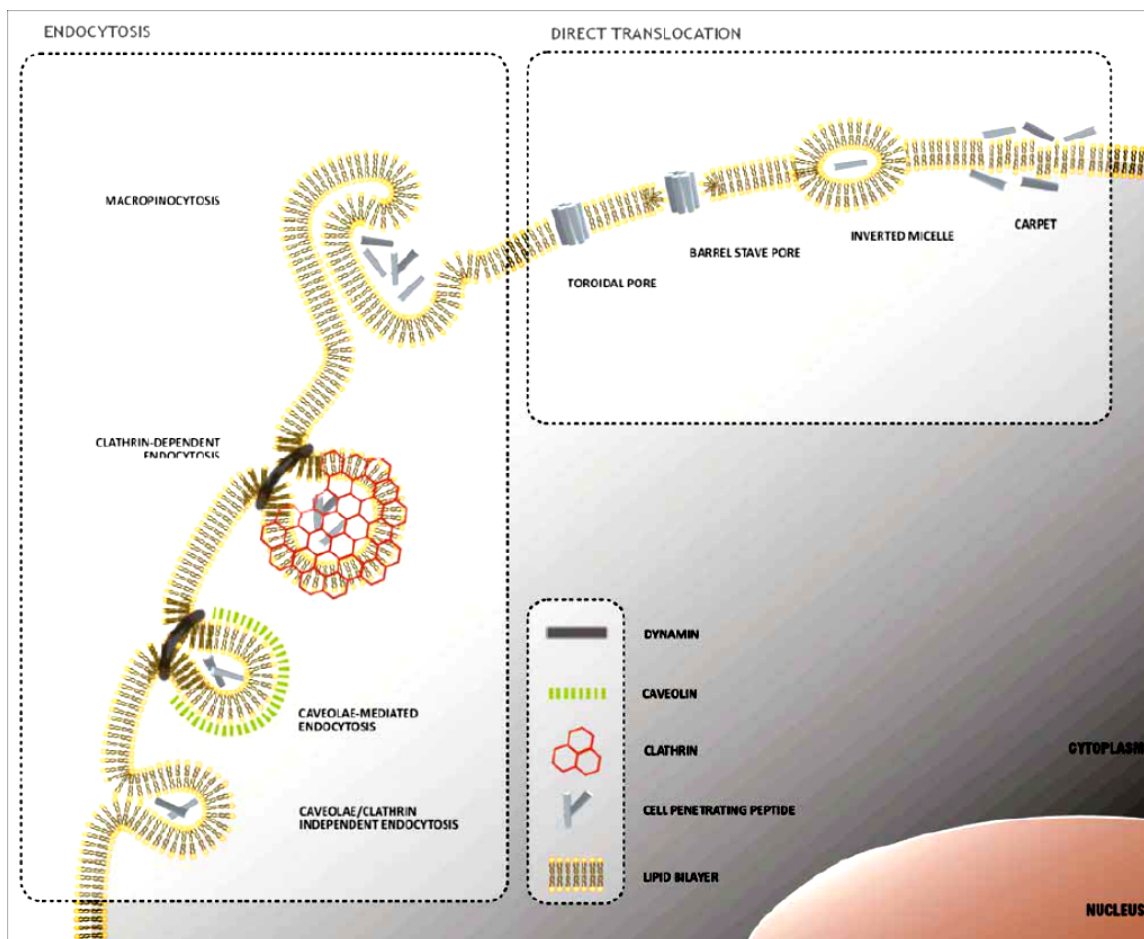


Figure 5. proposed mechanisms to explain cellular uptake of cell-penetrating peptides

A variety of internalization mechanisms have been proposed to explain cellular uptake of CPPs. These mechanisms include well-characterized energy-dependent pathways, based on vesicle formation (endocytosis), and direct translocation or cell penetration, which involve the formation of hydrophilic pores or local destabilization of the lipid bilayer⁹⁹.

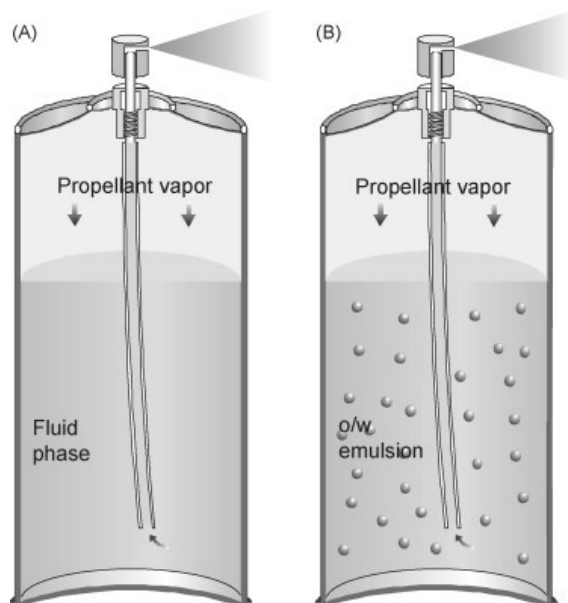


Figure 6. Types of Aerosol Foams

In two-phase systems (A) the liquefied propellant is solved in the solution of a foaming agent under pressure. In this case, the aerosol canister contains a continuous liquid and a gas phase. The liquid phase consists of the foam concentrate and partially dissolved propellant, whereas the gas phase is composed of propellant vapor. Three-phase systems represent an o/w or w/o emulsion (B). The propellant is solved in the lipid phase, which is emulsified with a water phase through addition of an emulsifier. The third phase is the vapor phase of the propellant over the emulsion. Both two-phase and three-phase systems should be shaken before application¹⁴.

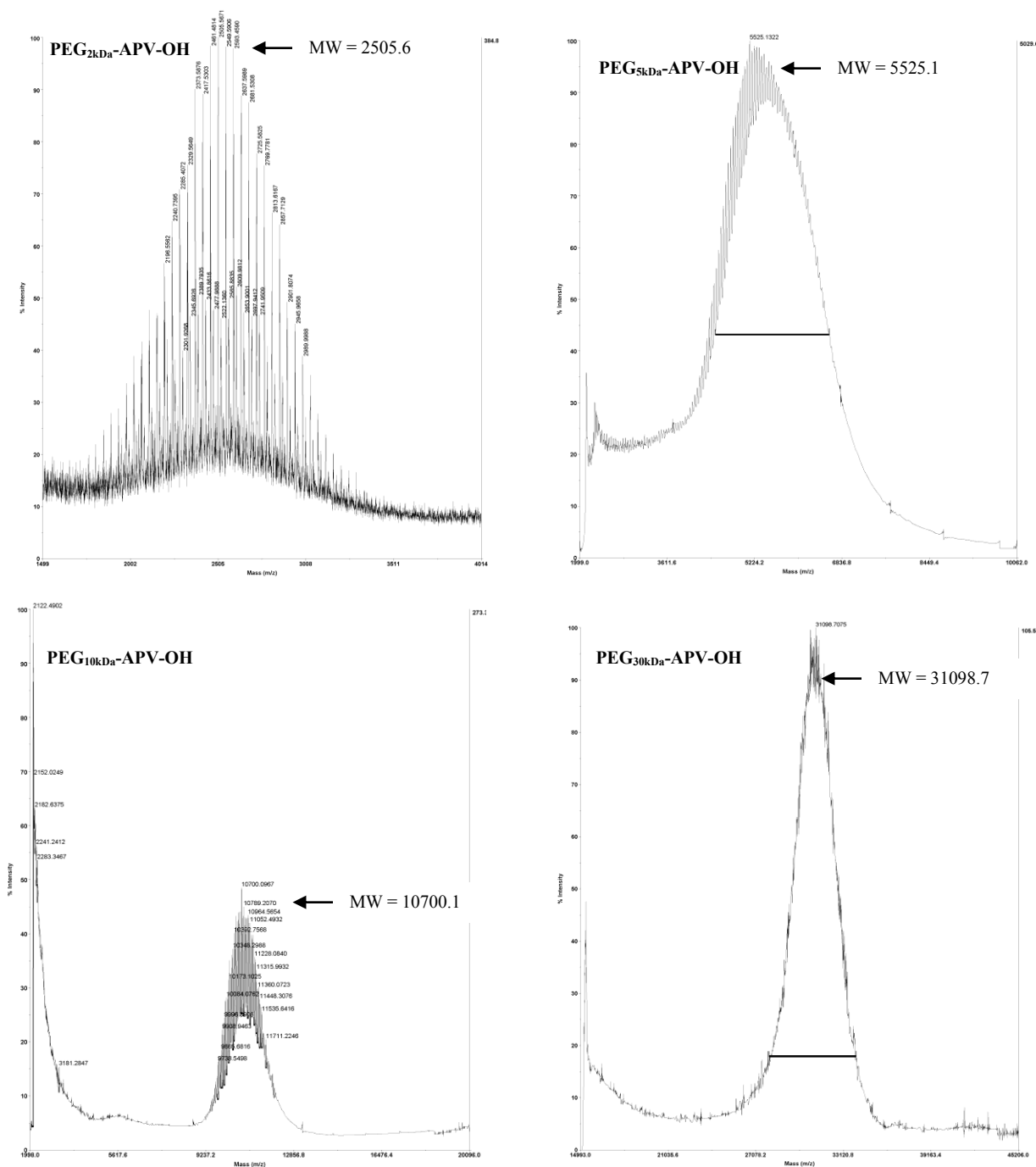


Figure 7. MALDI-TOF-MS (m/z) profiles of purified PEG-APV conjugates

The peaks showing molecular weights at 2505.6, 5525.1, 10700.1 and 31098.7 Da confirm successful reaction of aromatic amino terminus of APV with respective 2, 5, 10 and 30 kDa PEGs.

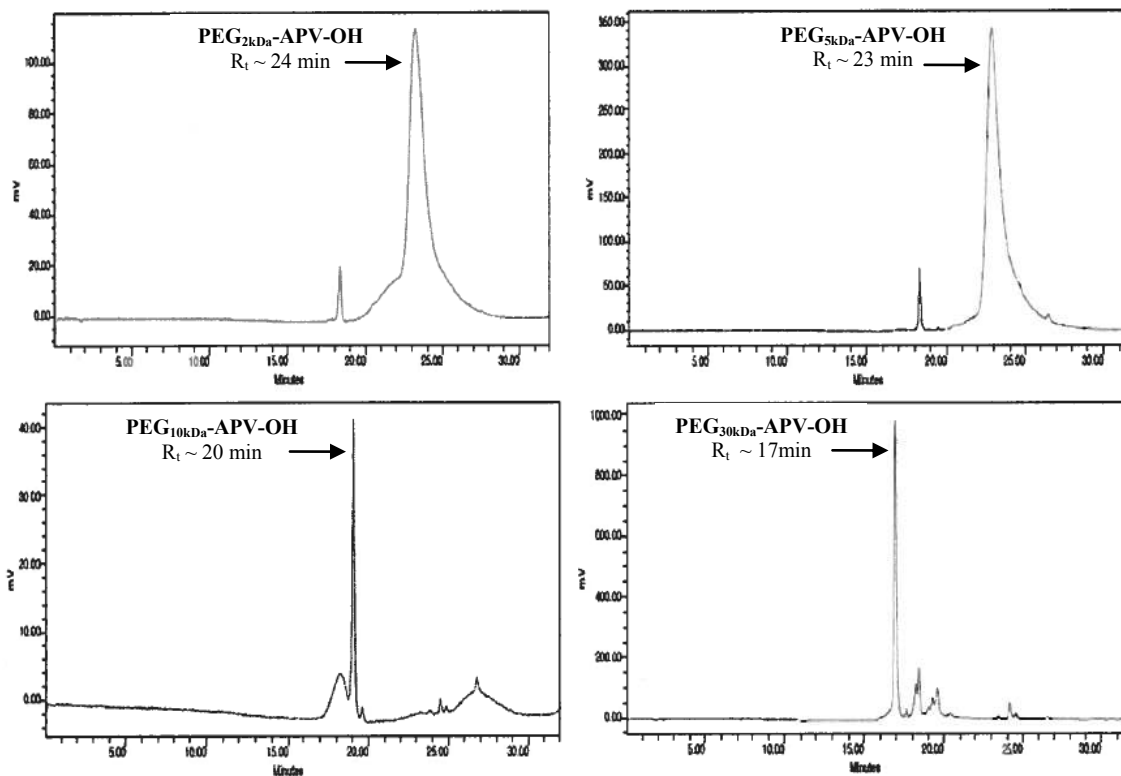


Figure 8. HPLC of PEG-APV conjugates

Size-exclusion chromatographic profile of purified PEG_X-APV-OH (X = 2, 5, 10 and 30 kDa) conjugates shows decrease in retention time with increase in PEG size.

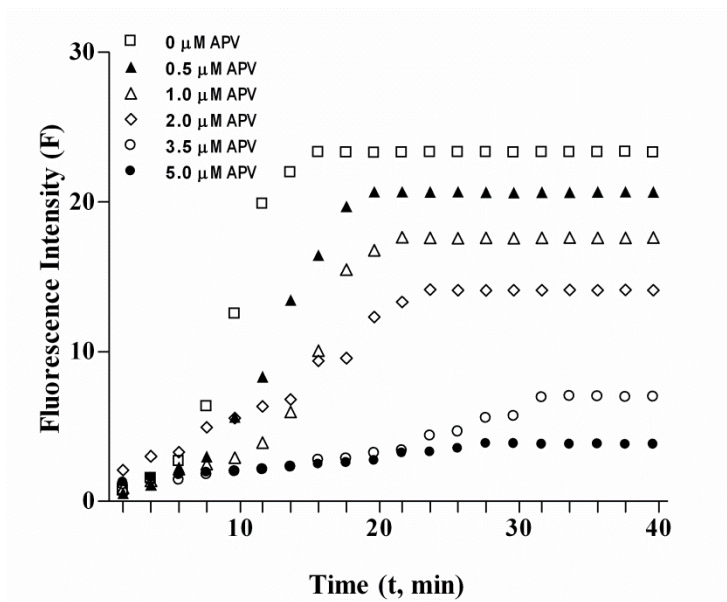


Figure 9. Cleavage kinetics of HIV-1 protease peptide substrate

Cleavage kinetics of HIV-1 protease FRET peptide substrate (5.0 μM) by recombinant HIV-1 protease (35.2 nM) was determined at 37 $^{\circ}\text{C}$ in the assay buffer in the presence of different APV concentrations (0.5–5.0 μM). All measurements were performed in triplicate and reported as mean \pm SD ($n = 3$). The effect of APV 3.5 μM and 5.0 μM was not significantly different ($p > 0.05$).

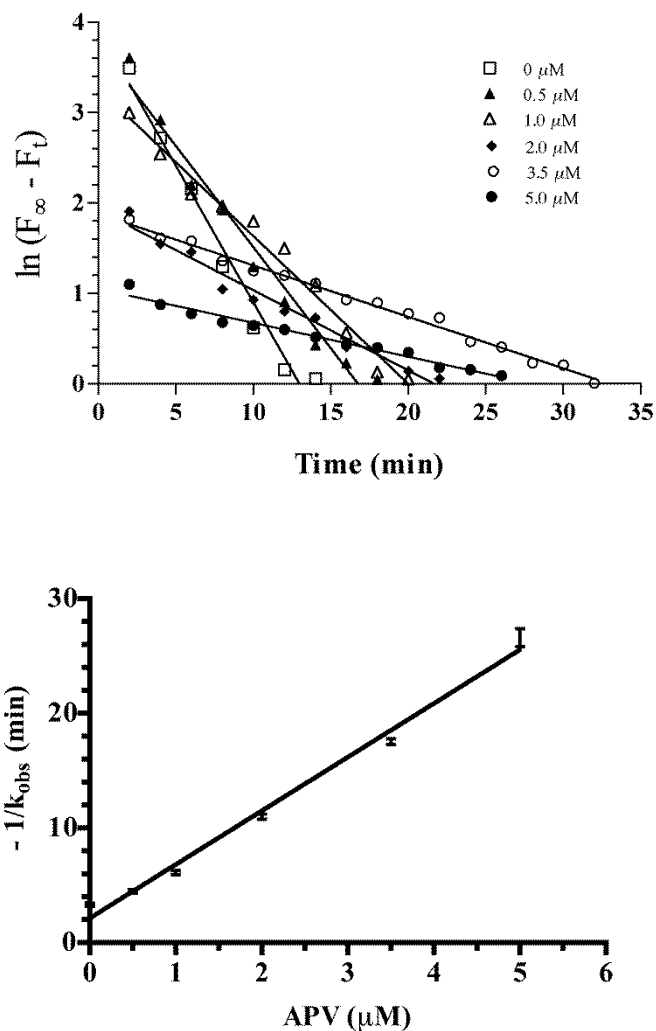


Figure 10. Determination of anti-HIV-1 activity of APV (0 – 5 μM)

Top: Plots of $\ln(F_{\infty} - F_t)$ vs. time for APV (0-5 μM) were prepared using the data obtained from Figure 9. F_{∞} is the maximum fluorescence intensity (0 μM of APV) and F_t is fluorescence intensity at time t (min). Linear regression analysis yielded straight lines ($R^2 \geq 0.9711$) and the slope of each line yields the rate constant (k_{obs} , min^{-1}). k_{obs} values: $-0.3027 (\pm 0.02341)$ for 0 μM , $-0.2239 (\pm 0.01459)$ for 0.5 μM , $-0.1638 (\pm 0.007995)$ for 1.0 μM , $-0.0890 (\pm 0.004938)$ for 2.0 μM , $-0.05704 (\pm 0.00144)$ for 3.5 μM , and $-0.03766 (\pm 0.00191)$ for 5.0 μM .

Bottom: Plot of negative reciprocal of observed rate constant [$-1/(k_{\text{obs}})$] vs. APV concentrations. The [$-1/(k_{\text{obs}})$] value increased with APV concentration in a linear manner ($R^2 = 0.9858$) which reflects the anti-HIV-1 protease activity of APV or an APV-PEG conjugate. This figure was used to derive the apparent APV concentration (APV_{app}) values for APV and each APV-PEG conjugate, all at 3.5 μM . The APV_{app} value was used as an indicator of anti-HIV-1 protease potency to compare APV with different APV-PEG conjugates (cf. Table 6).

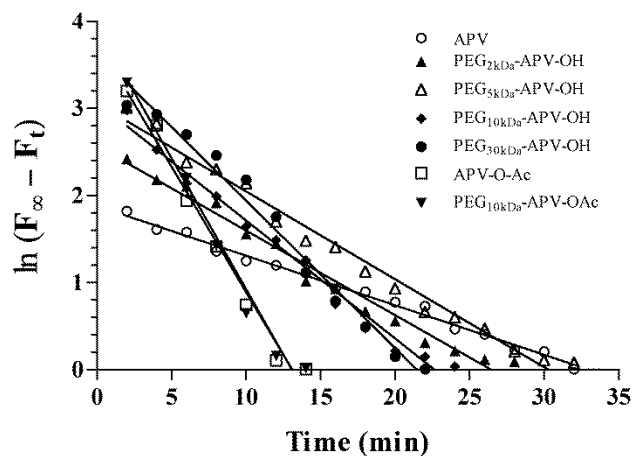


Figure 11. Plots of $\ln(F_{\infty} - F_t)$ vs. time for PEG-APV conjugates

Plots of $\ln(F_{\infty} - F_t)$ vs. time were for APV, PEG-APV conjugates and the two negative controls, all at $3.5\mu\text{M}$ APV-equivalent concentrations. Linear regression yielded straight lines ($R^2 \geq 0.9655$) and the slope of each line yields the rate constant (k_{obs} , min^{-1}). The k_{obs} values are: $-0.05704 (\pm 0.001439)$ for APV, $-0.09743 (\pm 0.004131)$ for $\text{PEG}_{2\text{kDa}}\text{-APV-OH}$, $-0.1011 (\pm 0.003616)$ for $\text{PEG}_{5\text{kDa}}\text{-APV-OH}$, $-0.1358 (\pm 0.005545)$ for $\text{PEG}_{10\text{kDa}}\text{-APV-OH}$, $-0.1695 (\pm 0.008027)$ for $\text{PEG}_{30\text{kDa}}\text{-APV-OH}$, $-0.2886 (\pm 0.01815)$ for APV-O-Ac, and $-0.3013 (\pm 0.02051)$ for $\text{PEG}_{10\text{kDa}}\text{-APV-O-Ac}$. The k_{obs} values were converted to $[-1/(k_{\text{obs}})]$ that were fitted into the linear regression equation derived from Fig. 10 (bottom) to yield the apparent APV concentration (APV_{app}) values for APV and APV-PEG conjugates. APV_{app} values (μM): $3.288 (\pm 0.095)$ for APV, $1.737 (\pm 0.093)$ for $\text{PEG}_{2\text{kDa}}\text{-APV-OH}$, $1.678 (\pm 0.109)$ for $\text{PEG}_{5\text{kDa}}\text{-APV-OH}$, $1.117 (\pm 0.064)$ for $\text{PEG}_{10\text{kDa}}\text{-APV-OH}$, $0.804 (\pm 0.060)$ for $\text{PEG}_{30\text{kDa}}\text{-APV-OH}$, $0.285 (\pm 0.047)$ for APV-O-Ac, and $0.254 (\pm 0.049)$ for $\text{PEG}_{10\text{kDa}}\text{-APV-O-Ac}$.

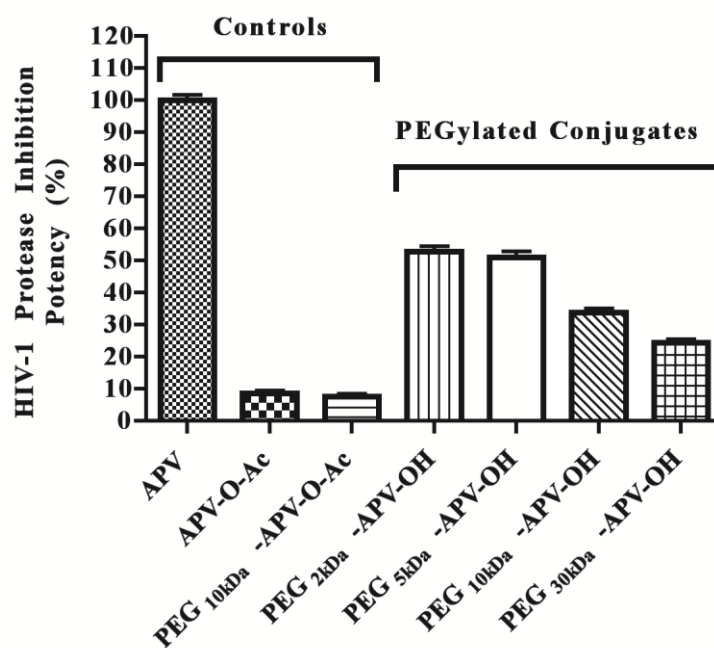


Figure 12. Effect of PEG size on the HIV-1 protease inhibition potency of APV-PEG conjugates

All compounds were tested at APV-equivalent concentration of $3.5 \mu\text{M}$. The potencies expressed as the apparent APV concentrations (APV_{app}) derived from figures 10 and 11 were referenced to the potency of APV (the APV reference being 100% potent). There was no significant difference between the potency of $\text{PEG}_{2\text{kDa}}\text{-APV-OH}$ and $\text{PEG}_{5\text{kDa}}\text{-APV-OH}$ ($p > 0.05$).

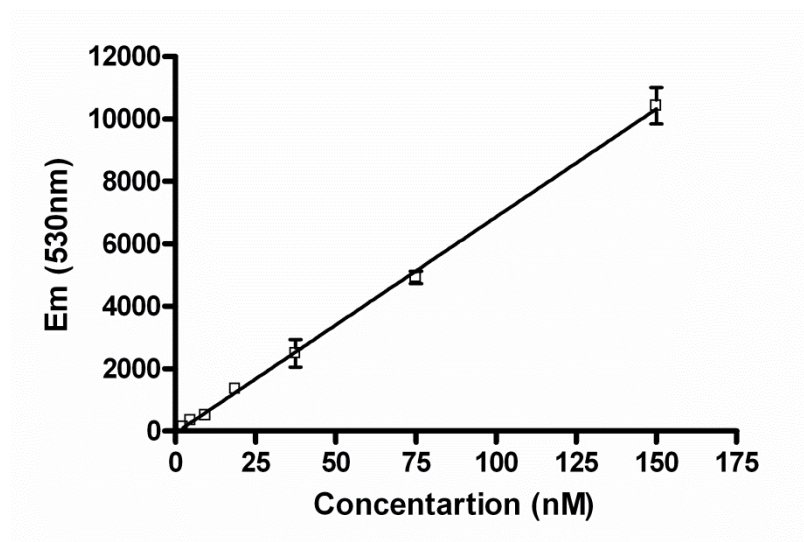


Figure 13. FITC-PEG Standard Curve

Fluorescence standard curve of FITC-PEG_{3.4kDa}-COOH in PBS was produced over the range of 2 to 150 nM in triplicates. Data was fit by nonlinear regression analysis to a first order polynomial equation. The fit regression line has a R^2 value of 0.9852. (Em: emission)

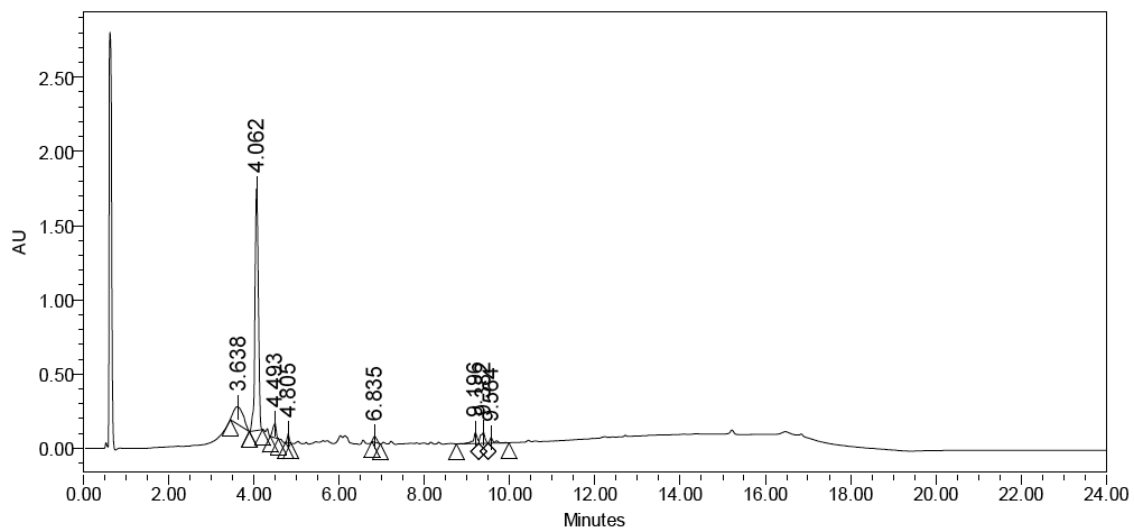


Figure 15. HPLC of Bac7 CPP

Analytical HPLC chromatogram of modified bactenecin 7 cell-penetrating peptide (Bac7 CPP). UV Absorbance was measured at 220nm and retention time was found to be 4.06 min.

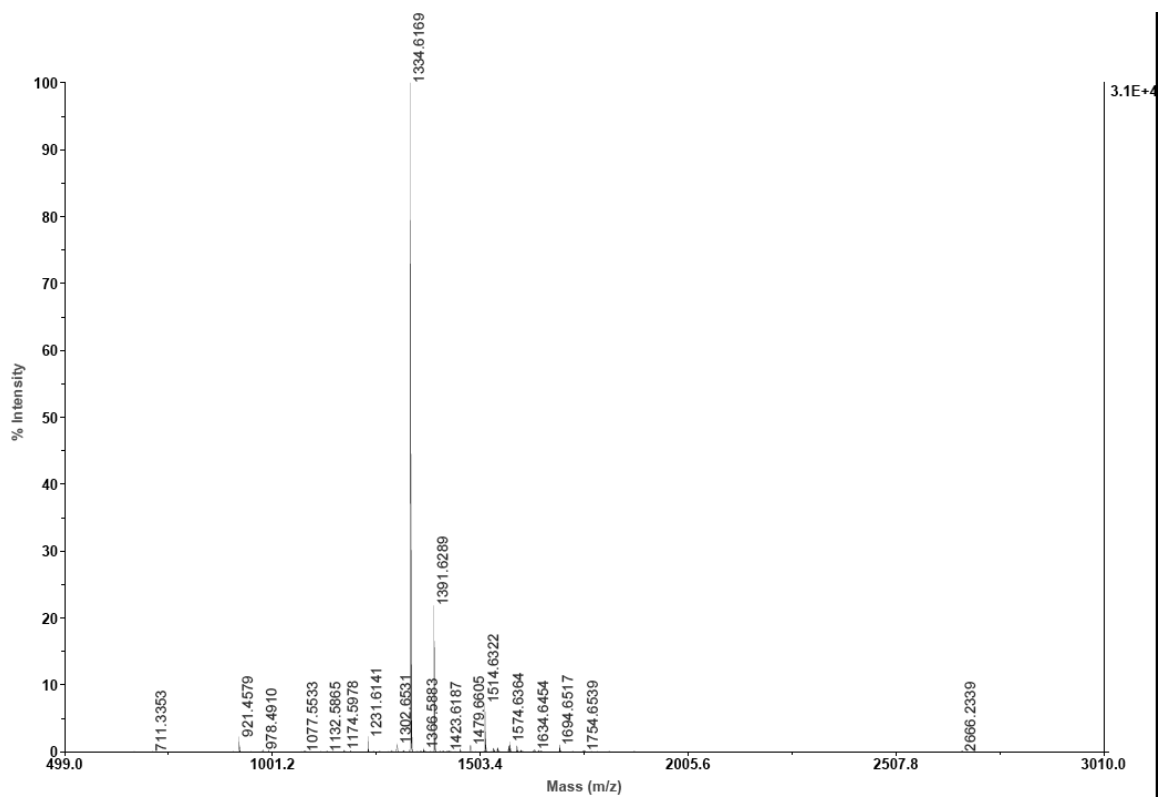


Figure 16. MALDI-TOF-MS of Bac7 CPP

MALDI-TOF mass spectrum of modified batenecin 7 cell-penetrating peptide (Bac7 CPP) was performed on an Applied Biosystems 4800 MALDITOF/TOF. The major peak at 1334.6 corresponds to the m/z of Bac7 CPP ($MW + H^+$).

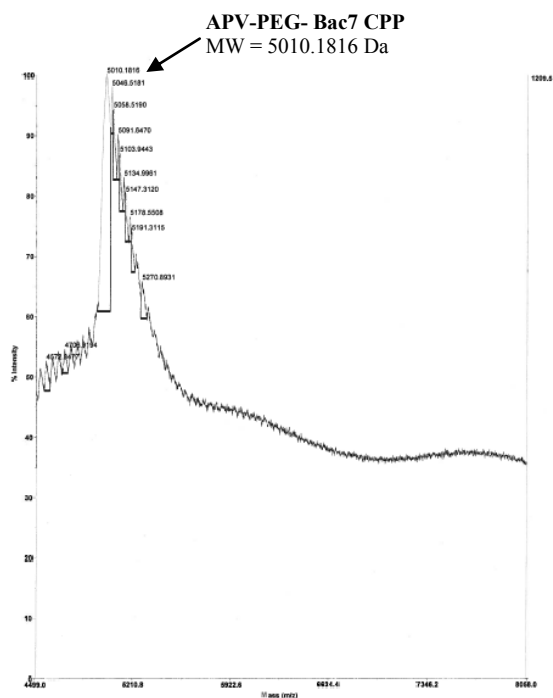


Figure 17. MALDI-TOF-MS of APV-PEG-Bac7 CPP

MALDI-TOF mass spectrum of APV-PEG_{3.4kDa}-Bac7 CPP (APB) was performed on an Applied Biosystems 4800 MALDITOF/TOF set to the linear mid mass mode.

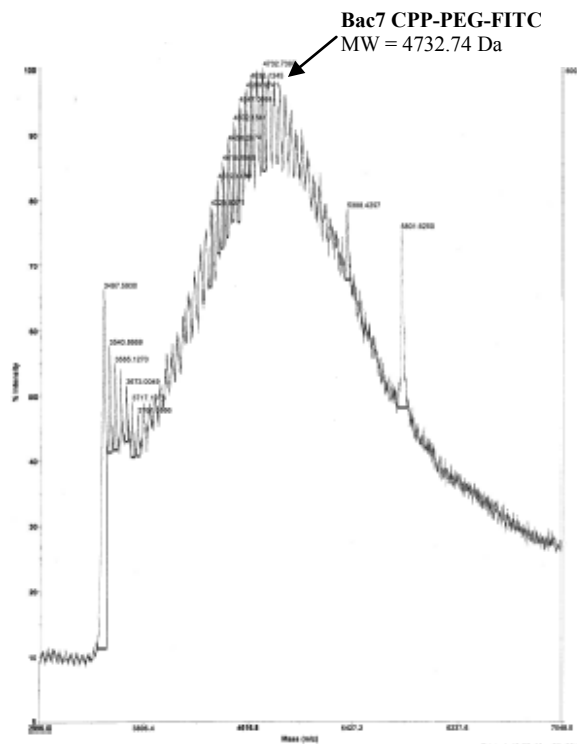


Figure 18. MALDI-TOF-MS of FITC-Labeled PEG-Bac7 CPP

MALDI-TOF mass spectrum of Bac7 CPP-PEG_{3.4kDa}-FITC (BPF) was performed on an Applied Biosystems 4800 MALDITOF/TOF.

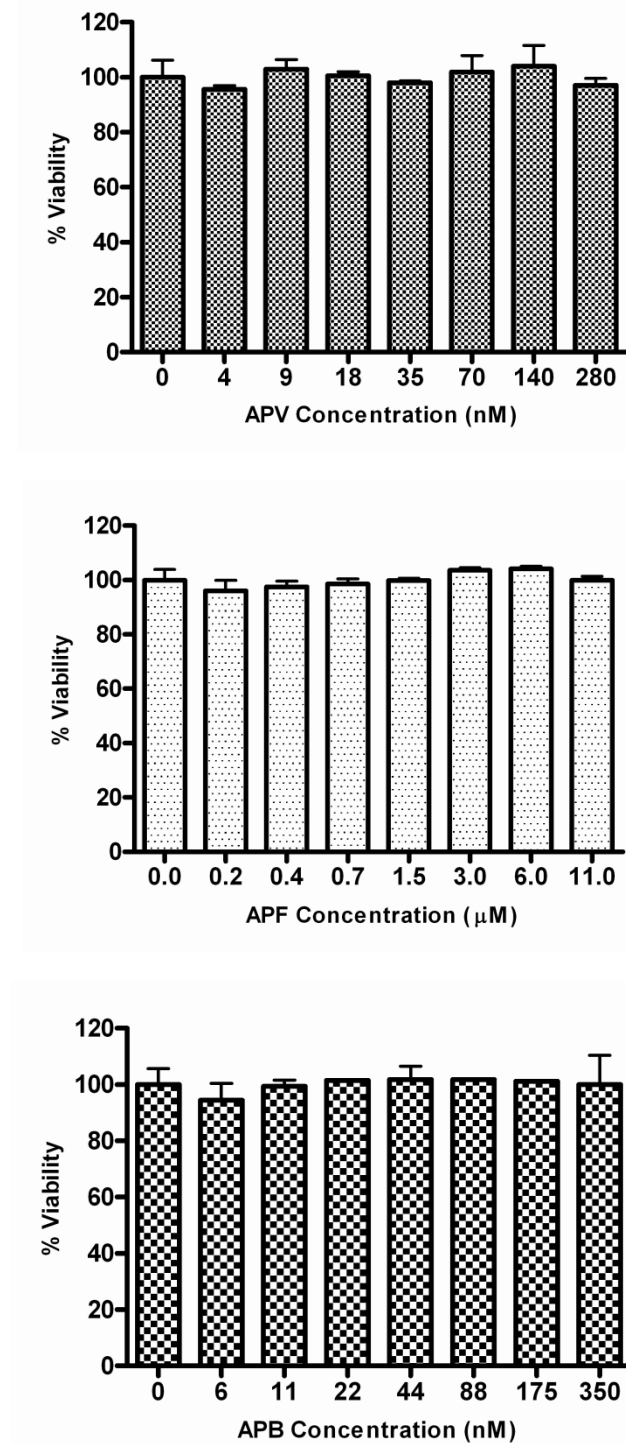


Figure 19. MTT Cytotoxicity Assay

Cytotoxicity of amprenavir (APV), APV-PEG_{3.4kDa}-Bac7 CPP (APB) and APV-PEG_{3.4kDa}-FITC (APF) was measured using the MTT assay. The conjugates were incubated at 37°C for 5 days with MT-2 T-cells. Data are presented as mean \pm SD (n = 3). No significant cytotoxicity was observed at several-fold higher than the compounds respective IC₅₀ values.

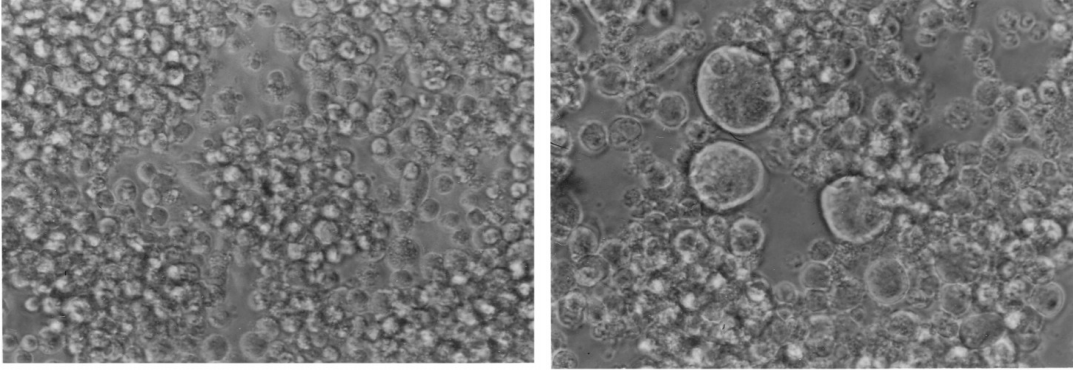


Figure 20. Syncytia Formation in MT-2 T-Cells

Left: normal MT-2 T-cells, Right: cell fusion and syncytia formation ¹⁹⁸.

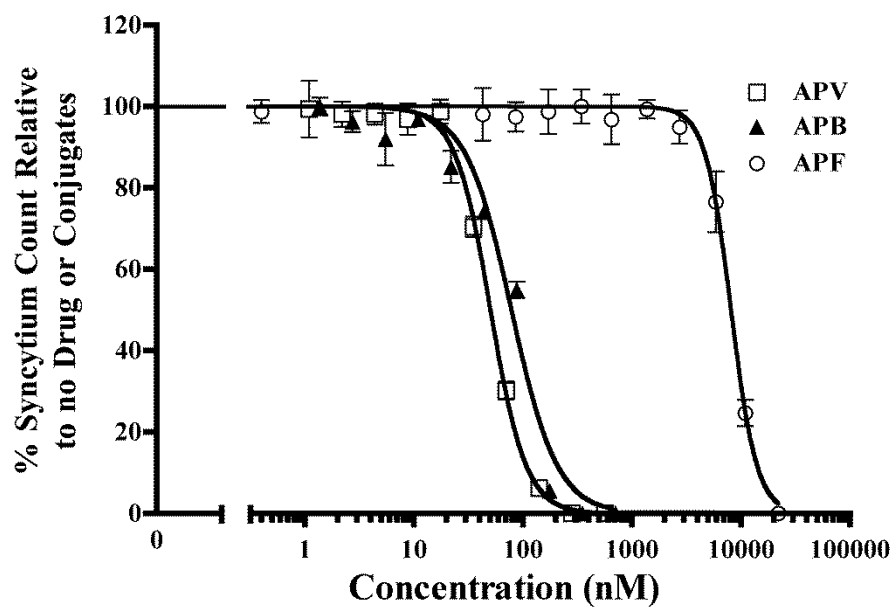


Figure 21. Anti-HIV-1 Activity of APV and APV-PEG Conjugates

The anti-HIV-1 activity was determined by the inhibition of syncytium formation in HIV-1 infected MT-2 T-cells and expressed as % of syncytium count of no treatment. Non-linear curve-fitting using the dose-response equation was used to determine the IC_{50} values. APF potency ($IC_{50} = 8064$ nM) was significantly lower than APV ($IC_{50} = 50.29$ nM) ($p < 0.001$). Further conjugation with Bac7 CPP (i.e., the APB conjugate, $IC_{50} = 78.29$ nM) almost completely restored APV activity with no significant difference in IC_{50} values ($p > 0.05$). Data are reported as mean \pm SD of three independent experiments ($n = 3$).

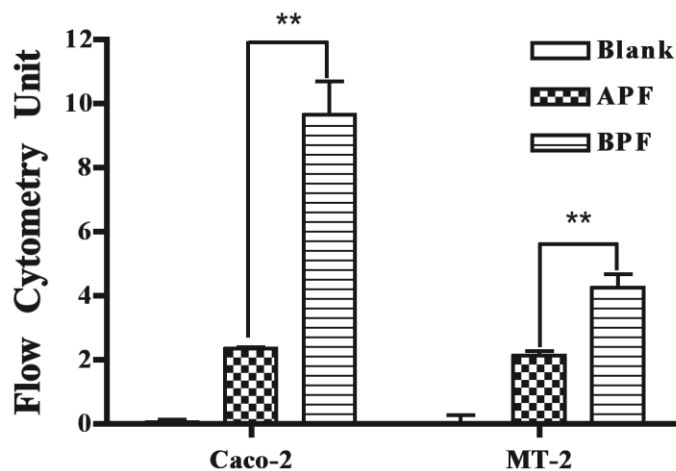


Figure 22. Quantitative Fluorescence-Activated Cell Sorting (FACTS) Assay

Caco-2 cells and MT2 cells were incubated with medium (Blank), and 10 μ M fluorescent equivalent of APF or BPF for 2 h. Intracellular delivery of the conjugates were studied with a Gallios flow cytometer. The mean \pm s.d. of gated fluorescent values of three independent experiments was obtained and ** indicates that the intracellular fluorescence of BPF in both cell types was significantly higher than that of APF ($p < 0.001$). One-way ANOVA analysis followed by Tukey multiple comparison test were performed.

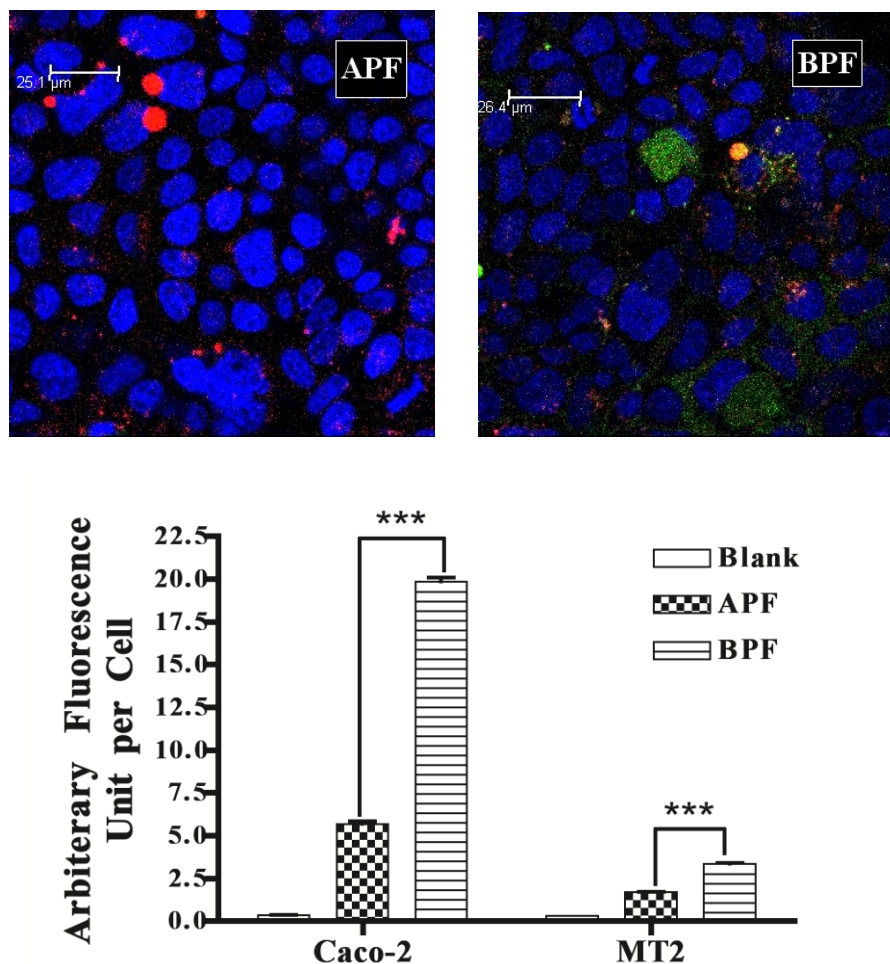


Figure 23. Confocal Microscopy

Top: Confocal microscopic images of Caco-2 cells incubated with APF (left) or BPF (right) at 2.47 \times -zoom. Caco-2 cells were incubated with 10 μ M fluorescent-equivalent of APF or BPF with DAPI and Rho-Dex for 4 h. A 40 \times objective was used for the acquisition of Z-stack of images in the XYZ mode for each treatment. Each image is produced from three separate blue, green and red-merged images. No cell surface fluorescence was observed, indicating that the fluorescence was exclusively intracellular. The lack of colocalization of green and red fluorescence in the BPF image (no orange color) indicates that most intracellular green fluorescence was located in the cytosolic compartment.

Bottom: Intracellular levels of APF and BPF in Caco-2 and MT2 cells were quantified for 500 cells per field using Leica microsystems LAS AF software. Each value is the mean \pm s.d. of fluorescence of 13 to 17 images of an entire stack and *** indicates that the intracellular fluorescence of BPF in both cell types was significantly higher than that of APF ($p < 0.0001$). One-way ANOVA analysis followed by Tukey multiple comparison test were performed.

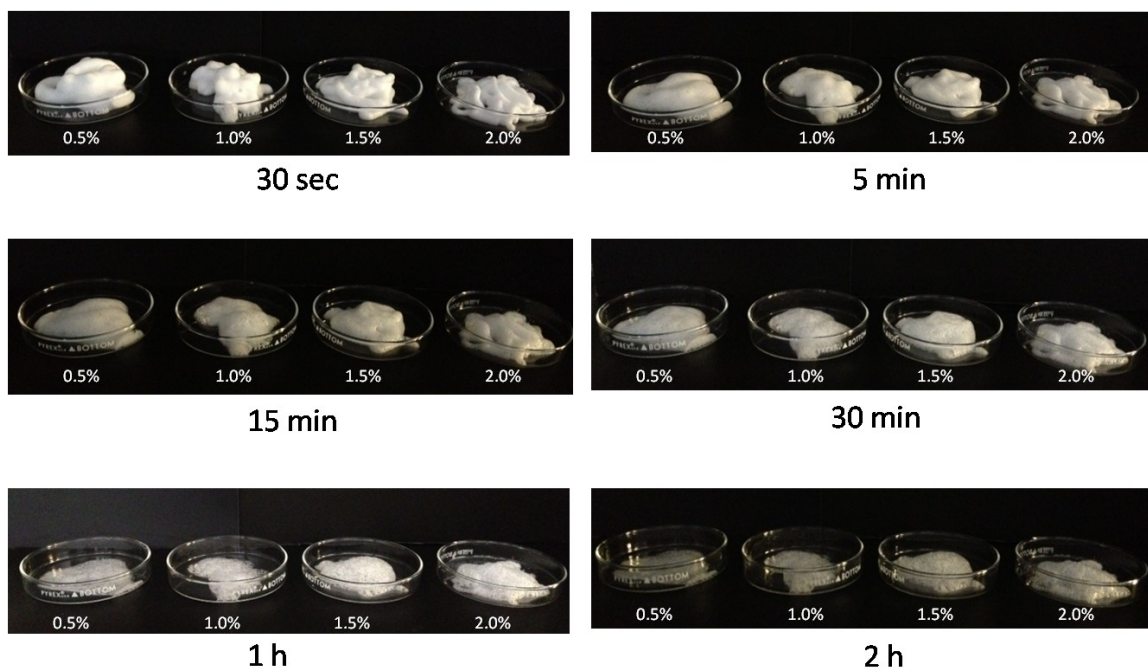
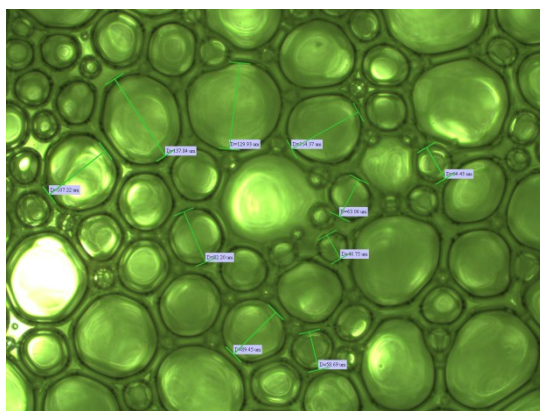
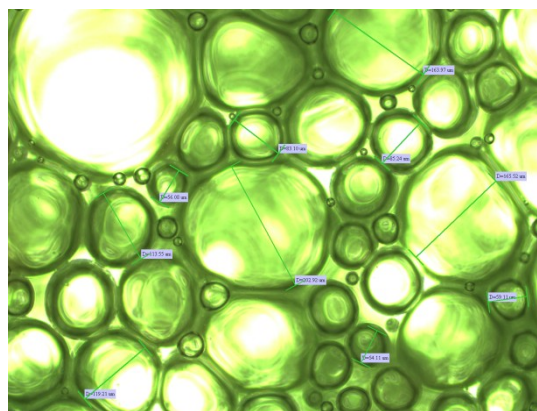
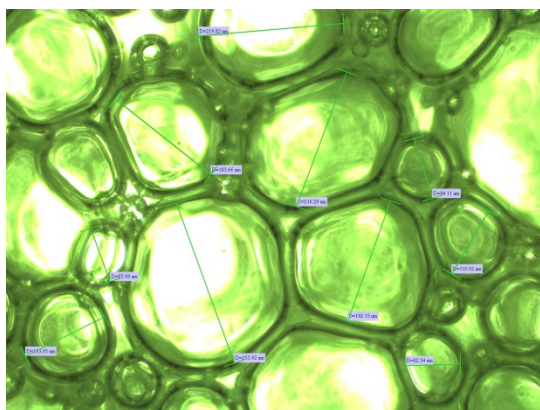
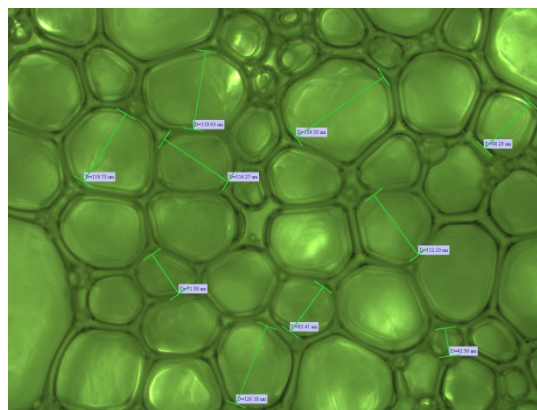


Figure 24. Macroscopic Foam Quality and stability at room temperature

A white to off-white foams were produced when the samples were expelled from the canister. All foams were characterized as being three-dimensional, semi-solid creamy structures that did not readily flow away from dispensing area when dispensed. The foams had relatively small bubble size and they exhibit characteristics like whipped cream. The foams with 1.5 to 2.0% XG could maintain over 70% of the original volume at the end the study where as the foams with lower XG concentration were less stable.

**0.5% XG****1.0% XG****1.5% XG****2.0% XG****Figure 25. Foam Light Microscopy Analysis**

An Olympus TH4-100 light microscope was used to capture the images with 10 × objective. Average diameter of the bubbles for each foam capture were measured as 87.82 μm, 110.28 μm, 157.27 μm and 104.7 μm for the foams containing 0.5%, 1.0%, 1.5% and 2.0% XG respectively.

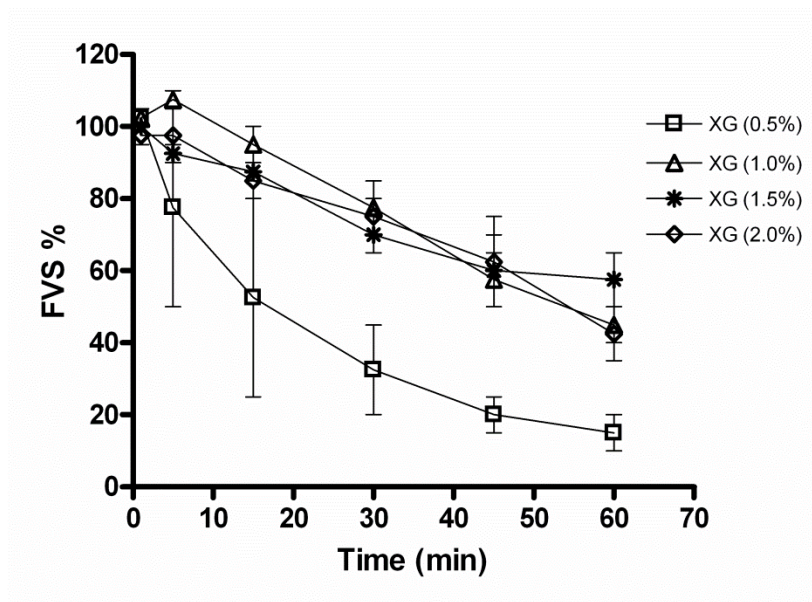


Figure 26. Foam Volume Stability (FVS) at Body Temperature

The foam samples were expelled into graded glass cylinders and the cylinders were immediately placed into a 38 °C water bath. The volume of the aged foams at each time point was compared with the initial volumes over a period of 60 min.

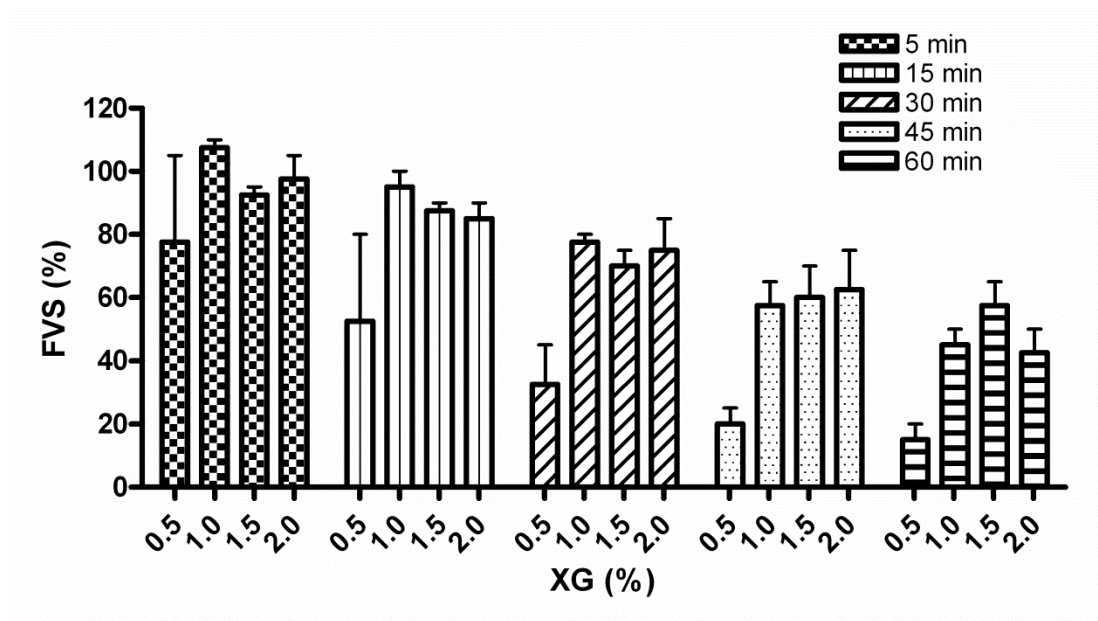


Figure 27. Foam Volume Stability (FVS) at Body Temperature (2)

FVS values were determined at 38°C over a period of 60 min after 20 ml of the foams (0.5 to 2.0% XG) were expelled in graded glass containers. The experiment was done in triplicates. The volume of the aged foams was compared with the initial volumes. Percentage of the foam volumes (FVS%) after 60 min compared with the initial foam volumes were determined as: 15.00 ± 7.071 for 1.5% XG, 45.00 ± 7.071 for 1.5% XG, 57.50 ± 10.61 for 1.5% XG and 42.50 ± 10.61 for 2.0% XG foam.

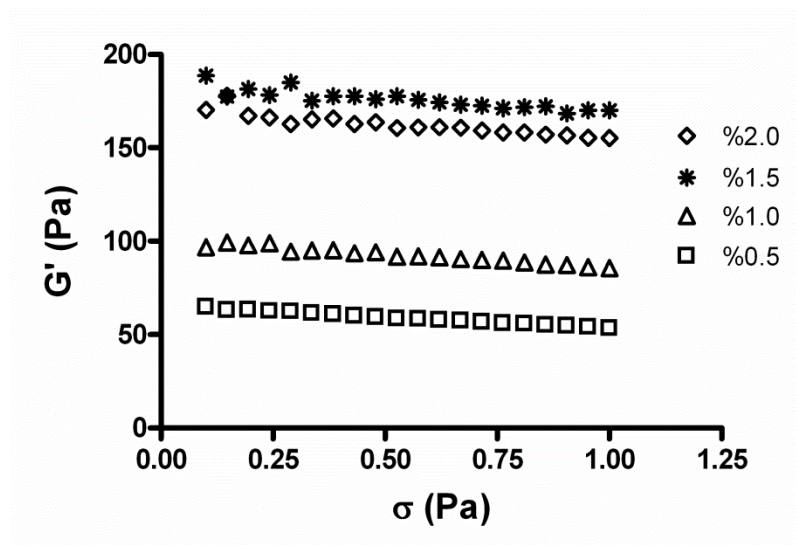


Figure 28. Determination of Linear Viscoelastic Region

The range of amplitude of oscillation for which the structure of the foam sample remains intact was determined by a Malvern Bohlin Gemini HRnano rheometer. The shear stress (σ) was gradually increased on the foam samples (XG %0.5 to 2.0%) at constant angular velocity (ω) of 5 rads/sec to find the range of amplitude of oscillation for which the structure of the sample remains intact ($n = 20$).

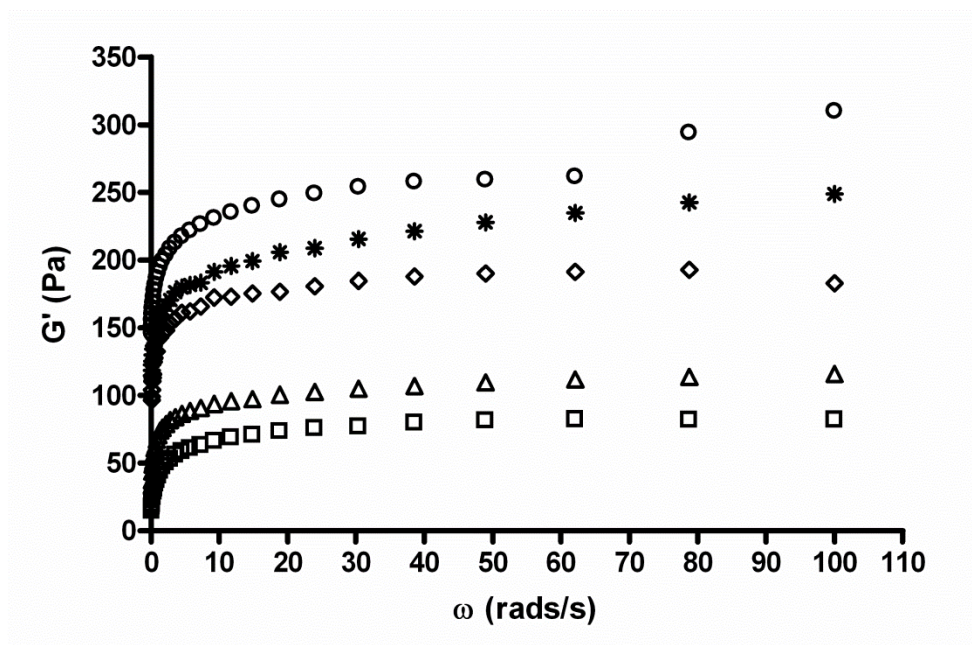


Figure 29. Evaluation of the Elastic Modulus, G' , for the Formulations at 38 °C

Determination of the G' provides a map of the behavior of the macrostructure of each formulation ($n = 30$). [o]: Gel (%1.5 XG), [◇]: Foam (%2.0 XG), [*]: Foam (%1.5 XG), [Δ]: Foam (%1.0 XG), [□]: Foam (%0.5 XG). The foam with 1.5% XG [*] has the highest elasticity among the foam formulations ($p < 0.001$).

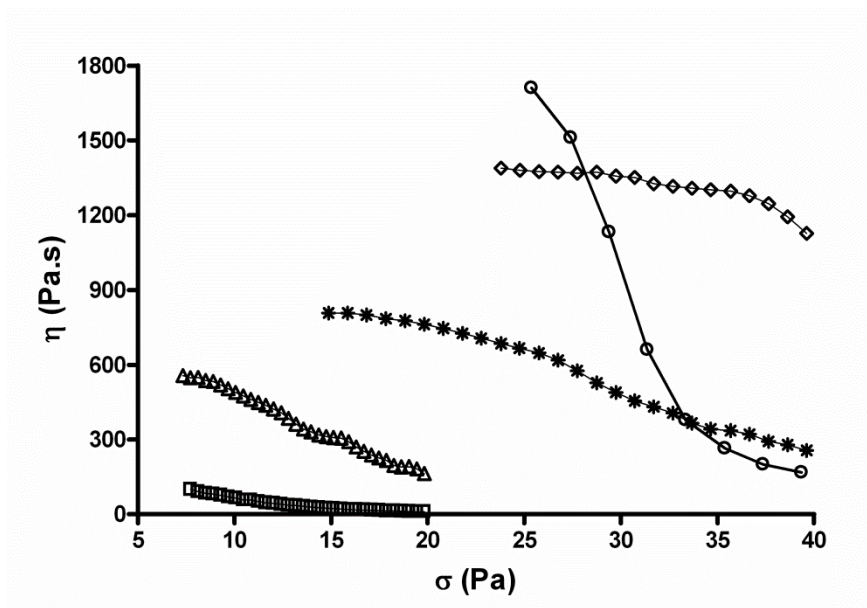


Figure 30. Changes in Instantaneous Viscosity, η , with Increase in Shear Stress

Formulations containing xanthan gum (XG) display shear-thinning behavior. [O]: Gel (%1.5 XG), [◇]: Foam (%2.0 XG), [*]: Foam (%1.5 XG), [Δ]: Foam (%1.0 XG), [□]: Foam (%0.5 XG). Measurements were taken at 38 °C. The shear-thinning behavior was significantly more obvious in the gel formulation [O].

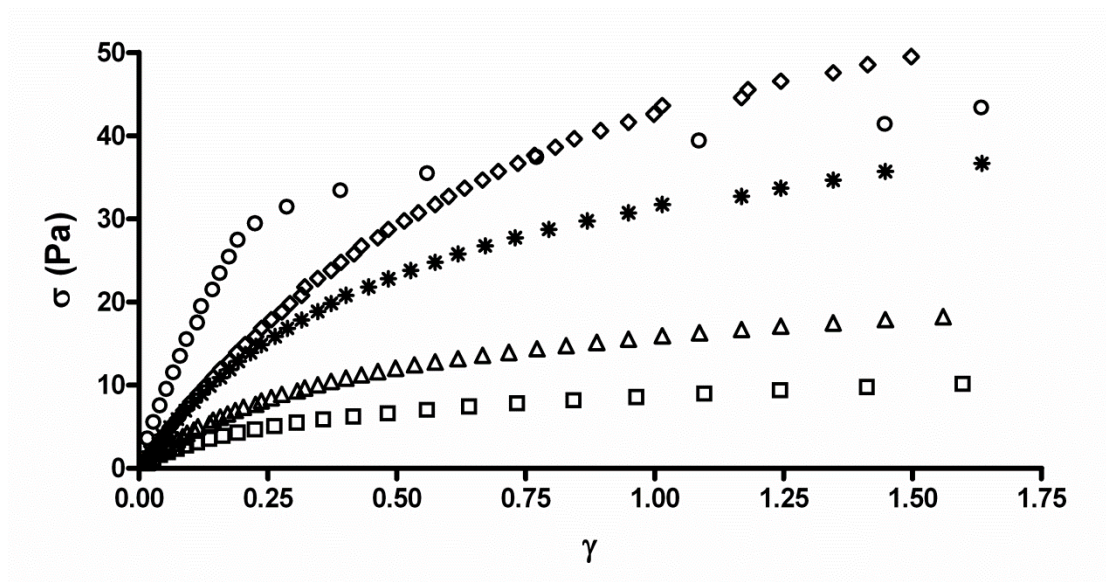


Figure 31. Determination of Yield Stress Values

The yield stress was determined by linearly increasing the shear stress from 1.0 to 50 Pa in a sweep time of 60 s and response of the sample was observed ($n = 50$). The location of the change in response from no flow to flow determined the yield point of the formulation. The calculated yield stress (Pa) values for [○]: Gel (%1.5 XG), [◇]: Foam (%2.0 XG), [*]: Foam (%1.5 XG), [Δ]: Foam (%1.0 XG), [□]: Foam (%0.5 XG) were 19.43, 25.77, 15.86, 7.33, and 3.43 respectively.

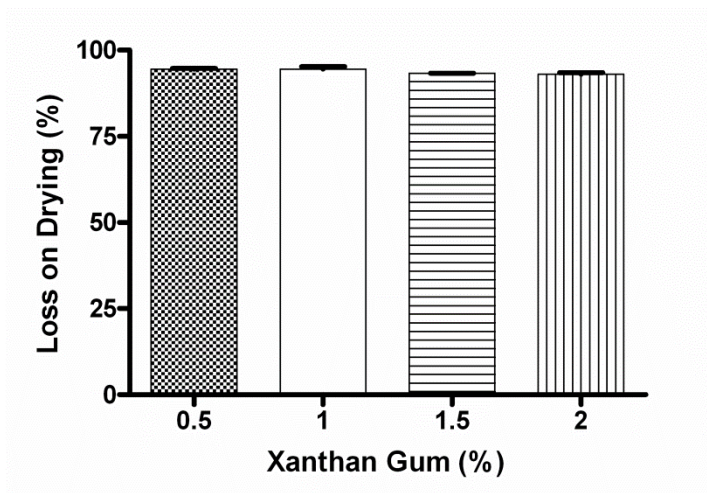


Figure 32. Loss on Drying

Percentage loss on drying was measured by comparing the weight of completely dried foam with the original weight after the foams were stored in a 65 °C oven for 7 days. The amount loss (93% to 95%) was not significantly different among the foams ($p > 0.05$).

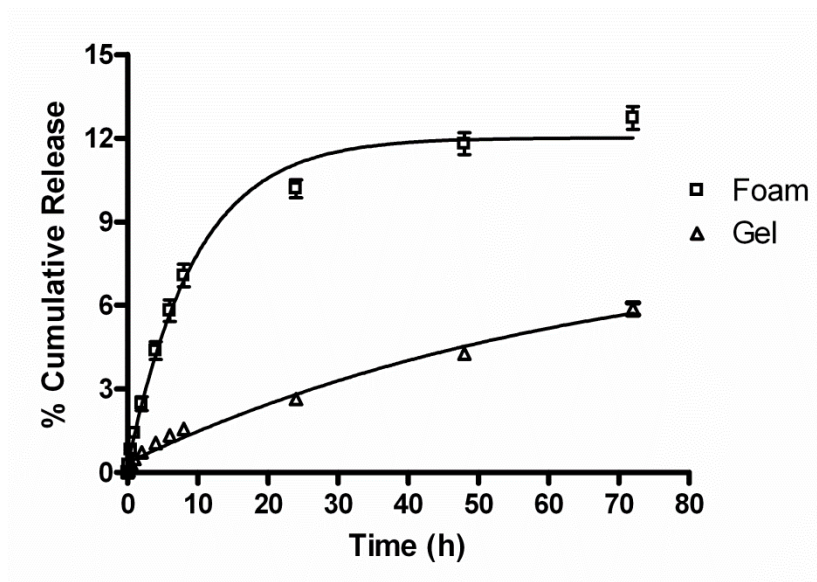


Figure 33. Kinetics of % Cumulative Release and the Release Rate of FITC-Labeled PEG

The Y-axis represents cumulative release of FITC-PEG_{3,4}-COOH (% of the total amount applied at $t = 0$) from the foam and the gel (both containing %1.5 XG) in medium, over a 72 h period. The near linear initial slopes of the curves used for calculation of the release rate. The release from the foam was significantly faster (4.6 fold) compare to the release form the gel ($p < 0.05$).

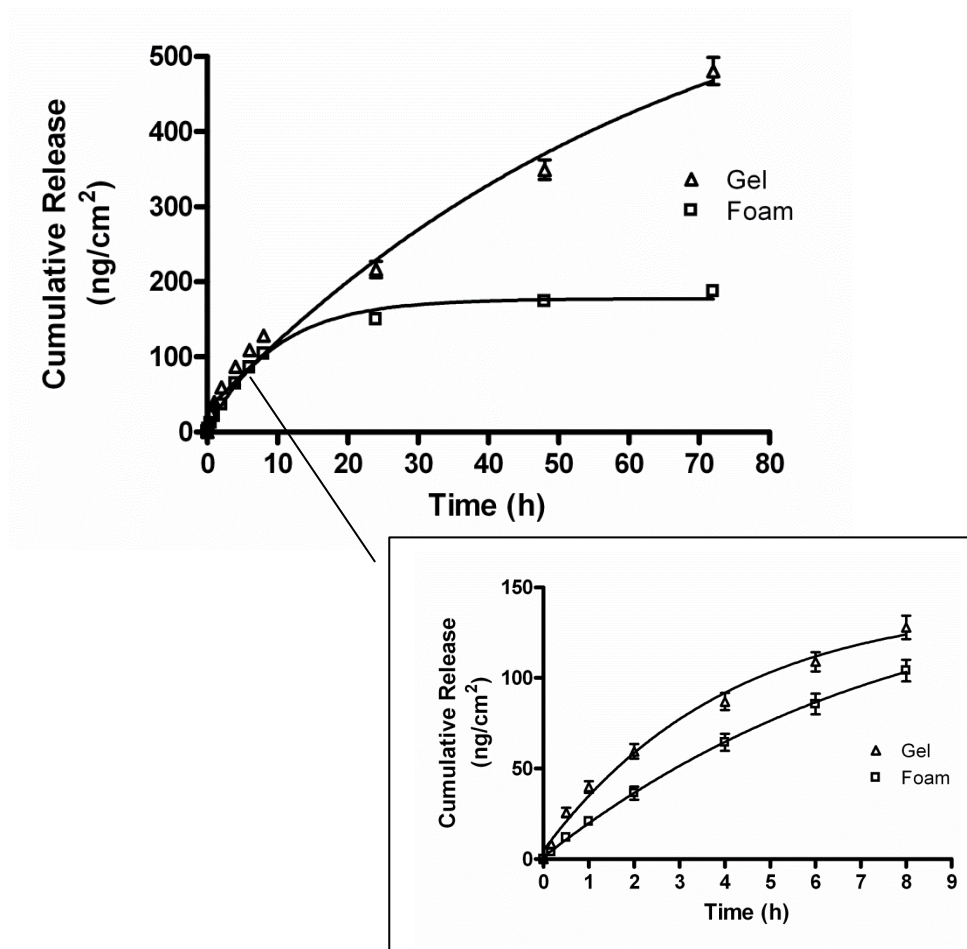


Figure 34. Kinetics of the Absolute Amount of FITC-Labeled PEG Release

The Y-axis represents the cumulative absolute amount of released FITC-PEG_{3,4kDa}-COOH from the foam and the gel (both containing %1.5 XG) in ng per cm² of the Transwell insert membrane (0 ng/cm² at t = 0). Compare to Fig. 33, over the period of the study (72h), more release was observed from the gel formulation because the formulation contains 10 fold more of the NC (w/v) compare to the foam. However, the period from 8h to 72h is irrelevant *in vivo* due to intestinal movement and defecation. The insert shows that during the first 8h period, the release of FITC-PEG_{3,4kDa}-COOH from the gel is not significantly different than that of the foam ($p > 0.05$).

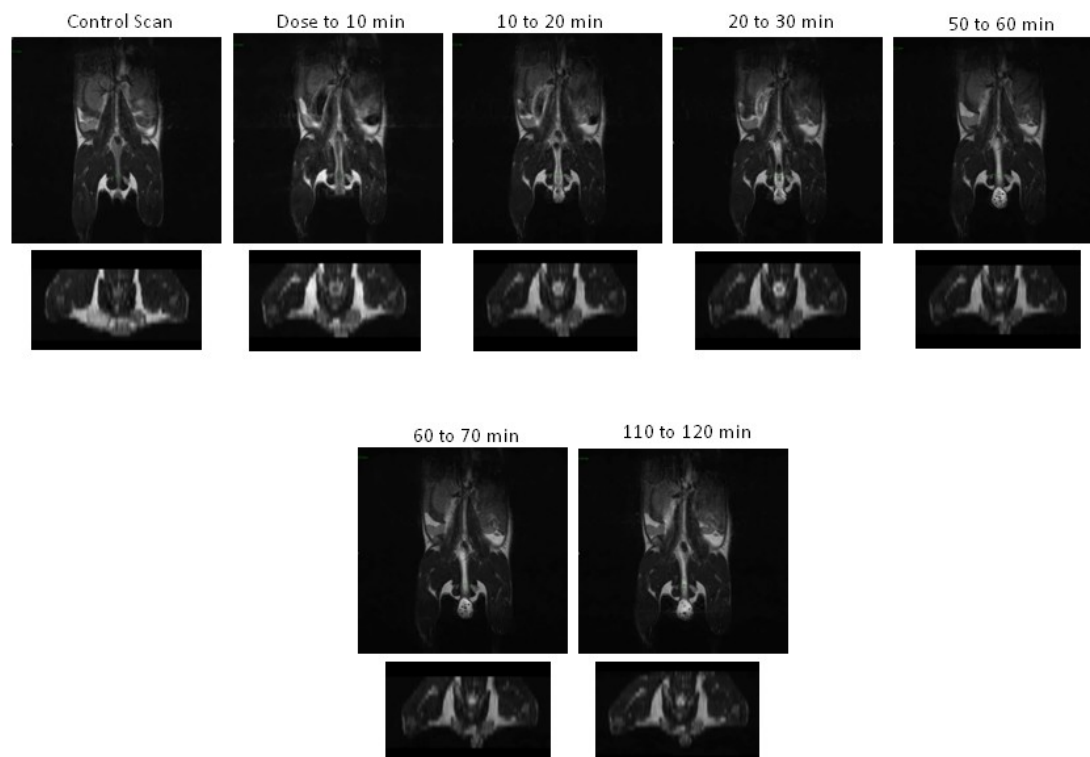


Figure 35. *In Vivo* Characterization of XG (1.5%) Foam in the Mice Rectum

Rectal distribution of the foam was investigated using an Aspect MRI. Coronal (top panels) and axial (lower panels) images show that the foam fully covers the inner wall of the rectum. An increase in the foam image intensities over time proves the foam is broken and condensed over time. An early rectal expansion after the foam application is fully recovered at the end of the study.

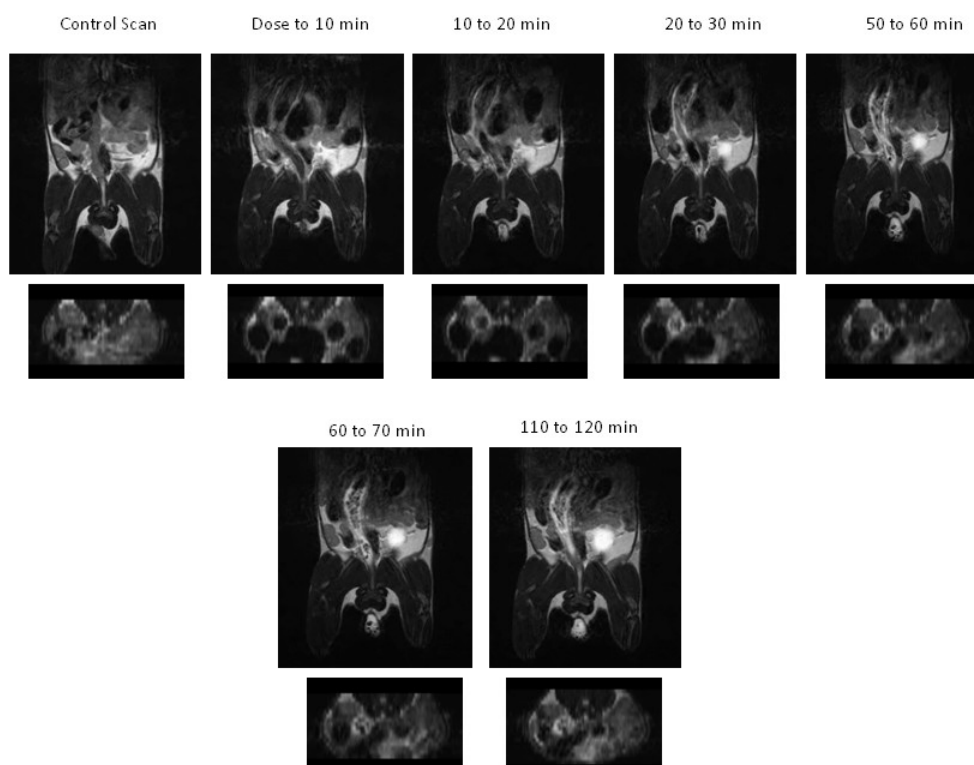


Figure 36. *In Vivo* Characterization of Foam in the Mice Colon

Distribution of the foam in the colon was investigated using an Aspect MRI. Coronal (top panels) and axial (lower panels) images show that the foam fully covers the inner wall of the descending colon. An increase in the foam image intensities over time proves the foam is broken and condensed over time. An early colonic expansion after the foam application serves to provide larger surface area for drug delivery and is partially recovered at the end of the study.

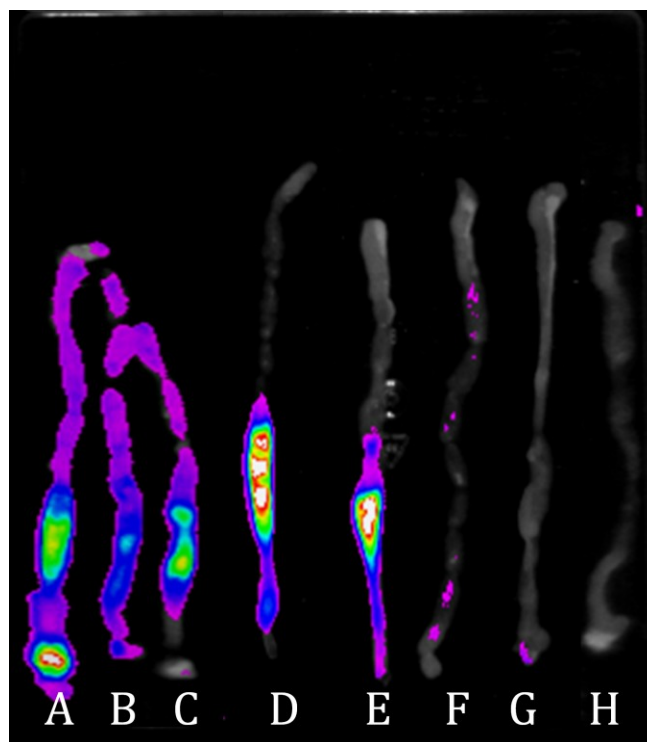


Figure 37. Colorectal Distribution of FITC-PEG_{3.4kDa}-COOH Loaded XG Foam

Distribution of the XG (1.5%) foam containing of a model NC (FITC-PEG_{3.4}-COOH) was investigated using a MS FX PRO small animal imaging system. Optical imaging results show the distribution of model NC is homogenous within the foam. A: 30 sec, B: 15 min, C: 30 min, D: 1h, E: 2 h, F: 3 h, G: 4 h, H: untreated. Colors: black-purple, lowest; yellow-orange-red, highest.

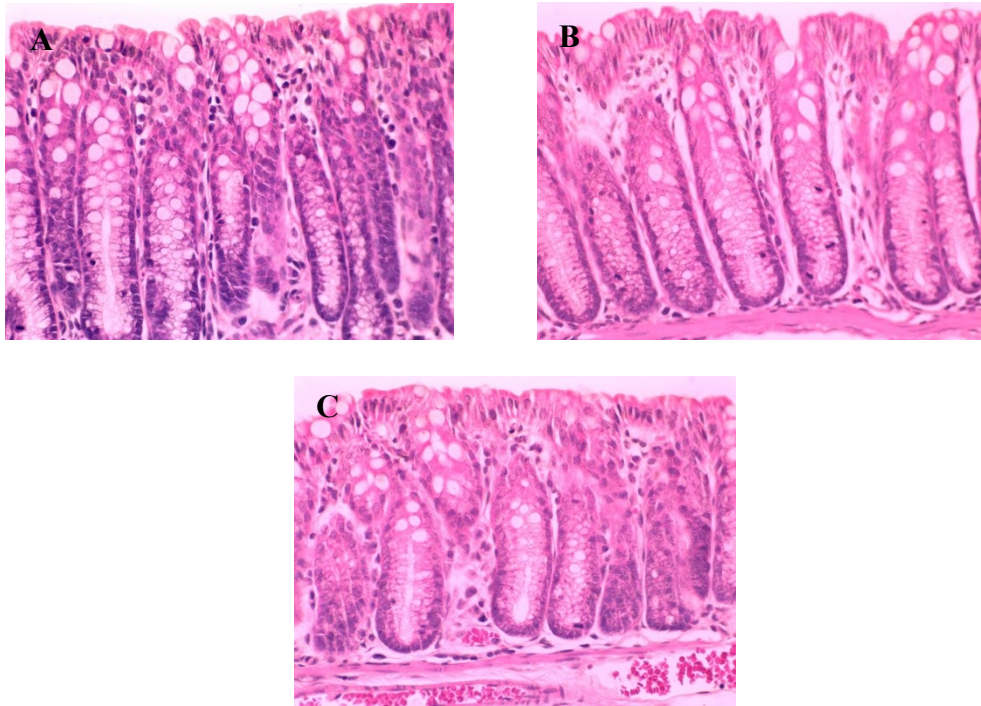


Figure 38. Mice Colorectal Irritation Test at Day 1 Post Dose

Light microscopic images of hematoxylin and eosin stained sections ($\times 400$) of the mice colon. A, untreated control; B, a single dose of saline enema; and C, a single dose of XG (1.5%) foam. The epithelium of all the three groups was normal with crypts and goblet cells arranged in series.

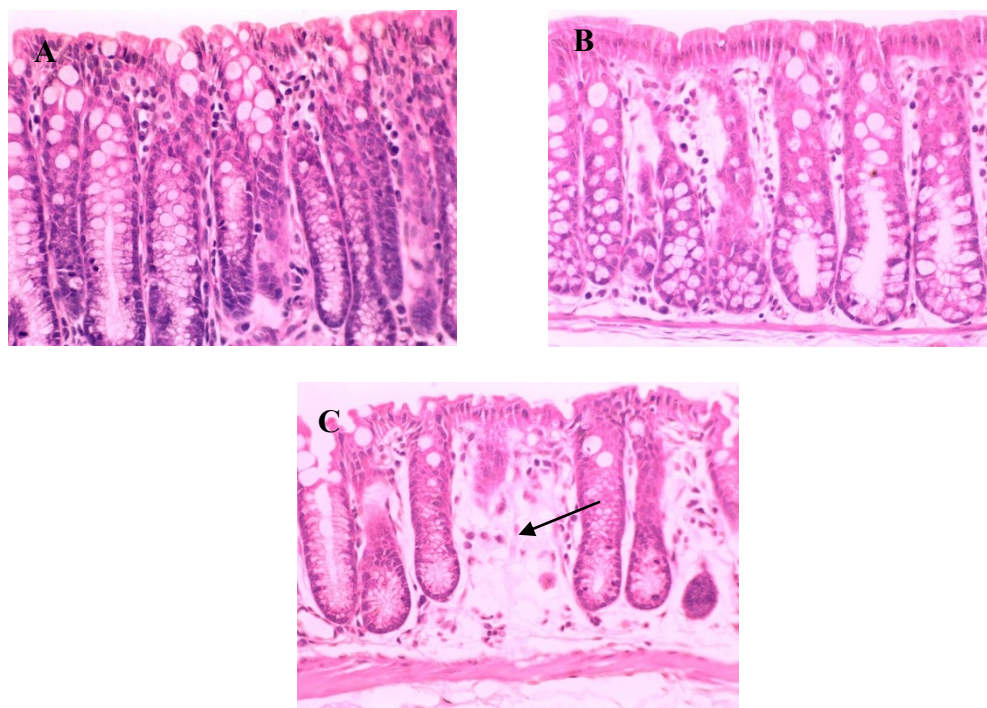


Figure 39. Mice Colorectal Irritation Test after 5 Consecutive Days of Dose Application

Light microscopic images of hematoxylin and eosin stained sections ($\times 400$) of the mice colon after five days of once in a day application. A, untreated control; B, saline enema; and C, XG (1.5%) foam. Occasional missing crypts (arrow) were observed with the foam formulation. No sign of moderate to severe inflammation or ulceration was reported.

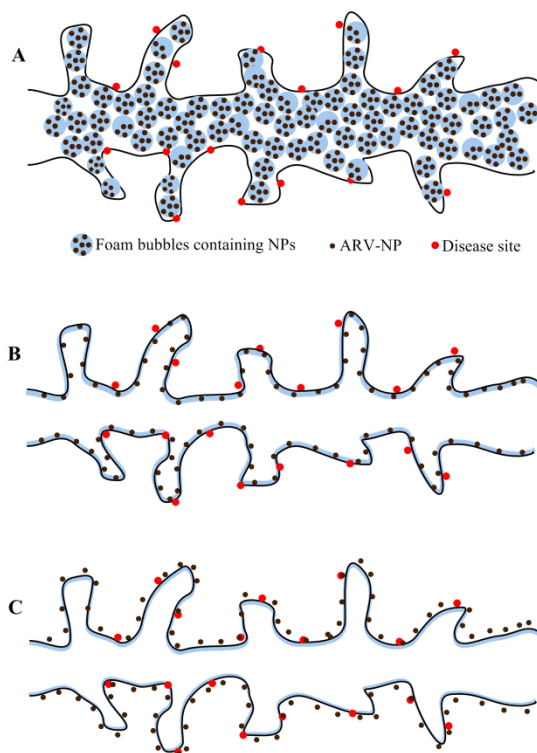


Figure 40. Mucosal Pre-Exposure Prophylaxis (PrEP) Concept

(A) Foam fills colonic lumen; (B) foam breaks depositing NPs in a gel layer on mucosal surface; and (C) NPs are taken up and implanted in the mucosa then deliver therapeutic agents slowly.

APPENDIX

8. Formulation of Pharmaceutical Foams

Foams contain two essential components:

1. Product concentrate (contains active ingredient or mixture of active ingredients and other such as solvents, surfactants and excipients)
2. Propellant (may be single or blend of various propellants)

Different types of propellants and their characteristics are listed in the following table ¹⁴,

127, 137.

Propellant	Characteristics	Example
ChloroFluorocarbons (CFCs)	Inertness, nontoxic, nonflammable, density greater than water Drawback: ozone depletion potential (ODP)	Trichlorofluoromethane, dichlorodifluoromethane, chlorotrifluoromethane, 1,1,2-Trichloro-1,2,2-trifluoroethane, 1,1,1-Trichloro-2,2,2-trifluoroethane, 1,2-Dichlorotetrafluoroethane, 1-Chloro-1,1,2,2,2-pentafluoroethane, Tetrachloro-1,2-difluoroethane, Tetrachloro-1,1-difluoroethane, 1,1,2-Trichlorotrifluoroethane
Compound gases	Drawbacks: producing wet sprays, greenhouse potential	Nitrogen ,CO ₂ , N ₂ O, SF ₆
HydroChlorofluorocarbons (HCFCs)	Inertness, nontoxic, nonflammable, density greater than water Drawback: ODP	Chlorofluoromethane, dichlorofluoromethane, chlorofluoromethane, 1,1-Dichloro-1-fluoroethane, 1-Chloro-1,1-difluoroethane, 1,1-Dichloro-2,2,3,3,3-pentafluoropropane, 1,3-Dichloro-1,2,2,3,3-pentafluoropropane
Hydrocarbons	Environmental acceptance, low toxicity, no reactivity.	Ethane, butane, isobutane (A31), propane,

	Drawbacks: Flammable, density lower than water, unpleasant odor	
Hydrofluorocarbons (HFCs)	Inertness, nontoxic, nonflammable, density greater than water, no ODP Drawback: greenhouse potential	1,1,1,2,3,3,3-heptafluoropropane (HFA-227), 1,1,1,2-tetrafluoroethane (Freon-134a, HFA-134a), 1,1,1,3,3,3-hexafluoropropane (R236-fa), ethylidene difluoride (HFC 152a)
Ethers	Flammable	Dimethyl ether

In the table below, different possible ingredients of pharmaceutical foams have been summarized ^{14, 199, 200}:

Ingredient	Function	Properties	Examples
Foaming agent (Surfactant)	Essential for foam generation	Anionic, cationic, non-ionic and, amphoteric surfactants; proteins	Anionic: ammonium lauryl sulfate, lauryl sarcosine, sodium cocoyl sulfate Cationic: distearyl dimethyl ammonium chloride, cetrimonium bromide Nonionic: sorbitan esters, cetyl octanoate Amphoteric: sodium lauroamphoacetate, lauryl betaine Proteins: collagen
Propellant	Developing the power pressure within the container, expels the product when the valve is opened	Liquefied or compress gas	CFCs, HCFCs, HFCs, compound gasses, ethers, hydrocarbons
Co-solvents	Increase solvating power	Volatile alcohols (flammable, can produce dryness and irritability)	Volatile alcohols (ethanol)
Foam Stabilizers	Enhance foam formation	Hydrocolloids	xanthan gum, hydroxypropylmethylcellulose, methylcellulose, alginates, agar-agar, esters of TWEEN
Foam Destabilizers	Reduce stability the foams	Oils, alcohols, solvents, polymers	Ethanol, fatty alcohols, silicon oils, glycerides, polyamide

Excipients	Pharmacologically inactive, used as a carrier for the active ingredients	Suspending agents	Bentonit, carbomer, xanthan gum, propylene glycol alginate
		Anti-oxidants	Alpha tocoferol, ascorbic acid, carotenes, uric acid
		Chelating agents	EDTA, nitrilotripropionic acid, pentatriacoaten hexahydrobromade
		Emollients	Cetyl alcohol, lanolin derivatives, mineral oil, cholesterol, glycerol
		Humectants	Glycerin, propylene glycol, sorbitol, triacetin
		pH modifying agents	Sodium hydroxide, acetic acid, calcium carbonate, potassium citrate
		preservatives	Benzoic acid, alkyl parabens, phenol, cetylpyridinium chloride

There are several classes of foam formulations being marketed and further classes under development, which are distinct from each other by their composition and functionality. Understanding the difference between different classes of foam formulations would allow selecting the right type of formulation for a given clinical condition. The parallels between various classes of foams and traditional topical dosage forms are given in the following table that is redrawn from ref. 14:

Class	Main Formulation Characteristics	Traditional Topical Dosage Form Designation	Attributes
Foam hydrophilic emulsion	Oil in water emulsion	Emulsion, Cream, Hydrophilic cream	-Emollient formulation
Foam lipophilic emulsion	Water in oil emulsion	Emulsion, Cream, Lipophilic cream	-Can carry lipophilic and hydrophilic APIs
Foam ointment	Single phase Petrolatum is a main ingredient	Ointment, white ointment, hydrophobic ointment	-Occlusive -Serves to keep medicaments in prolonged contact with the skin -In the absence of water, protects water sensitive actives -Does not require preservatives
Foam hydrophilic ointment	Single phase Main ingredient is PEG or other hydrophilic solvents	Polyethylene glycol ointment, hydrophilic ointment	-Greaseless ointment base -Serves to solubilize medicaments, thus rendering them more bioavailable -In the absence of water, protects water sensitive actives -Does not require preservatives
Foam oil	Single phase Liquid oil is main component	Oil solution, oil suspension	-Partially occlusive -Nourishes and lubricates the skin -Serves to keep medicaments in prolonged contact with the skin -In the absence of water, protects water sensitive actives -Does not require preservatives
Hydro-ethanolic foam	Lower MW alcohols and water are main ingredients	Solution, tincture	-Serves to solubilize medicaments, thus rendering them more bioavailable -Adequate for oily skin areas -Does not require preservatives
Aqueous foam	Main ingredients are water, gelling agents and surfactants	Gel	-Non-greasy
Foam suspension	Suspended API in a foam formulation	Topical suspension	-Non-greasy - Desiccative

Depending on the way of pharmaceutical application rectal, vaginal and dermal foams can be defined. Table below represents examples of different pharmaceutical foams available in the market ^{14, 130, 201}:

Products	Active Ingredients	Indications
Dermal Foams:		
Extina	Ketoconazole	Mycoses
Evoclin	Clindamycin	Acne vulgaris
Olux, Clarelux	Clobethasol	Dermatosis, Psoriasis
Luxiq, Deflatop	Bethamethason	Scalp dermatosis (eg. psoriasis)
Epifoam	Hydrocortison and pramoxin	Skin inflammations and itching
Ibuleve	Ibuprofen	Fast pain relief (eg. backache)
Desenex	Undecylenate	Antifungal, Antibacterial
Saccharide Foam	Saccharide and Honey	Wound and burn therapy
Scytera	Coal tar	Psoriasis
Rectal Foams:		
Proctofoam	Hydrocortison and Pramoxine	Haemorrhoids, Anal fissures
Claversal	Mesalazine	Crohn disease, Colitis ulcerosa
Vaginal Foams:		
Patentex	Nonoxynol-9	Contraceptive, HIV infection prevention
Gynefoamix	None	For different gynecological drugs administration

Examples of different foam formulations and their stability at room temperature (RT) and body temperature (BT) are illustrated below. The effect of a hydrocarbon propellant (AP-70) and an HFC propellant (134a) on the structure of the produced foams indicates that the formulations containing AP-70 expand more after expelled from the canisters. Formulations containing ethyl alcohol (ethanol) are not recommended for mucosal application for possible irritability and dryness.

Foam Formulation A:

Ingredient	Function	% w/w
Cetyl Alcohol	Fatty alcohol; QBF agent (adjuvant)	1.1
Stearyl Alcohol	Fatty alcohol; QBF agent (adjuvant)	0.5
Polysorbate 60	Surface active agent; foaming agent, Enhances fatty alcohol solubility	0.4
Dehydrated Ethanol	Solvent for alcoholic phase, Skin penetration enhancer	57.00
Purified Water	Solvent for aqueous phase	33.00
Propylene Glycol	Humectant	2.00
Citric Acid Anhydrous	Buffering agent (pH : 4.5)	0.073
Potassium Citrate	Buffering agent (pH : 4.5)	0.027
1,1,1,2- Tetrafluoroethane	Propellant, solvent for fatty alcohols	5.9
		100

Stability and Appearance of Formulation A:

Formulation Stability at RT

30 sec

1 min

2 min

3 min

4 min

5 min

Propellant: AP70



Propellant: 134a



Formulation Stability at BT

30 sec

1 min

2 min

3 min

4 min

5 min

Propellant: AP70



Propellant: 134a



Foam Formulation B:

Ingredient	Function	% w/w
Emulsifying wax	Emulsifier	3.27
PEG (40) stearate	Emulsifiers	2.32
Polysorbate 80	Surface active agent; foaming agent	0.95
Acrylate/octylacrylamide copolymer	Film former	2.18
Dehydrated Ethanol	Solvent for alcoholic phase, Skin penetration enhancer	23.87
Purified Water	Solvent for aqueous phase	61.35
Sodium Benzoate	Anti-corrosion protection	0.22
di-sodium EDTA	Chelating agent	0.115
1,1,1,2- Tetrafluoroethane	Propellant, solvent for fatty alcohols	5.725
		100

Stability and Appearance of Formulation B:

Formulation Stability at RT

30 sec

1 min

2 min

3 min

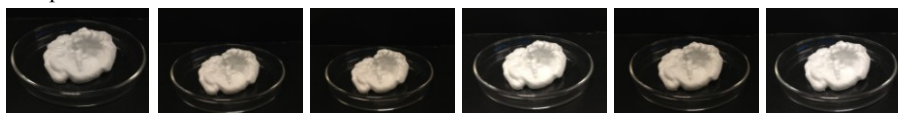
4 min

5 min

Propellant: AP70



Propellant: 134a



Formulation Stability at BT

30 sec

1 min

2 min

3 min

4 min

5 min

Propellant: AP70



Propellant: 134a

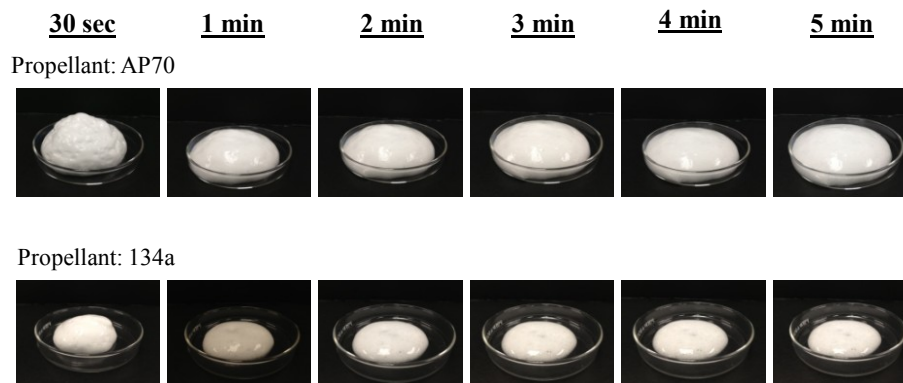


Foam Formulation C:

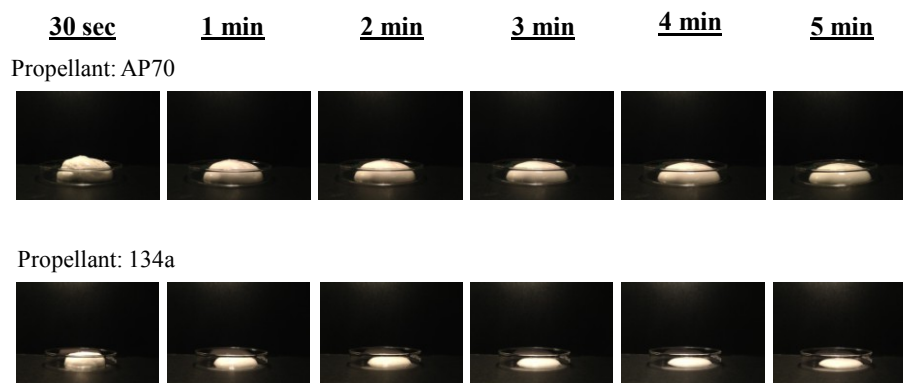
Ingredient	Function	% w/w
Brij L23	Surface active agent; foaming agent	3.8
Methyl-hydroxybenzoate	Antioxidant, preservative	0.19
Xanthan gum	Stabilizer, natural film forming agent	0.95
Dehydrated Ethanol	Skin penetration enhancer	9.5
Purified Water	Solvent for aqueous phase	72.56
di-sodium EDTA	Chelating agent	0.48
Propellant	Blowing agent	5.0
		100

Stability and Appearance of Formulation C:

Formulation Stability at RT



Formulation Stability at BT



9. Caco-2 Cell Culture for Prediction of Intestinal Absorption of Nanoparticles

Materials and Methods

Caco-2 cells were purchased from American type culture collection (ATCC, Manassas, VA) and T7 trinucleotide-encoded 12-mer peptide library from NCI-Frederick (Frederick, MD). Dulbecco's modified Eagle's medium (DMEM), Hank's balance salt solution (HBSS), fetal bovine serum (FBS), penicillin/streptomycin 100× solution and 0.05% trypsin-EDTA were obtained from purchased from Invitrogen/Life Technologies Corp (Grand Island, NY). Transwell[®] polycarbonate membrane cell culture inserts (3 μm pore size) and cell culture plastics were purchased from Corning (Corning, NY).

Caco-2 Cell Culture

Human colon carcinoma Caco-2 cells were grown in a culture flask containing complete DMEM supplemented with 10% FBS, 100 UI/ml penicillin and 100 μg/ml streptomycin. The culture flask was incubated at 37 °C under 5% CO₂. After the cells proliferated and reached confluency (in about 10 to 14 days), Caco-2 cells were trypsinized and washed twice with DMEM. In each Transwell[®] polycarbonate membrane cell culture insert, 500 μl of Caco-2 cell suspension in DMEM were seeded at 1.5×10^4 cells/inserts. The receiver compartments were filled with 1500 μl of DMEM and the plates were incubated at 37 °C. During the 21 days incubation, mediums in inserts and receiver compartments were changed every other day and the transepithelial electrical resistance (TEER) was measured by special probes attached to a voltohmmeter (EVOM, World Precision Instrument, Sarasota, Fl). After 21 days incubation, the insert wells with TEER value about $200 \Omega \text{ cm}^2$ were selected for detection of nanoparticles absorption.

Phage Display and Caco-2 Cell Transport

The T7 phage trinucleotide-encoded 12-mer peptide library had a complexity (library size) of 1.2×10^9 different 12-mer peptide sequences. The library was lightly ($18 \times$) amplified before use in phage display by infecting *E. coli* host cells and purified by PEG precipitation according to Novagen's T7 phage display protocol. Four rounds of selection for rare phage that were able to cross Caco-2 monolayers to the basolateral side were conducted. At each round of selection, 0.5 ml of phage suspension at the apical side and 1.5 ml of HBSS at the basolateral side of the insert was added and the plate was incubated at 37°C in a regular incubator without CO_2 supply while shaking for 1 hr in the absence or presence of chylomicron-forming lipid micelles. The lipid micelles in the apical side HBSS resembled the digested lipid composition in small intestine lumen after a normal fat-containing meal. After the selection step, 50 μl samples of the HBSS at the basolateral side of the Transwell were used to determine the titer of recovered phage (output). The selection process (success or failure) was monitored by the ratio of output phage number to input phage number. Individual phage plaques were cloned using glass Pasteur pipettes and amplified. Isolated phage clones were DNA sequenced and deduced peptide sequences were used as cues to search for possible similarity to known protein sequences in protein database using the web-based Protein Blast tool (NCBI/Blast Home).

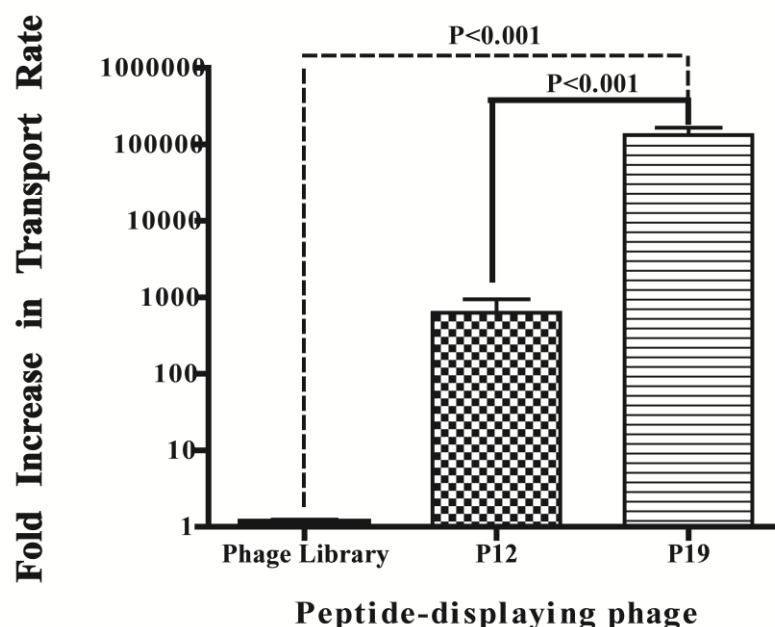
Results and Discussion

While the oral delivery of drugs in nanoparticle (NP) form is highly desirable, it has proven to be a significant challenge with only very limited success. T7 phage, a natural spherical NP ($\sim 65\text{ nm}$) was used to identify peptidic ligands that promote

intestinal NP translocation. There were always some phage particles translocated to the basolateral side because of the very high input phage number (e.g., 2.4×10^{11} phage particles in the first round of selection) and the baseline leakiness of the Caco-2 cell monolayers. This served as the background translocation rate (at about one in a million or less). In the absence of lipid, there was no phage enrichment (expressed in the output/input ratio) in any of the four selection trials suggesting that lipid was necessary for effective translocation of the phage across intestinal cells. In the presence of lipid, a sporadic increase in the ratio was seen during the first three trials of selection but the enrichment disappeared in the next round of selection. The result suggested that the specific phage in a selected phage pool was not significantly different than the non-specific phage during subsequent amplification of the selected phage pool. Only in the last trial a consistent sequential enrichment was observed from round 1 to round 3 but not from round 3 to round 4. This result suggested that it was possible to isolate specific orally absorbable phage in the presence of lipid. The lipid did not increase TEER or the rate of phage translocation compared to the rate in the absence of lipid. There was about 5000 fold increase in the ratio for round 3 and 4 of the fourth trial as compared to the ratio of the starting phage library (round 1). Our previous experience with T7 phage peptide libraries showed that peptide-displaying phage are prone to DNA rearrangement, which may partially explain why it was difficult to enrich specific phage.

Thirty-six phage plaques were randomly chosen from the selected phage pool of the fourth round selection of the successful trial. They were amplified and tested for translocation efficiency across Caco-2 monolayers. Three of the 36 clones (P12, P19 and P23) exhibited significantly higher transport rate than the starting phage library while 33

clones exhibited the same transport rate as the starting phage peptide library. DNA sequencing of the three phage clones revealed that P23 had undergone DNA rearrangement resulting in a 17-mer peptide. Therefore, the P23 clone was not pursued. The following figure shows that compared to starting phage library, the transport efficiency of P12 and P19 phages were 629 fold and 132,600 fold higher, respectively.



Transport rates of phage clones P12 and P19 relative to that of the starting phage library. The transport rate of the starting phage library (based on output/input ratio) is considered to be 1 \times . The transport was carried out through Caco-2 cell monolayer by incubating the samples for 1 hr at 37 °C incubator with shaking. The data were expressed as mean \pm s.d. of three experiments. Compare to the starting phage library, the transport rates for P12 and P19 were 629 and 132,600 fold higher, respectively.

REFERENCES

1. Granich, R.; Crowley, S.; Vitoria, M.; Smyth, C.; Kahn, J. G.; Bennett, R.; Lo, Y. R.; Souteyrand, Y.; Williams, B., Highly active antiretroviral treatment as prevention of HIV transmission: review of scientific evidence and update. *Curr Opin HIV AIDS* **2010**, *5* (4), 298-304.
2. Puskas, C. M.; Forrest, J. I.; Parashar, S.; Salters, K. A.; Cescon, A. M.; Kaida, A.; Miller, C. L.; Bangsberg, D. R.; Hogg, R. S., Women and vulnerability to HAART non-adherence: a literature review of treatment adherence by gender from 2000 to 2011. *Current HIV/AIDS Reports* **2011**, *8* (4), 277-87.
3. Cohen, J., Tissue Says Blood Is Misleading, Confusing HIV Cure Efforts. *Science* **2011**, *334* (6063), 1614.
4. Sandkovsky, U.; Swindells, S.; Robbins, B. L.; Nelson, S. R.; Acosta, E. P.; Fletcher, C. V., Measurement of plasma and intracellular concentrations of raltegravir in patients with HIV infection. *AIDS* **2012**, *26* (17), 2257-9.
5. Girard, M. P.; Osmanov, S.; Assossou, O. M.; Kieny, M.-P., Human immunodeficiency virus (HIV) immunopathogenesis and vaccine development: A review. *Vaccine* **2011**, *29* (37), 6191-6218.
6. Haase, A. T., Targeting early infection to prevent HIV-1 mucosal transmission. *Nature* **2010**, *464* (7286), 217-23.
7. Hladik, F.; McElrath, M. J., Setting the stage: host invasion by HIV. *Nat Rev Immunol* **2008**, *8* (6), 447-57.
8. Hladik, F.; Hope, T. J., HIV infection of the genital mucosa in women. *Curr HIV/AIDS Rep* **2009**, *6* (1), 20-8.
9. Shacklett, B. L.; Anton, P. A., HIV Infection and Gut Mucosal Immune Function: Updates on Pathogenesis with Implications for Management and Intervention. *Curr Infect Dis Rep* **2010**, *12* (1), 19-27.
10. Wang, X.; Rasmussen, T.; Pahar, B.; Poonia, B.; Alvarez, X.; Lackner, A. A.; Veazey, R. S., Massive infection and loss of CD4+ T cells occurs in the intestinal tract of neonatal rhesus macaques in acute SIV infection. *Blood* **2007**, *109* (3), 1174-1181.
11. Keele, B. F.; Giorgi, E. E.; Salazar-Gonzalez, J. F.; Decker, J. M.; Pham, K. T.; Salazar, M. G.; Sun, C.; Grayson, T.; Wang, S.; Li, H.; Wei, X.; Jiang, C.; Kirchherr, J. L.; Gao, F.; Anderson, J. A.; Ping, L.-H.; Swanstrom, R.; Tomaras, G. D.; Blattner, W. A.; Goepfert, P. A.; Kilby, J. M.; Saag, M. S.; Delwart, E. L.; Busch, M. P.; Cohen, M. S.; Montefiori, D. C.; Haynes, B. F.; Gaschen, B.; Athreya, G. S.; Lee, H. Y.; Wood, N.; Seoighe, C.; Perelson, A. S.; Bhattacharya, T.; Korber, B. T.; Hahn, B. H.; Shaw, G. M., Identification and characterization of transmitted and early founder virus envelopes in primary HIV-1 infection. *Proceedings of the National Academy of Sciences* **2008**, *105* (21), 7552-7557.
12. Abdool Karim, Q.; Abdool Karim, S. S.; Frohlich, J. A.; Grobler, A. C.; Baxter, C.; Mansoor, L. E.; Kharsany, A. B. M.; Sibeko, S.; Mlisana, K. P.; Omar, Z.; Gengiah, T. N.; Maarschalk, S.; Arulappan, N.; Mlotshwa, M.; Morris, L.; Taylor, D.; Group, o. b.

- o. t. C. T., Effectiveness and Safety of Tenofovir Gel, an Antiretroviral Microbicide, for the Prevention of HIV Infection in Women. *Science* **2010**, *329* (5996), 1168-1174.
13. Mehendale, S.; Deshpande, S.; Kohli, R.; Tsui, S.; Tolley, E., Acceptability of coitally-associated versus daily use of 1% tenofovir vaginal gel among women in Pune, India. *International Health* **2012**, *4* (1), 63-69.
 14. Arzhavitina, A.; Steckel, H., Foams for pharmaceutical and cosmetic application. *International Journal of Pharmaceutics* **2010**, *394* (1-2), 1-17.
 15. Garg, A. B.; Nuttall, J.; Romano, J., The future of HIV microbicides: challenges and opportunities. *Antivir Chem Chemother* **2009**, *19* (4), 143-50.
 16. Herrera, C.; Cranage, M.; McGowan, I.; Anton, P.; Shattock, R. J., Reverse transcriptase inhibitors as potential colorectal microbicides. *Antimicrob Agents Chemother* **2009**, *53* (5), 1797-807.
 17. Harper, D. R., *Viruses Biology, Applications, Control*. **2012**.
 18. Pinna, G.; Kakalou, E.; Rosenberg, T., Access to Affordable Highly Active Anti-Retroviral Therapy (HAART) for HIV/AIDS Patients. Where Do We Stand? *Hospital Chronicles* **2012**, *7* (3), 133-142.
 19. Fanales-Belasio, E.; Raimondo, M.; Suligo, B.; Buttò, S., HIV virology and pathogenetic mechanisms of infection: a brief overview. *Annali dell'Istituto Superiore di Sanità* **2010**, *46*, 5-14.
 20. Ferguson, L. M.; Rohan, L. C., The importance of the vaginal delivery route for antiretrovirals in HIV prevention. *Therapeutic delivery* **2011**, *2* (12), 1535-50.
 21. Veazey, R. S.; Lackner, A. A., Getting to the guts of HIV pathogenesis. *The Journal of experimental medicine* **2004**, *200* (6), 697-700.
 22. Pal, R.; Taylor, B.; Foulke, J. S.; Woodward, R.; Merges, M.; Praschunus, R.; Gibson, A.; Reitz, M., Characterization of a simian human immunodeficiency virus encoding the envelope gene from the CCR5-tropic HIV-1 Ba-L. *Journal of acquired immune deficiency syndromes* **2003**, *33* (3), 300-7.
 23. Tsai, C. C.; Emau, P.; Jiang, Y.; Tian, B.; Morton, W. R.; Gustafson, K. R.; Boyd, M. R., Cyanovirin-N gel as a topical microbicide prevents rectal transmission of SHIV89.6P in macaques. *AIDS Res Hum Retroviruses* **2003**, *19* (7), 535-41.
 24. Li, Q.; Estes, J. D.; Schlievert, P. M.; Duan, L.; Brosnahan, A. J.; Southern, P. J.; Reilly, C. S.; Peterson, M. L.; Schultz-Darken, N.; Brunner, K. G.; Nephew, K. R.; Pambuccian, S.; Lifson, J. D.; Carlis, J. V.; Haase, A. T., Glycerol monolaurate prevents mucosal SIV transmission. *Nature* **2009**, *458* (7241), 1034-8.
 25. Brechley, J. M.; Douek, D. C., HIV infection and the gastrointestinal immune system. *Mucosal Immunol* **2008**, *1* (1), 23-30.
 26. McElrath, M. J.; Smythe, K.; Randolph-Habecker, J.; Melton, K. R.; Goodpaster, T. A.; Hughes, S. M.; Mack, M.; Sato, A.; Diaz, G.; Steinbach, G.; Novak, R. M.; Curlin, M. E.; Lord, J. D.; Maenza, J.; Duerr, A.; Frahm, N.; Hladik, F., Comprehensive assessment of HIV target cells in the distal human gut suggests increasing HIV susceptibility toward the anus. *J Acquir Immune Defic Syndr* **2013**, *63* (3), 263-71.
 27. Ganesan, A.; Chattopadhyay, P. K.; Brodie, T. M.; Qin, J.; Gu, W.; Mascola, J. R.; Michael, N. L.; Follmann, D. A.; Roederer, M., Immunologic and Virologic Events in Early HIV Infection Predict Subsequent Rate of Progression. *Journal of Infectious Diseases* **2010**, *201* (2), 272-284.

28. Lerner, P.; Guadalupe, M.; Donovan, R.; Hung, J.; Flamm, J.; Prindiville, T.; Sankaran-Walters, S.; Syvanen, M.; Wong, J. K.; George, M. D.; Dandekar, S., The gut mucosal viral reservoir in HIV-infected patients is not the major source of rebound plasma viremia following interruption of highly active antiretroviral therapy. *J Virol* **2011**, *85* (10), 4772-82.
29. Hladik, F.; Doncel, G. F., Preventing mucosal HIV transmission with topical microbicides: Challenges and opportunities. *Antiviral Research* **2010**, *88*, Supplement (0), S3-S9.
30. Ray, M.; Logan, R.; Sterne, J. A.; Hernandez-Diaz, S.; Robins, J. M.; Sabin, C.; Bansi, L.; van Sighem, A.; de Wolf, F.; Costagliola, D.; Lanoy, E.; Bucher, H. C.; von Wyl, V.; Esteve, A.; Casbona, J.; del Amo, J.; Moreno, S.; Justice, A.; Goulet, J.; Lodi, S.; Phillips, A.; Seng, R.; Meyer, L.; Perez-Hoyos, S.; Garcia de Olalla, P.; Hernan, M. A., The effect of combined antiretroviral therapy on the overall mortality of HIV-infected individuals. *AIDS* **2010**, *24* (1), 123-37.
31. Alconcel, S. N. S.; Baas, A. S.; Maynard, H. D., FDA-approved poly(ethylene glycol)-protein conjugate drugs. *Polymer Chemistry* **2011**, *2* (7), 1442-1448.
32. Wensing, A. M. J.; van Maarseveen, N. M.; Nijhuis, M., Fifteen years of HIV Protease Inhibitors: raising the barrier to resistance. *Antiviral Research* **2010**, *85* (1), 59-74.
33. Craig, J. C.; Duncan, I. B.; Hockley, D.; Grief, C.; Roberts, N. A.; Mills, J. S., Antiviral properties of Ro 31-8959, an inhibitor of human immunodeficiency virus (HIV) proteinase. *Antiviral Research* **1991**, *16* (4), 295-305.
34. Kempf, D. J.; Marsh, K. C.; Jon, F. D.; McDonald, E.; Vasavanonda, S.; Flentge, C. A.; Green, B. E.; Fino, L.; Park, C. H.; Kong, X.-P.; Wideburg, N. E.; Saldivar, A.; Ruiz, L.; Kati, W. M.; Sham, H. L.; Robins, T.; Stewart, K. D.; Hsu, A.; Plattner, J. J.; Leonard, J. M.; Norbeck, D. W., ABT-538 is a Potent Inhibitor of Human Immunodeficiency Virus Protease and has High Oral Bioavailability in Humans. *Proceedings of the National Academy of Sciences of the United States of America* **1995**, *92* (7), 2484-2488.
35. Koh, Y.; Nakata, H.; Maeda, K.; Ogata, H.; Bilcer, G.; Devasamudram, T.; Kincaid, J. F.; Boross, P.; Wang, Y. F.; Tie, Y.; Volarath, P.; Gaddis, L.; Harrison, R. W.; Weber, I. T.; Ghosh, A. K.; Mitsuya, H., Novel bis-tetrahydrofuranylurethane-containing nonpeptidic protease inhibitor (PI) UIC-94017 (TMC114) with potent activity against multi-PI-resistant human immunodeficiency virus in vitro. *Antimicrob Agents Chemother* **2003**, *47* (10), 3123-9.
36. Partaledis, J. A.; Yamaguchi, K.; Tisdale, M.; Blair, E. E.; Falcione, C.; Maschera, B.; Myers, R. E.; Pazhanisamy, S.; Futer, O.; Cullinan, A. B.; et al., In vitro selection and characterization of human immunodeficiency virus type 1 (HIV-1) isolates with reduced sensitivity to hydroxyethylamino sulfonamide inhibitors of HIV-1 aspartyl protease. *J Virol* **1995**, *69* (9), 5228-35.
37. Patick, A. K.; Mo, H.; Markowitz, M.; Appelt, K.; Wu, B.; Musick, L.; Kalish, V.; Kaldor, S.; Reich, S.; Ho, D.; Webber, S., Antiviral and resistance studies of AG1343, an orally bioavailable inhibitor of human immunodeficiency virus protease. *Antimicrob Agents Chemother* **1996**, *40* (2), 292-7.
38. Robinson, B. S.; Riccardi, K. A.; Gong, Y. F.; Guo, Q.; Stock, D. A.; Blair, W. S.; Terry, B. J.; Deminie, C. A.; Djang, F.; Colonno, R. J.; Lin, P. F., BMS-232632, a highly

potent human immunodeficiency virus protease inhibitor that can be used in combination with other available antiretroviral agents. *Antimicrob Agents Chemother* **2000**, *44* (8), 2093-9.

39. Sham, H. L.; Kempf, D. J.; Molla, A.; Marsh, K. C.; Kumar, G. N.; Chen, C. M.; Kati, W.; Stewart, K.; Lal, R.; Hsu, A.; Betebenner, D.; Korneyeva, M.; Vasavanonda, S.; McDonald, E.; Saldivar, A.; Wideburg, N.; Chen, X.; Niu, P.; Park, C.; Jayanti, V.; Grabowski, B.; Granneman, G. R.; Sun, E.; Japour, A. J.; Leonard, J. M.; Plattner, J. J.; Norbeck, D. W., ABT-378, a highly potent inhibitor of the human immunodeficiency virus protease. *Antimicrob Agents Chemother* **1998**, *42* (12), 3218-24.

40. Vacca, J. P.; Dorsey, B. D.; Schleif, W. A.; Levin, R. B.; McDaniel, S. L.; Darke, P. L.; Zugay, J.; Quintero, J. C.; Blahy, O. M.; Roth, E.; et al., L-735,524: an orally bioavailable human immunodeficiency virus type 1 protease inhibitor. *Proc Natl Acad Sci U S A* **1994**, *91* (9), 4096-100.

41. Hruz, P. W., HIV protease inhibitors and insulin resistance: lessons from in-vitro, rodent and healthy human volunteer models. *Current Opinion in HIV and AIDS* **2008**, *3* (6), 660-665 10.1097/COH.0b013e3283139134.

42. Bradbury, R. A.; Samaras, K., Antiretroviral therapy and the human immunodeficiency virus – improved survival but at what cost? *Diabetes, Obesity and Metabolism* **2008**, *10* (6), 441-450.

43. Boyd, M. A.; Siangphoe, U.; Ruxrungtham, K.; Duncombe, C. J.; Stek, M.; Lange, J. M. A.; Cooper, D. A.; Phanuphak, P., Indinavir/ritonavir 800/100 mg bid and efavirenz 600 mg qd in patients failing treatment with combination nucleoside reverse transcriptase inhibitors: 96-week outcomes of HIV-NAT 009. *HIV Medicine* **2005**, *6* (6), 410-420.

44. Gathe, J. C., Jr.; Pierone, G.; Piliero, P.; Arasteh, K.; Rubio, R.; Lalonde, R. G.; Cooper, D.; Lazzarin, A.; Kohlbrenner, V. M.; Dohnanyi, C.; Sabo, J.; Mayers, D., Efficacy and safety of three doses of tipranavir boosted with ritonavir in treatment-experienced HIV type-1 infected patients. *AIDS Res Hum Retroviruses* **2007**, *23* (2), 216-23.

45. Sension, M.; Andrade Neto, J. L.; Grinsztejn, B.; Molina, J. M.; Zavala, I.; Gonzalez-Garcia, J.; Donnelly, A.; Phiri, P.; Ledesma, E.; McGrath, D., Improvement in lipid profiles in antiretroviral-experienced HIV-positive patients with hyperlipidemia after a switch to unboosted atazanavir. *J Acquir Immune Defic Syndr* **2009**, *51* (2), 153-62.

46. Polli, J. W.; Jarrett, J. L.; Studenberg, S. D.; Humphreys, J. E.; Dennis, S. W.; Brouwer, K. R.; Woolley, J. L., Role of P-glycoprotein on the CNS disposition of amprenavir (141W94), an HIV protease inhibitor. *Pharm Res* **1999**, *16* (8), 1206-12.

47. Wire, M. B.; Shelton, M. J.; Studenberg, S., Fosamprenavir : clinical pharmacokinetics and drug interactions of the amprenavir prodrug. *Clin Pharmacokinet* **2006**, *45* (2), 137-68.

48. Huang, L.; Wring, S. A.; Woolley, J. L.; Brouwer, K. R.; Serabjit-Singh, C.; Polli, J. W., Induction of P-glycoprotein and cytochrome P450 3A by HIV protease inhibitors. *Drug Metab Dispos* **2001**, *29* (5), 754-60.

49. Sadler, B. M.; Chittick, G. E.; Polk, R. E.; Slain, D.; Kerkering, T. M.; Studenberg, S. D.; Lou, Y.; Moore, K. H.; Woolley, J. L.; Stein, D. S., Metabolic disposition and pharmacokinetics of [¹⁴C]-amprenavir, a human immunodeficiency virus

type 1 (HIV-1) protease inhibitor, administered as a single oral dose to healthy male subjects. *J Clin Pharmacol* **2001**, *41* (4), 386-96.

50. Polk, R. E.; Crouch, M. A.; Israel, D. S.; Pastor, A.; Sadler, B. M.; Chittick, G. E.; Symonds, W. T.; Gouldin, W.; Lou, Y., Pharmacokinetic interaction between ketoconazole and amprenavir after single doses in healthy men. *Pharmacotherapy* **1999**, *19* (12), 1378-84.

51. Polk, R. E.; Brophy, D. F.; Israel, D. S.; Patron, R.; Sadler, B. M.; Chittick, G. E.; Symonds, W. T.; Lou, Y.; Kristoff, D.; Stein, D. S., Pharmacokinetic Interaction between amprenavir and rifabutin or rifampin in healthy males. *Antimicrob Agents Chemother* **2001**, *45* (2), 502-8.

52. Rerks-Ngarm, S.; Pitisuttithum, P.; Nitayaphan, S.; Kaewkungwal, J.; Chiu, J.; Paris, R.; Premisri, N.; Namwat, C.; de Souza, M.; Adams, E.; Benenson, M.; Gurunathan, S.; Tartaglia, J.; McNeil, J. G.; Francis, D. P.; Stablein, D.; Birx, D. L.; Chunsuttiwat, S.; Khamboonruang, C.; Thongcharoen, P.; Robb, M. L.; Michael, N. L.; Kunasol, P.; Kim, J. H., Vaccination with ALVAC and AIDSVAX to Prevent HIV-1 Infection in Thailand. *New England Journal of Medicine* **2009**, *361* (23), 2209-2220.

53. Haynes, B. F.; Gilbert, P. B.; McElrath, M. J.; Zolla-Pazner, S.; Tomaras, G. D.; Alam, S. M.; Evans, D. T.; Montefiori, D. C.; Karnasuta, C.; Sutthent, R.; Liao, H.-X.; DeVico, A. L.; Lewis, G. K.; Williams, C.; Pinter, A.; Fong, Y.; Janes, H.; DeCamp, A.; Huang, Y.; Rao, M.; Billings, E.; Karasavvas, N.; Robb, M. L.; Ngauy, V.; de Souza, M. S.; Paris, R.; Ferrari, G.; Bailer, R. T.; Soderberg, K. A.; Andrews, C.; Berman, P. W.; Frahm, N.; De Rosa, S. C.; Alpert, M. D.; Yates, N. L.; Shen, X.; Koup, R. A.; Pitisuttithum, P.; Kaewkungwal, J.; Nitayaphan, S.; Rerks-Ngarm, S.; Michael, N. L.; Kim, J. H., Immune-Correlates Analysis of an HIV-1 Vaccine Efficacy Trial. *New England Journal of Medicine* **2012**, *366* (14), 1275-1286.

54. Prejean, J.; Song, R.; Hernandez, A.; Ziebell, R.; Green, T.; Walker, F.; Lin, L. S.; An, Q.; Mermin, J.; Lansky, A.; Hall, H. I., Estimated HIV incidence in the United States, 2006-2009. *PLoS One* **2011**, *6* (8), e17502.

55. Padian, N. S.; McCoy, S. I.; Balkus, J. E.; Wasserheit, J. N., Weighing the gold in the gold standard: challenges in HIV prevention research. *AIDS* **2010**, *24* (5), 621-35.

56. Cohen, M. S.; Chen, Y. Q.; McCauley, M.; Gamble, T.; Hosseinipour, M. C.; Kumarasamy, N.; Hakim, J. G.; Kumwenda, J.; Grinsztejn, B.; Pilotto, J. H.; Godbole, S. V.; Mehendale, S.; Chariyalertsak, S.; Santos, B. R.; Mayer, K. H.; Hoffman, I. F.; Eshleman, S. H.; Piwowar-Manning, E.; Wang, L.; Makhema, J.; Mills, L. A.; de Bruyn, G.; Sanne, I.; Eron, J.; Gallant, J.; Havlir, D.; Swindells, S.; Ribaud, H.; Elharrar, V.; Burns, D.; Taha, T. E.; Nielsen-Saines, K.; Celentano, D.; Essex, M.; Fleming, T. R., Prevention of HIV-1 infection with early antiretroviral therapy. *N Engl J Med* **2011**, *365* (6), 493-505.

57. Graham, S. M.; Holte, S. E.; Peshu, N. M.; Richardson, B. A.; Panteleeff, D. D.; Jaoko, W. G.; Ndinya-Achola, J. O.; Mandaliya, K. N.; Overbaugh, J. M.; McClelland, R. S., Initiation of antiretroviral therapy leads to a rapid decline in cervical and vaginal HIV-1 shedding. *AIDS* **2007**, *21* (4), 501-7.

58. Vernazza, P. L.; Troiani, L.; Flepp, M. J.; Cone, R. W.; Schock, J.; Roth, F.; Boggian, K.; Cohen, M. S.; Fiscus, S. A.; Eron, J. J.; Swiss, H. I. V. C. S., Potent antiretroviral treatment of HIV-infection results in suppression of the seminal shedding of HIV. *AIDS* **2000**, *14* (2), 117-121.

59. Watts, C.; Vickerman, P., The impact of microbicides on HIV and STD transmission: model projections. *AIDS* **2001**, *15*, S43-S44.
60. Li, W.; Zhan, P.; De Clercq, E.; Lou, H.; Liu, X., Current drug research on PEGylation with small molecular agents. *Progress in Polymer Science* **2012**, (0).
61. Brocchini, S.; Godwin, A.; Balan, S.; Choi, J.-w.; Zloh, M.; Shaunak, S., Disulfide bridge based PEGylation of proteins. *Advanced Drug Delivery Reviews* **2008**, *60* (1), 3-12.
62. Abuchowski, A.; McCoy, J. R.; Palczuk, N. C.; van Es, T.; Davis, F. F., Effect of covalent attachment of polyethylene glycol on immunogenicity and circulating life of bovine liver catalase. *J Biol Chem* **1977**, *252* (11), 3582-6.
63. Abuchowski, A.; van Es, T.; Palczuk, N. C.; Davis, F. F., Alteration of immunological properties of bovine serum albumin by covalent attachment of polyethylene glycol. *Journal of Biological Chemistry* **1977**, *252* (11), 3578-81.
64. Cattel, L.; Ceruti, M.; Dosio, F., From conventional to stealth liposomes: a new Frontier in cancer chemotherapy. *J Chemother* **2004**, *16 Suppl 4*, 94-7.
65. Immordino, M. L.; Dosio, F.; Cattel, L., Stealth liposomes: review of the basic science, rationale, and clinical applications, existing and potential. *Int J Nanomedicine* **2006**, *1* (3), 297-315.
66. Working Peter, K.; Newman Mary, S.; Johnson, J.; Cornacoff Joel, B., Safety of Poly(ethylene glycol) and Poly(ethylene glycol) Derivatives. In *Poly(ethylene glycol)*, American Chemical Society: 1997; Vol. 680, pp 45-57.
67. Richter, A. W.; Akerblom, E., Antibodies against polyethylene glycol produced in animals by immunization with monomethoxy polyethylene glycol modified proteins. *Int Arch Allergy Appl Immunol* **1983**, *70* (2), 124-31.
68. Richter, A. W.; Akerblom, E., Polyethylene glycol reactive antibodies in man: titer distribution in allergic patients treated with monomethoxy polyethylene glycol modified allergens or placebo, and in healthy blood donors. *Int Arch Allergy Appl Immunol* **1984**, *74* (1), 36-9.
69. Cheng, T. L.; Wu, P. Y.; Wu, M. F.; Chern, J. W.; Roffler, S. R., Accelerated clearance of polyethylene glycol-modified proteins by anti-polyethylene glycol IgM. *Bioconjug Chem* **1999**, *10* (3), 520-8.
70. Pasut, G.; Sergi, M.; Veronese, F. M., Anti-cancer PEG-enzymes: 30 years old, but still a current approach. *Advanced Drug Delivery Reviews* **2008**, *60* (1), 69-78.
71. Milla, P.; Dosio, F.; Cattel, L., PEGylation of proteins and liposomes: a powerful and flexible strategy to improve the drug delivery. *Current drug metabolism* **2012**, *13* (1), 105-119.
72. Roberts, M. J.; Bentley, M. D.; Harris, J. M., Chemistry for peptide and protein PEGylation. *Advanced Drug Delivery Reviews* **2002**, *54* (4), 459-476.
73. Molineux, G., The design and development of pegfilgrastim (PEG-rmetHuG-CSF, Neulasta). *Curr Pharm Des* **2004**, *10* (11), 1235-44.
74. Greenwald, R. B.; Yang, K.; Zhao, H.; Conover, C. D.; Lee, S.; Filpula, D., Controlled release of proteins from their poly(ethylene glycol) conjugates: drug delivery systems employing 1,6-elimination. *Bioconjug Chem* **2003**, *14* (2), 395-403.
75. Filpula, D.; Zhao, H., Releasable PEGylation of proteins with customized linkers. *Adv Drug Deliv Rev* **2008**, *60* (1), 29-49.

76. Pasut, G.; Mero, A.; Caboi, F.; Scaramuzza, S.; Sollai, L.; Veronese, F. M., A new PEG-beta-alanine active derivative for releasable protein conjugation. *Bioconjug Chem* **2008**, *19* (12), 2427-31.
77. Foster, G. R., Pegylated interferons for the treatment of chronic hepatitis C: pharmacological and clinical differences between peginterferon-alpha-2a and peginterferon-alpha-2b. *Drugs* **2010**, *70* (2), 147-65.
78. Bentley, M. D.; Roberts, M. J.; Shen, X.; Cheng, L. Polymer conjugates of opioid antagonists. 2010.
79. Kang, J. S.; Deluca, P. P.; Lee, K. C., Emerging PEGylated drugs. *Expert Opin Emerg Drugs* **2009**, *14* (2), 363-80.
80. Kozlowski, A.; Huntsville, A. L.; McManus, S. P.; Riggs-Sauthier, J.; Shen, X.; Zhang, W. Multi-arm polymeric alkanoate conjugates. 2011.
81. Li, C.; Wallace, S., Polymer-drug conjugates: recent development in clinical oncology. *Adv Drug Deliv Rev* **2008**, *60* (8), 886-98.
82. Vicent, M. J.; Ringsdorf, H.; Duncan, R., Polymer therapeutics: clinical applications and challenges for development. *Adv Drug Deliv Rev* **2009**, *61* (13), 1117-20.
83. Veronese, F. M.; Pasut, G., PEGylation, successful approach to drug delivery. *Drug Discov Today* **2005**, *10* (21), 1451-8.
84. Caliceti, P.; Veronese, F. M., Pharmacokinetic and biodistribution properties of poly(ethylene glycol)-protein conjugates. *Adv Drug Deliv Rev* **2003**, *55* (10), 1261-77.
85. Minko, T., Soluble polymer conjugates for drug delivery. *Drug Discovery Today: Technologies* **2005**, *2* (1), 15-20.
86. Mahato, R.; Tai, W.; Cheng, K., Prodrugs for improving tumor targetability and efficiency. *Advanced Drug Delivery Reviews* **2011**, *63* (8), 659-670.
87. Chen, C.; Constantinou, A.; Deonarain, M., Modulating antibody pharmacokinetics using hydrophilic polymers. *Expert Opinion on Drug Delivery* **2011**, *8* (9), 1221-1236.
88. Markovsky, E.; Baabur-Cohen, H.; Eldar-Boock, A.; Omer, L.; Tiram, G.; Ferber, S.; Ofek, P.; Polyak, D.; Scomparin, A.; Satchi-Fainaro, R., Administration, distribution, metabolism and elimination of polymer therapeutics. *J Control Release* **2012**, *161* (2), 446-60.
89. Zhao, H.; Greenberger, L. M.; Horak, I. D., Drug Conjugates with Poly(Ethylene Glycol). In *Drug Delivery in Oncology*, Wiley-VCH Verlag GmbH & Co. KGaA: 2011; pp 627-665.
90. Gunaseelan, S.; Debrah, O.; Wan, L.; Leibowitz, M. J.; Rabson, A. B.; Stein, S.; Sinko, P. J., Synthesis of poly(ethylene glycol)-based saquinavir prodrug conjugates and assessment of release and anti-HIV-1 bioactivity using a novel protease inhibition assay. *Bioconjug Chem* **2004**, *15* (6), 1322-33.
91. Li, W.; Chang, Y.; Zhan, P.; Zhang, N.; Liu, X.; Pannecouque, C.; De Clercq, E., Synthesis, in vitro and in vivo release kinetics, and anti-HIV activity of a sustained-release prodrug (mPEG-AZT) of 3'-azido-3'-deoxythymidine (AZT, Zidovudine). *ChemMedChem* **2010**, *5* (11), 1893-8.
92. Li, W.; Wu, J.; Zhan, P.; Chang, Y.; Pannecouque, C.; De Clercq, E.; Liu, X., Synthesis, drug release and anti-HIV activity of a series of PEGylated zidovudine conjugates. *Int J Biol Macromol* **2012**, *50* (4), 974-80.

93. Zacchigna, M.; Di Luca, G.; Maurich, V.; Boccu, E., Syntheses, chemical and enzymatic stability of new poly(ethylene glycol)-acyclovir prodrugs. *Farmaco* **2002**, *57* (3), 207-14.
94. Splith, K.; Neundorff, I., Antimicrobial peptides with cell-penetrating peptide properties and vice versa. *Eur Biophys J* **2011**, *40* (4), 387-97.
95. Morris, M. C.; Deshayes, S.; Heitz, F.; Divita, G., Cell-penetrating peptides: from molecular mechanisms to therapeutics. *Biology of the Cell* **2008**, *100* (4), 201-217.
96. Khafagy, E.-S.; Morishita, M., Oral biodrug delivery using cell-penetrating peptide. *Advanced Drug Delivery Reviews* **2012**, *64* (6), 531-539.
97. Jarver, P.; Mager, I.; Langel, U., In vivo biodistribution and efficacy of peptide mediated delivery. *Trends Pharmacol Sci* **2010**, *31* (11), 528-35.
98. Brogden, K. A., Antimicrobial peptides: pore formers or metabolic inhibitors in bacteria? *Nat Rev Microbiol* **2005**, *3* (3), 238-50.
99. Trabulo, S.; Cardoso, A. L.; Mano, M.; De Lima, M. C. P., Cell-Penetrating Peptides—Mechanisms of Cellular Uptake and Generation of Delivery Systems. *Pharmaceuticals* **2010**, *3* (4), 961-993.
100. Räägel, H.; Säälük, P.; Hansen, M.; Langel, Ü.; Pooga, M., CPP–protein constructs induce a population of non-acidic vesicles during trafficking through endo-lysosomal pathway. *Journal of Controlled Release* **2009**, *139* (2), 108-117.
101. Dubikovskaya, E. A.; Thorne, S. H.; Pillow, T. H.; Contag, C. H.; Wender, P. A., Overcoming multidrug resistance of small-molecule therapeutics through conjugation with releasable octaarginine transporters. *Proceedings of the National Academy of Sciences* **2008**, *105* (34), 12128-12133.
102. Lindgren, M.; Rosenthal-Aizman, K.; Saar, K.; Eiríksdóttir, E.; Jiang, Y.; Sassian, M.; Östlund, P.; Hällbrink, M.; Langel, Ü., Overcoming methotrexate resistance in breast cancer tumour cells by the use of a new cell-penetrating peptide. *Biochemical Pharmacology* **2006**, *71* (4), 416-425.
103. Scocchi, M.; Tossi, A.; Gennaro, R., Proline-rich antimicrobial peptides: converging to a non-lytic mechanism of action. *Cell Mol Life Sci* **2011**, *68* (13), 2317-30.
104. Matsuzaki, K., Control of cell selectivity of antimicrobial peptides. *Biochimica et Biophysica Acta (BBA) - Biomembranes* **2009**, *1788* (8), 1687-1692.
105. Gennaro, R.; Zanetti, M.; Benincasa, M.; Podda, E.; Miani, M., Pro-rich antimicrobial peptides from animals: structure, biological functions and mechanism of action. *Curr Pharm Des* **2002**, *8* (9), 763-78.
106. Podda, E.; Benincasa, M.; Pacor, S.; Micali, F.; Mattiuzzo, M.; Gennaro, R.; Scocchi, M., Dual mode of action of Bac7, a proline-rich antibacterial peptide. *Biochimica et Biophysica Acta (BBA) - General Subjects* **2006**, *1760* (11), 1732-1740.
107. Dmitriev, R. I.; Ropiak, H. M.; Yashunsky, D. V.; Ponomarev, G. V.; Zhdanov, A. V.; Papkovsky, D. B., Bactenecin 7 peptide fragment as a tool for intracellular delivery of a phosphorescent oxygen sensor. *Febs J* **2010**, *277* (22), 4651-61.
108. Benincasa, M.; Scocchi, M.; Podda, E.; Skerlavaj, B.; Dolzani, L.; Gennaro, R., Antimicrobial activity of Bac7 fragments against drug-resistant clinical isolates. *Peptides* **2004**, *25* (12), 2055-61.
109. Chan, Y. R.; Zanetti, M.; Gennaro, R.; Gallo, R. L., Anti-microbial activity and cell binding are controlled by sequence determinants in the anti-microbial peptide PR-39. *J Invest Dermatol* **2001**, *116* (2), 230-5.

110. Wade, D.; Boman, A.; Wåhlin, B.; Drain, C. M.; Andreu, D.; Boman, H. G.; Merrifield, R. B., All-D amino acid-containing channel-forming antibiotic peptides. *Proceedings of the National Academy of Sciences* **1990**, *87* (12), 4761-4765.
111. Benincasa, M.; Pacor, S.; Gennaro, R.; Scocchi, M., Rapid and reliable detection of antimicrobial peptide penetration into gram-negative bacteria based on fluorescence quenching. *Antimicrob Agents Chemother* **2009**, *53* (8), 3501-4.
112. Pujals, S.; Giralt, E., Proline-rich, amphipathic cell-penetrating peptides. *Adv Drug Deliv Rev* **2008**, *60* (4-5), 473-84.
113. Sadler, K.; Eom, K. D.; Yang, J. L.; Dimitrova, Y.; Tam, J. P., Translocating proline-rich peptides from the antimicrobial peptide bactenecin 7. *Biochemistry* **2002**, *41* (48), 14150-7.
114. Tomasinsig, L.; Skerlavaj, B.; Papo, N.; Giabbai, B.; Shai, Y.; Zanetti, M., Mechanistic and Functional Studies of the Interaction of a Proline-rich Antimicrobial Peptide with Mammalian Cells. *Journal of Biological Chemistry* **2006**, *281* (1), 383-391.
115. Lee, V. H. L., Mucosal Drug Delivery. *JNCI Monographs* **2001**, *2001* (29), 41-44.
116. Tukker, J., Rectal and Vaginal Drug Delivery. In *Pharmaceutics, the science of dosage form design*, second ed.; Aulton, A. E., Ed. 2002; pp 534-543.
117. Desai, A., Rectal, vaginal and urethral delivery. In *Gibaldi's Drug Delivery Systems in Pharmaceutical Care*, Desai, A.; Lee, M., Eds. 2007; pp 95-102.
118. Block, L. H., Medicated Topicals. In *Remington*, 21 ed.; 2005; pp 871-888.
119. Flashner, M.; Lerner, E. I.; Penhasi, A. Local delivery of drugs to the colon for local treatment of colonic diseases. 2000.
120. Woodley, J. In *Peptidase activity in the GI tract: distribution between luminal contents and mucosal tissue*, Proc Int Symp Contr Rel Bioact Mater, 1991; p 337.
121. Moore, J. A.; Pletcher, S. A.; Ross, M. J., Absorption enhancement of growth hormone from the gastrointestinal tract of rats. *International Journal of Pharmaceutics* **1986**, *34* (1-2), 35-43.
122. Li, W.-Z.; Zhao, N.; Zhou, Y.-Q.; Yang, L.-B.; Xiao-Ning, W.; Bao-Hua, H.; Peng, K.; Chun-Feng, Z., Post-expansile hydrogel foam aerosol of PG-liposomes: A novel delivery system for vaginal drug delivery applications. *European Journal of Pharmaceutical Sciences* **2012**, *47* (1), 162-169.
123. Bulletti, C.; de Ziegler, D.; Flamigni, C.; Giacomucci, E.; Polli, V.; Bolelli, G.; Franceschetti, F., Targeted drug delivery in gynaecology: the first uterine pass effect. *Hum Reprod* **1997**, *12* (5), 1073-9.
124. Cicinelli, E.; de Ziegler, D.; Bulletti, C.; Matteo, M. G.; Schonauer, L. M.; Galantino, P., Direct transport of progesterone from vagina to uterus. *Obstetrics & Gynecology* **2000**, *95* (3), 403-406.
125. Levine, H.; Watson, N., Comparison of the pharmacokinetics of Crinone 8% administered vaginally versus Prometrium administered orally in postmenopausal women. *Fertility and Sterility* **2000**, *73* (3), 516-521.
126. Kealy, T.; Abram, A.; Hunt, B.; Buchta, R., The rheological properties of pharmaceutical foam: implications for use. *Int J Pharm* **2008**, *355* (1-2), 67-80.
127. Sciarra, J. J.; Sciarra, C. J., Aerosols. In *Remington, The Science and Practice of Pharmacy*, 21 ed.; 2005; pp 1000-1017.

128. Patel, P. D.; Stripp, A. M.; Fry, J. C., Whipping test for the determination of foaming capacity of protein: a collaborative study. *International Journal of Food Science & Technology* **1988**, *23* (1), 57-63.
129. Poole, S., The foam-enhancing properties of basic biopolymers. *International Journal of Food Science & Technology* **1989**, *24* (2), 121-137.
130. Loew, B. J.; Siegel, C. A., Foam preparations for the treatment of ulcerative colitis. *Curr Drug Deliv* **2012**, *9* (4), 338-44.
131. Valenta, C., The use of mucoadhesive polymers in vaginal delivery. *Advanced Drug Delivery Reviews* **2005**, *57* (11), 1692-1712.
132. Kieweg, S. L.; Katz, D. F., Squeezing Flows of Vaginal Gel Formulations Relevant to Microbicide Drug Delivery. *Journal of Biomechanical Engineering* **2006**, *128* (4), 540-553.
133. das Neves, J.; Bahia, M. F., Gels as vaginal drug delivery systems. *International Journal of Pharmaceutics* **2006**, *318* (1-2), 1-14.
134. Barnhart, K. T.; Pretorius, E. S.; Timbers, K.; Shera, D.; Shabbout, M.; Malamud, D., In vivo distribution of a vaginal gel: MRI evaluation of the effects of gel volume, time and simulated intercourse. *Contraception* **2004**, *70* (6), 498-505.
135. Zhou, F.; Kraehenbuhl, J. P.; Neutra, M. R., Mucosal IgA response to rectally administered antigen formulated in IgA-coated liposomes. *Vaccine* **1995**, *13* (7), 637-44.
136. Watarai, S.; Han, M.; Tana; Kodama, H., Antibody response in the intestinal tract of mice orally immunized with antigen associated with liposomes. *J Vet Med Sci* **1998**, *60* (9), 1047-50.
137. Zhao, Y.; Brown, M. B.; Jones, S. A., Pharmaceutical foams: are they the answer to the dilemma of topical nanoparticles? *Nanomedicine: Nanotechnology, Biology and Medicine* **2010**, *6* (2), 227-236.
138. Zhao, Y.; Moddarese, M.; Jones, S. A.; Brown, M. B., A dynamic topical hydrofluoroalkane foam to induce nanoparticle modification and drug release in situ. *Eur J Pharm Biopharm* **2009**, *72* (3), 521-8.
139. Zhao, Y.; Brown, M. B.; Jones, S. A., The topical delivery of benzoyl peroxide using elegant dynamic hydrofluoroalkane foams. *Journal of Pharmaceutical Sciences* **2010**, *99* (3), 1384-1398.
140. Farese-Di Giorgio, A.; Rouquayrol, M.; Greiner, J.; Aubertin, A. M.; Vierling, P.; Guedj, R., Synthesis and anti-HIV activity of prodrugs derived from saquinavir and indinavir. *Antivir Chem Chemother* **2000**, *11* (2), 97-110.
141. Bilello, J. A.; Bilello, P. A.; Stellrecht, K.; Leonard, J.; Norbeck, D. W.; Kempf, D. J.; Robins, T.; Drusano, G. L., Human serum alpha 1 acid glycoprotein reduces uptake, intracellular concentration, and antiviral activity of A-80987, an inhibitor of the human immunodeficiency virus type 1 protease. *Antimicrob Agents Chemother* **1996**, *40* (6), 1491-7.
142. Denissen, J. F.; Grabowski, B. A.; Johnson, M. K.; Buko, A. M.; Kempf, D. J.; Thomas, S. B.; Surber, B. W., Metabolism and disposition of the HIV-1 protease inhibitor ritonavir (ABT-538) in rats, dogs, and humans. *Drug Metab Dispos* **1997**, *25* (4), 489-501.
143. Kempf, D. J.; Marsh, K. C.; Kumar, G.; Rodrigues, A. D.; Denissen, J. F.; McDonald, E.; Kukulka, M. J.; Hsu, A.; Granneman, G. R.; Baroldi, P. A.; Sun, E.; Pizzuti, D.; Plattner, J. J.; Norbeck, D. W.; Leonard, J. M., Pharmacokinetic enhancement

of inhibitors of the human immunodeficiency virus protease by coadministration with ritonavir. *Antimicrob Agents Chemother* **1997**, *41* (3), 654-60.

144. Sadler, B. M.; Stein, D. S., Clinical pharmacology and pharmacokinetics of amprenavir. *Ann Pharmacother* **2002**, *36* (1), 102-18.

145. Yu, L.; Bridgers, A.; Polli, J.; Vickers, A.; Long, S.; Roy, A.; Winnike, R.; Coffin, M., Vitamin E-TPGS Increases Absorption Flux of an HIV Protease Inhibitor by Enhancing Its Solubility and Permeability. *Pharmaceutical Research* **1999**, *16* (12), 1812-1817.

146. Vierling, P.; Greiner, J., Prodrugs of HIV protease inhibitors. *Curr Pharm Des* **2003**, *9* (22), 1755-70.

147. Zalipsky, S., Chemistry of polyethylene glycol conjugates with biologically active molecules. *Adv Drug Deliv Rev* **1995**, *16*, 157-182.

148. Greenwald, R. B.; Pendri, A.; Conover, C.; Gilbert, C.; Yang, R.; Xia, J., Drug delivery systems. 2. Camptothecin 20-O-poly(ethylene glycol) ester transport forms. *J Med Chem* **1996**, *39* (10), 1938-40.

149. Zhao, H.; Rubio, B.; Sapra, P.; Wu, D.; Reddy, P.; Sai, P.; Martinez, A.; Gao, Y.; Lozanguiez, Y.; Longley, C.; Greenberger, L. M.; Horak, I. D., Novel prodrugs of SN38 using multiarm poly(ethylene glycol) linkers. *Bioconjug Chem* **2008**, *19* (4), 849-59.

150. Greenwald, R. B.; Gilbert, C. W.; Pendri, A.; Conover, C. D.; Xia, J.; Martinez, A., Drug delivery systems: water soluble taxol 2'-poly(ethylene glycol) ester prodrugs-design and in vivo effectiveness. *J Med Chem* **1996**, *39* (2), 424-31.

151. Li, C.; Yu, D.; Inoue, T.; Yang, D. J.; Milas, L.; Hunter, N. R.; Kim, E. E.; Wallace, S., Synthesis and evaluation of water-soluble polyethylene glycol-paclitaxel conjugate as a paclitaxel prodrug. *Anticancer Drugs* **1996**, *7* (6), 642-8.

152. Antonian, L., K. Burton, R. Goodin, et al, PEGylation governs the disposition and metabolism of irinotecan following administration of a novel PEG-Irinotecan conjugate. *Eur J Cancer* **2007**, *5* (Suppl).

153. Sahner d, p. h., marcantonio a, eldon m, Results from a phase 1, double-blind, randomized, placebo-controlled, multiple-dose study evaluating the safety, tolerability, and pharmacokinetics of oral doses of NKTR-118. *J Pain* **2007**, *9* (suppl 1).

154. Paranjpe, P. V.; Chen, Y.; Kholodovych, V.; Welsh, W.; Stein, S.; Sinko, P. J., Tumor-targeted bioconjugate based delivery of camptothecin: design, synthesis and in vitro evaluation. *J Control Release* **2004**, *100* (2), 275-92.

155. Matayoshi, E. D.; Wang, G. T.; Krafft, G. A.; Erickson, J., Novel fluorogenic substrates for assaying retroviral proteases by resonance energy transfer. *Science* **1990**, *247* (4945), 954-8.

156. Wan, L.; Zhang, X.; Pooyan, S.; Palombo, M. S.; Leibowitz, M. J.; Stein, S.; Sinko, P. J., Optimizing Size and Copy Number For PEG-fMLF (N-Formyl-methionyl-leucyl-phenylalanine) Nanocarrier Uptake by Macrophages. *Bioconjugate Chemistry* **2007**, *19* (1), 28-38.

157. Wan, L.; Pooyan, S.; Hu, P.; Leibowitz, M.; Stein, S.; Sinko, P., Peritoneal Macrophage Uptake, Pharmacokinetics and Biodistribution of Macrophage-Targeted PEG-fMLF (N-Formyl-Methionyl-Leucyl-Phenylalanine) Nanocarriers for Improving HIV Drug Delivery. *Pharmaceutical Research* **2007**, *24* (11), 2110-2119.

158. Pooyan, S.; Qiu, B.; Chan, M. M.; Fong, D.; Sinko, P. J.; Leibowitz, M. J.; Stein, S., Conjugates Bearing Multiple Formyl-Methionyl Peptides Display Enhanced Binding

- to but Not Activation of Phagocytic Cells. *Bioconjugate Chemistry* **2002**, *13* (2), 216-223.
159. Mallipedi, R.; Rohan, L. C., Progress in antiretroviral drug delivery using nanotechnology. *Int J Nanomedicine* **2010**, *5*, 533-47.
160. Ellman, G. L., A colorimetric method for determining low concentrations of mercaptans. *Arch Biochem Biophys* **1958**, *74* (2), 443-50.
161. Mosmann, T., Rapid colorimetric assay for cellular growth and survival: application to proliferation and cytotoxicity assays. *J. Immunol. Methods* **1983**, *65*, 55-63.
162. Nara, P. L.; Hatch, W. C.; Dunlop, N. M.; Robey, W. G.; Arthur, L. O.; Gonda, M. A.; Fischinger, P. J., Simple, rapid, quantitative, syncytium-forming microassay for the detection of human immunodeficiency virus neutralizing antibody. *AIDS Res Hum Retroviruses* **1987**, *3* (3), 283-302.
163. Zacchigna, M.; Cateni, F.; Drioli, S.; Bonora, G. M., Multimeric, Multifunctional Derivatives of Poly(ethylene glycol). *Polymers* **2011**, *3*, 1076-1090.
164. Ziegler, A.; Seelig, J., Contributions of glycosaminoglycan binding and clustering to the biological uptake of the nonamphipathic cell-penetrating peptide WR9. *Biochemistry* **2011**, *50* (21), 4650-64.
165. Salomone, F.; Cardarelli, F.; Di Luca, M.; Boccardi, C.; Nifosi, R.; Bardi, G.; Di Bari, L.; Serresi, M.; Beltram, F., A novel chimeric cell-penetrating peptide with membrane-disruptive properties for efficient endosomal escape. *J Control Release* **2012**, *163* (3), 293-303.
166. Mueller J, K. I., Volkmer R, Boisguerin P., Comparison of cellular uptake using 22 CPPs in 4 different cell lines. *Bioconjug Chem.* **2008**, *19*, 2363-74.
167. Lindgren, M.; Langel, U., Classes and prediction of cell-penetrating peptides. *Methods Mol Biol* **2011**, *683*, 3-19.
168. Futaki, S.; Nakase, I.; Tadokoro, A.; Takeuchi, T.; Jones, A. T., Arginine-rich peptides and their internalization mechanisms. *Biochem Soc Trans* **2007**, *35* (Pt 4), 784-7.
169. Zhang, X.; Jin, Y.; Plummer, M. R.; Pooyan, S.; Gunaseelan, S.; Sinko, P. J., Endocytosis and membrane potential are required for HeLa cell uptake of R.I.-CKTat9, a retro-inverso Tat cell penetrating peptide. *Mol Pharm* **2009**, *6* (3), 836-48.
170. Kumar, R.; Kulkarni, A.; Nabulsi, J.; Nagesha, D.; Cormack, R.; Makrigiorgos, M.; Sridhar, S., Facile synthesis of PEGylated PLGA nanoparticles encapsulating doxorubicin and its in vitro evaluation as potent drug delivery vehicle. *Drug Delivery and Translational Research* **2013**, 1-10.
171. Bansal, T.; Akhtar, N.; Jaggi, M.; Khar, R. K.; Talegaonkar, S., Novel formulation approaches for optimising delivery of anticancer drugs based on P-glycoprotein modulation. *Drug Discovery Today* **2009**, *14* (21-22), 1067-1074.
172. McGowan, I., The development of rectal microbicides for HIV prevention. *Expert Opin Drug Deliv* **2014**, *11* (1), 69-82.
173. Hardy, E.; Jiménez, A. L.; de Pádua, K. S.; Zaneveld, L. J. D., Women's preferences for vaginal antimicrobial contraceptives III: Choice of a formulation, applicator, and packaging. *Contraception* **1998**, *58* (4), 245-249.
174. das Neves, J.; Amaral, M. H.; Bahia, M. F., Performance of an in vitro mucoadhesion testing method for vaginal semisolids: Influence of different testing

conditions and instrumental parameters. *European Journal of Pharmaceutics and Biopharmaceutics* **2008**, *69* (2), 622-632.

175. McCarty, A.; Feldman, S., Study of patient preferences for ointment, cream and foam formulations. *Journal of the American Academy of Dermatology* **2004**, *50* (3), P150.

176. Abram, A.; Fuchshuber, L. Pharmaceutical Foam. 2010.

177. Talukdar, M. M.; Kinget, R., Swelling and drug release behaviour of xanthan gum matrix tablets. *International Journal of Pharmaceutics* **1995**, *120* (1), 63-72.

178. Rinaudo, M., Relation between the molecular structure of some polysaccharides and original properties in sol and gel states. *Food Hydrocolloids* **2001**, *15* (4-6), 433-440.

179. Katzbauer, B., Properties and applications of xanthan gum. *Polymer Degradation and Stability* **1998**, *59* (1-3), 81-84.

180. Beneventi, D.; Carre, B.; Gandini, A., Role of surfactant structure on surface and foaming properties. *Colloids and Surfaces A: Physicochemical and Engineering Aspects* **2001**, *189* (1-3), 65-73.

181. Zhao, Y.; Brown, M. B.; Jones, S. A., Engineering novel topical foams using hydrofluoroalkane emulsions stabilised with pluronic surfactants. *European Journal of Pharmaceutical Sciences* **2009**, *37* (3-4), 370-377.

182. Sund-Levander, M.; Forsberg, C.; Wahren, L. K., Normal oral, rectal, tympanic and axillary body temperature in adult men and women: a systematic literature review. *Scand J Caring Sci* **2002**, *16* (2), 122-8.

183. Lunkenheimer, K.; Malysa, K., Simple and generally applicable method of determination and evaluation of foam properties. *Journal of Surfactants and Detergents* **2003**, *6* (1), 69-74.

184. Pinazo, A.; Pérez, L.; Infante, M. R.; Franses, E. I., Relation of foam stability to solution and surface properties of gemini cationic surfactants derived from arginine. *Colloids and Surfaces A: Physicochemical and Engineering Aspects* **2001**, *189* (1-3), 225-235.

185. Arnaudov, L.; Denkov, N. D.; Surcheva, I.; Durbut, P.; Broze, G.; Mehreteab, A., Effect of Oily Additives on Foamability and Foam Stability. 1. Role of Interfacial Properties. *Langmuir* **2001**, *17* (22), 6999-7010.

186. Pugh, R. J., Foaming, foam films, antifoaming and defoaming. *Advances in Colloid and Interface Science* **1996**, *64*, 67-142.

187. Murray, B. S.; Ettelaie, R., Foam stability: proteins and nanoparticles. *Current Opinion in Colloid & Interface Science* **2004**, *9* (5), 314-320.

188. Horozov, T. S., Foams and foam films stabilised by solid particles. *Current Opinion in Colloid & Interface Science* **2008**, *13* (3), 134-140.

189. Denkov, N. D., Foam Rheology. In *Foam Engineering: Fundamentals and Applications*, Stevenson, P., Ed. Wiley-Blackwell: 2012; pp 90-120.

190. Widengren, J.; Terry, B.; Rigler, R., Protonation kinetics of GFP and FITC investigated by FCS — aspects of the use of fluorescent indicators for measuring pH. *Chemical Physics* **1999**, *249* (2-3), 259-271.

191. Peng, J.; He, X.; Wang, K.; Tan, W.; Wang, Y.; Liu, Y., Noninvasive monitoring of intracellular pH change induced by drug stimulation using silica nanoparticle sensors. *Analytical and Bioanalytical Chemistry* **2007**, *388* (3), 645-654.

192. Lorenz, J. N.; Gruenstein, E., A simple, nonradioactive method for evaluating single-nephron filtration rate using FITC-inulin. *American Journal of Physiology - Renal Physiology* **1999**, *276* (1), F172-F177.
193. Norris, D. A.; Puri, N.; Sinko, P. J., The effect of physical barriers and properties on the oral absorption of particulates. *Advanced Drug Delivery Reviews* **1998**, *34* (2–3), 135-154.
194. Norris, D. A.; Sinko, P. J., Effect of size, surface charge, and hydrophobicity on the translocation of polystyrene microspheres through gastrointestinal mucin. *Journal of Applied Polymer Science* **1997**, *63* (11), 1481-1492.
195. Berestovsky, G. N.; Ternovsky, V. I.; Kataev, A. A., Through pore diameter in the cell wall of *Chara corallina*. *Journal of Experimental Botany* **2001**, *52* (359), 1173-1177.
196. Linegar, K. L.; Adeniran, A. E.; Kostko, A. F.; Anisimov, M. A., Hydrodynamic radius of polyethylene glycol in solution obtained by dynamic light scattering. *Colloid Journal* **2010**, *72* (2), 279-281.
197. Pokorná, J.; Machala, L.; Řezáčová, P.; Konvalinka, J., Current and Novel Inhibitors of HIV Protease. *Viruses* **2009**, *1* (3), 1209-1239.
198. Hildreth, J. E. K., Syncytium-Inhibiting Monoclonal Antibodies Produced against Human T-Cell Lymphotropic Virus Type 1-Infected Cells Recognize Class II Major Histocompatibility Complex Molecules and Block by Protein Crowding. *Journal of Virology* **1998**, *72* (12), 9544-9552.
199. Tamarkin, D.; Berman, T.; Eini, M.; Friedman, D.; Schuz, D. Stable non-alcoholic foamable pharmaceutical emulsion compositions with an unctuous emollient and their uses. 2007.
200. Shinde, N. G.; Aloorkar, N. H.; Bangar, B. N.; Deshmukh, S. M., Pharmaceutical Foam Drug Delivery System: General Considerations. *Indo American Journal of Pharmaceutical Research* **2013**, *3* (12), 1322-1327.
201. Grimes, D. A.; Lopez, L.; Raymond, E. G.; Halpern, V.; Nanda, K.; Schulz, K. F., Spermicide used alone for contraception. *Cochrane Database Syst Rev* **2005**, (4), CD005218.